LBL-19510
c.2

Lawrence Berkeley Laboratory

UNIVERSITY OF CALIFORNIA

RECEIVED
LAWRENCE
BERKELEY LABORATORY
JUN 4 1985
LIBRARY AND
DOCUMENTS SECTION

CHEMICAL BIODYNAMICS DIVISION

PICOSECOND STUDIES OF EXCITED STATE
PROTON TRANSFER REACTIONS

S.P. Webb
(Ph.D. Thesis)

TWO-WEEK LOAN COPY

This is a Library Circulating Copy
which may be borrowed for two weeks.

April 1985

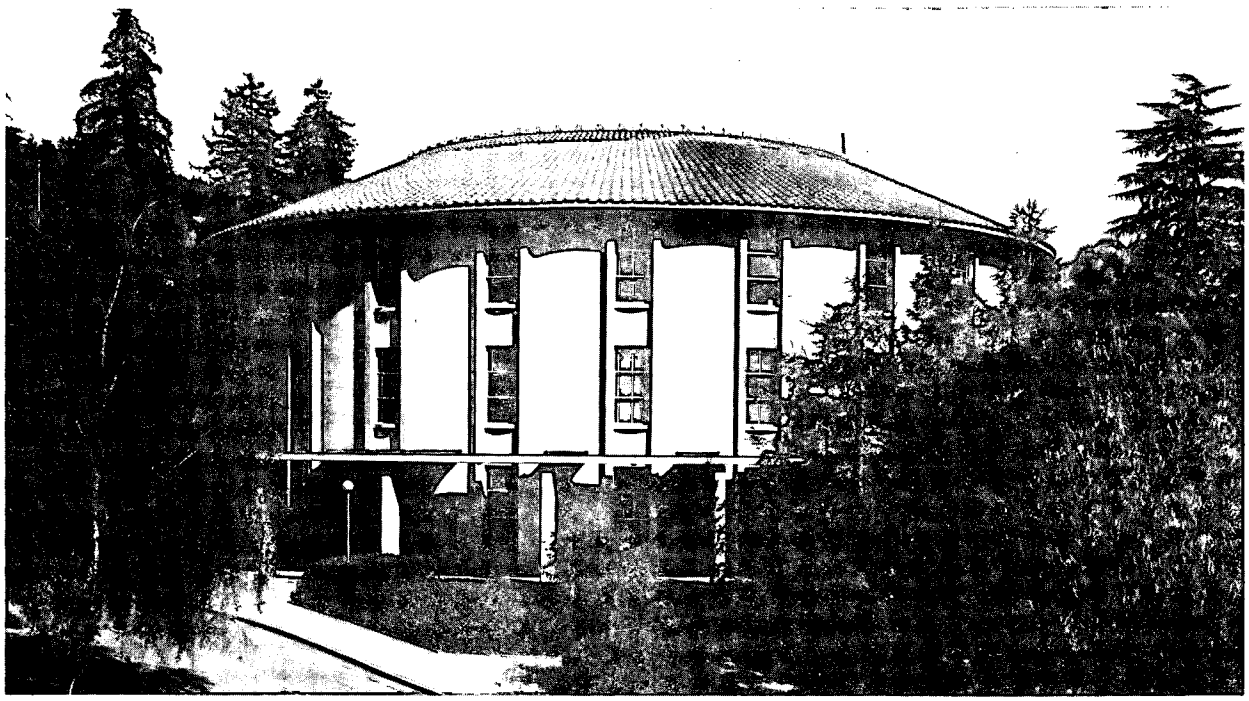

Prepared for the U.S. Department of Energy under Contract DE-AC03-76SF00098

LBL-19510
c.2

DISCLAIMER

This document was prepared as an account of work sponsored by the United States Government. While this document is believed to contain correct information, neither the United States Government nor any agency thereof, nor the Regents of the University of California, nor any of their employees, makes any warranty, express or implied, or assumes any legal responsibility for the accuracy, completeness, or usefulness of any information, apparatus, product, or process disclosed, or represents that its use would not infringe privately owned rights. Reference herein to any specific commercial product, process, or service by its trade name, trademark, manufacturer, or otherwise, does not necessarily constitute or imply its endorsement, recommendation, or favoring by the United States Government or any agency thereof, or the Regents of the University of California. The views and opinions of authors expressed herein do not necessarily state or reflect those of the United States Government or any agency thereof or the Regents of the University of California.

LBL-19510

Picosecond Studies of Excited State Proton Transfer Reactions

Steven Paul Webb
Ph.D. Thesis

Lawrence Berkeley Laboratory
University of California
Berkeley, California 94720

April 1985

This work was supported by the Director, Office of Energy Research, Office of Basic Energy Sciences, Chemical Sciences Division of the U. S. Department of Energy under Contract No. DE-AC03-76SF00098.

Picosecond Studies of Excited State Proton Transfer Reactions

Steven Paul Webb

Abstract

The detailed kinetic processes for the excited state proton transfer (ESPT) of 1-naphthol in H_2O and D_2O are investigated. This process is studied using both time dependent and steady state techniques. This work has resulted in the most accurate determination yet made for the many, excited state rate constants for this system. Previously unobtainable measurements of the extremely faint fluorescence of the 1-naphthol neutral species are carried out using time resolved and steady state methods. Questions regarding the nature of the solute/solvent system are discussed with respect to the effect of the solvent on the excited state processes. The use of the proton transfer process as a probe of solvent interactions is also considered.

Twenty picosecond, 266 nm pulses from a Nd:YAG laser were used for excitation in the time resolved study. The very rapid fluorescence decays were determined using a streak camera system that was capable of extensive real time data correction and signal averaging. Steady state spectral measurements were carried out using a sensitive, computer-controlled spectrofluorimeter.

The data from both types of measurements were analyzed and evaluated in terms of a two-state (excited state) system involving adiabatic ESPT and diabatic proton quenching of both the neutral and anionic 1-naphthol species. Only by combining the techniques of time dependent and steady state measurements and by performing experiments that are capable of measuring both very weak and very rapidly evolving signals

can the ESPT reaction of 1-naphthol be adequately understood.

A model based on data obtained using both these techniques is presented. Computer simulations based on this model are compared to the actual temporal and spectral data. Analyses of the data based on the reaction scheme and kinetic model presented here yield the rates for proton transfer and reprotonation as: 2.5×10^{10} sec^{-1} and 6.8×10^{10} M^{-1} sec^{-1} in H_2O ($pK_a^* = 0.4$); and 7.9×10^{9} sec^{-1} and 4.8×10^{10} M^{-1} sec^{-1} in D_2O ($pK_a^* = 0.8$), respectively. The numerous other rate constants necessary to fully describe the ESPT reactions in 1-naphthol are also accurately determined. Comparisons between the results obtained in H_2O and D_2O are made with respect to the influence of the solvent. Investigations involving added salts, mixed solvents, and applied pressure permit a the qualitative assessment of the role of the solvent environment in the ESPT process.

Table of Contents

Chapter	Page
Acknowledgements	iii
List of Figures	iv
List of Tables	vii
I. Chapter One: Introduction	
A. Background	1
B. Excited State Proton Transfer in 1-Naphthol	10
II. Chapter Two: Experimental Apparatus and Techniques	
A. Introduction	14
B. Experimental Apparatus	
1. Picosecond Laser System	18
2. Streak Camera System	28
C. Analyses, Calibrations, and Corrections	30
D. Comparative Features of the Laser and Detection Systems	41
E. Applications	43
F. Sample Preparation and Steady State Methods	57
III. Chapter Three: Theory	
A. Introduction	60
B. Theoretical Model and Methods	63
C. Method of Analysis	70
D. Calculations of the Acid Strength	73
E. Computer Modelling	75

Chapter Page

IV. Chapter Four: Results and Discussion

A. Introduction..... 77

B. Experimental Observables..... 78

C. Method of Analysis..... 91

D. Investigations of the Effects of Solvent Structure on Excited State Proton Transfer in 1-Naphthol..... 133

V. Chapter Five: Conclusions..... 149

VI. References..... 151

VII. Appendix

A. The Excited State Proton Transfer Rate Equations..... A1

B. Equilibrium Conditions..... A3

C. Steady State Method and Quantum Yields..... A6

D. Analytic Expressions Employing Steady State and Kinetic Measurements vs. pH..... A12

Acknowledgements

The number of people deserving my thanks would alone fill this thesis. My parents, whose love, faith, and caring have always been tremendous, are worthy of my highest thanks and I love them. My family, Jeanne, Dave, and Judy (and Jeff, Dave, and Robin) have also been a source of strength and support.

My research group has been a nice assortment of people. I would like to thank my boss, John, for giving me the opportunity and the freedom to pursue my own interests. Especially important to me is my good friend and partner, Laura, who has done so many things for me that I could not list them here. She has been an inspiration. (Mark, we will see.) My very good friends, Howard (my role model) and Lisa (and, of course, Matilde who has helped me through many a bleak night), have been very close and I will miss them alot. Marion and the youngster, Steve, have given me hope for the youth of today.

My bridge-buddies: John, John, and Bruce (may we call you John), have shown me that work and play can go well together. John Casey and clan (not to forget Sasha) have been more than roommates, but also very good friends. Lennie, too, has been one of the few people I could look up to. My fellow softballers have been a wonderful group to know and I'm proud to be a part of the team. My friends in the Lee group will be greatly missed. To my friends, Don and Fred, back home, we will keep in touch.

I gratefully acknowledge my professional associates: Gary Scott, Alex Glazer, and Laren Tolbert; it's good to have friends on the inside.

To those I've missed, and there are plenty, you're in my heart, but I'm out of space.

List of Figures

Figure	Description	Page
1	1- and 2-Naphthol Molecules	3
2	Förster Cycle Thermodynamic Model	6
3	Active/Passive Nd:YAG Laser Cavity	20
4	Output Pulse Train from the Modelocked Nd:YAG Laser.	23
5	Schematic Representation of the Experimental Layout: Laser System and Detection Apparati for 266 nm Experiments	24
6	Etalon Pulses for Time Calibration	35
7	Normalized Etalon Spacing vs. Position on the Detector	36
8	Potential Energy Diagram for Excited State, Solute/Solvent Re-equilibration	40
9	Simultaneous, Spectral and Temporal Pulse Diagnostics: Dependence of Spectral and Temporal Width on Pulse Selection from the Train	45
10	Vertical and Horizontal Components of Fluorescence of Rhodamine 6G in Ethanol	46
11	Rotational Reorientation Time vs. Excitation Energy for Rhodamine 6G in Ethanol	48
12	Maximum Rotational Anisotropy, r(0), vs. Excitation Energy for Rhodamine 6G in Ethanol	49
13	Time-Evolving Spectra of 4-Aminophthalimide	50
14	Signal Averaging and Laser Power Dependence: Phycobilisomes	51
15	Time Resolved Emission from Ruthenium tris(Bipyridine)$^{++}$ Using 532 nm and 355 nm Excitation	54
16	Rotational Reorientation Lifetime for Rhodamine 6G vs. Viscosity: Linear Alcohols versus Ethanol under Pressure	56
17	The Excited State Proton Transfer Kinetic Scheme for 2-Naphthol	61

Figure	Description	Page
18	The Excited State Proton Transfer Kinetic Scheme for 1-Naphthol	64
19	Absorption Spectra for 1-Naphthol (Neutral, pH 6.5) and 1-Naphtholate (Anion, pH 12) in H_2O and D_2O Solutions	79
20	Emission Spectra for 1-Naphthol Neutral and Anion at pH 6.5 in H_2O	81
21	Emission Spectra for 1-Naphthol Neutral and Anion at pD 6.5 in D_2O	83
22	Time Resolved Fluorescence of 1-Naphtholate (pH 7 and 12) and 1-Naphthol (pH 7)	86
23	Fluorescence Decay and Log Plot for 1-Naphtholate at pH 1.1	88
24	Fluorescence Decays of 1-Naphtholate as a Function of pH	89
25	Time Resolved Emission Spectra of 1-Naphthol at pH 6.5	92
26	Time-Evolving Emission Spectra of 1-Naphthol at pH 6.5 in H_2O	93
27	Time-Evolving Emission Spectra of 1-Naphthol at pD 6.5 in D_2O	94
28	Normalized Excitation Spectra for the Neutral and Anion in Water and Their Ratio (ϕ_A/ϕ_{A^-})	96
29	Fluorescence Titration Curves for the Neutral and Anion in H_2O	105
30	Fluorescence Titration Curves for the Neutral and Anion in D_2O	106
31	Plot of the Relative Emission Yields (Neutral/Anion) vs. (H^+) (Eq. (A71)) in H_2O	108
32	Plot of the Relative Emission Yields (Neutral/Anion) vs. (D^+) (Eq. (A71)) in D_2O	109
33	Plot of $G_1 + G_2$ vs. (H^+) (Eq. (A72)) in H_2O	113
34	Plot of $G_1 + G_2$ vs. (D^+) (Eq. (A72)) in D_2O	114
35	Plot of Eq. (A66b) for 1-Naphthol in H_2O	118

Figure	Description	Page
36	Plot of Eq. (A66b) for 1-Naphthol in D_2O.....	119
37	Plot of $G_1 * G_2 - k_3k_4$ vs. (H^+) (Eq. (A73)) in H_2O..	121
38	Plot of $G_1 * G_2 - k_3k_4$ vs. (D^+) (Eq. (A73)) in D_2O..	122
39	Computer Simulated Fluorescence Titration Curves for the Neutral and Anion in H_2O.....	125
40	Computer Simulated Fluorescence Titration Curves for the Neutral and Anion in D_2O.....	126
41	Computer Simulated Fluorescence Curves with the H_2O Data at pH: 7.1, 1.3, and -0.08.....	127
42	Computer Simulated Fluorescence Curves with the D_2O Data at pD: 5.5, 1.3, and 0.06.....	128
43	Effect on the Anion Rise Time of Added Salt: 0 and 5 M NaCl in Water at pH 6.5.....	137
44	Effect on the Anion Rise Time of Mixed Solvents: 0, 20, and 40 % Ethanol in Water at pH 6.5.....	141
45	Effect of Applied Pressure on the Anion Rise Time in Water at pH 6.2: 1, 1500, and 3000 bar.....	147

List of Tables

Table	Description	Page
I	Concentrations, pHs, and Corrections Used in the Spectral and Temporal Analysis of 1-Naphthol in H_2O	99
II	Concentrations, pDs, and Corrections Used in the Spectral and Temporal Analysis of 1-Naphthol in D_2O	100
III	Data from Time Resolved Experiments for 1-Naphthol in H_2O	101
IV	Data from Time Resolved Experiments for 1-Naphthol in D_2O	102
V	Data from Steady State Experiments for 1-Naphthol in H_2O	103
VI	Data from Steady State Experiments for 1-Naphthol in D_2O	104
VII	Temporal Fits to Eqs. (A72) and (A73) Calculated from the H_2O data	111
VIII	Temporal Fits to Eqs. (A72) and (A73) Calculated from the D_2O data	112
IX	Steady State Data for Eq. (A66b) Calculated from the H_2O Data	116
X	Steady State Data for Eq. (A66b) Calculated from the D_2O Data	117
XI	Rate Constants for the Excited State Proton Transfer Reaction of 1-Naphthol in H_2O and D_2O: Comparison with Values from the Literature	124
XII	Time Resolved Results for 1-Naphthol in Water at Various Salt Concentrations	136
XIII	Time Resolved Results for 1-Naphthol in Mixed Solvents: Acetonitrile/Water and Ethanol/Water	142
XIV	1-Naphtholate Anion Decay in Mixed Solvents: Acetonitrile/H_2O and Ethanol/H_2O	143
XV	Time Resolved Measurements for 1-Naphthol in H_2O under Pressure	146

Chapter One

Introduction

A. Background

The interactions of acids and bases are some of the most fundamental processes in chemistry. The original model of acid/base reactions depicted acids and bases as simple proton donors and acceptors (Brønsted definition). The scope of the theory was later expanded by the more general idea of electron pair donors and acceptors (Lewis definition)[1]. The thrust of many investigations in organic and physical chemistry has been to uncover the role which acids play in a reaction. Proton transfer reactions are the simplest in the general theory of acids. Although proton transfer is an elementary reaction, attaining a complete understanding of this fundamental process is a difficult problem. The almost countless experiments performed to provide new insight into this phenomenon attest to its actual complexity.

The study of proton transfer reactions encompasses both solute and solvent interactions. Solute studies probe the structural properties that determine the acid/base properties of a molecule. Gas phase studies of acidity focus on these molecular features, since the molecules are isolated from any solvent interactions. In liquids, where most chemistry occurs, proton transfer is complicated by solvent effects as well. Not only is the solvent directly involved in the proton transfer process, but it may also act to stabilize the resultant conjugate base. Therefore, the solvent influences the motion of the proton in a manner which is very different from that in the isolated solute. The great disparity between gas phase and solution phase

acidities emphasizes this difference[1]. In addition to the solute structure, interactions between solute and solvent molecules raise new questions concerning solvent structure. For example, the orientation of the solute with respect to neighboring solvent molecules would be expected to influence the rate of proton transfer. Investigations of acids and bases in solution are aimed at answering some of the questions involving the role of the solvent in proton transfer reactions. Expanding our theoretical and experimental knowledge of this simplest of acids, the proton, builds the foundations of chemical understanding.

Numerous and varied approaches have been used in the analysis of the proton transfer process[2-17]. This work describes the investigation of excited state proton transfer (ESPT). ESPT refers to a proton transfer process which occurs along an excited potential energy surface. The aromatic acid, 1-naphthol (Fig. 1), was chosen for this study. Like many aromatic acids[31], the acidity of 1-naphthol increases dramatically upon electronic excitation, resulting in proton transfer to the solvent. This reaction results in the formation of the electronically excited conjugate base. Since these fundamental molecular processes occur on rapid timescales, their direct observation requires an equally rapid experimental technique. In this work, the ESPT process is initiated by excitation using a picosecond laser. Fluorescence from the excited acid and its conjugate base is monitored to identify the events occuring on the excited surface. Finally, a kinetic analysis of the data provides insights into the mechanism of these events.

Excited state photochemical reactions are used to investigate proton transfer phenomena for two reasons. First, it is experi-

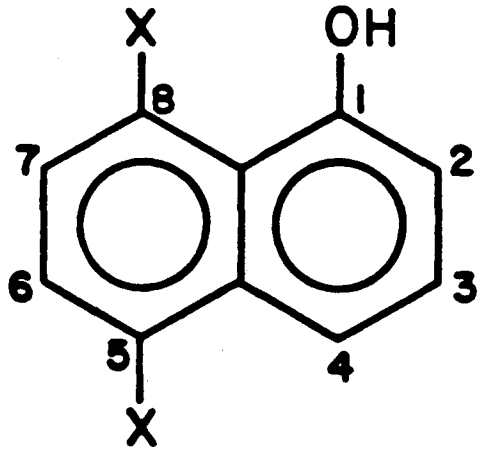

X = H : 1-Naphthol

X = D : 5,8-Dideutero-1-Naphthol

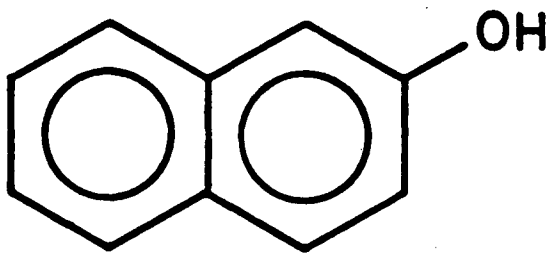

2-Naphthol

Fig. 1: The molecules investigated in these experiments: 1-naphthol, 5,8-dideutero-1-naphthol, and 2-naphthol.

mentally feasible to monitor the detailed kinetics on a very fast timescale. This information is not accessible with other methods[18-20]. Second, electronically excited species have a different electronic charge distribution than the ground state species. Thus the study of excited species probes electronic characteristics which affect the reaction mechanisms and rates.

ESPT dynamics have direct application to the study of other processes. In biological systems[21], the ESPT process is used to analyze protein structure. Since the proton transfer process is sensitive to solvent properties (e.g. polarity, basicity, or hydrogen bonding), the ESPT reaction can be used to probe the environment immediately surrounding an ESPT-active molecule. A moiety capable of ESPT is incorporated into a specific site of a protein. If the probe resides in a region where water is excluded (hydrophobic region), then the proton transfer rate will be reduced compared to a water-rich location (hydrophilic region). Therefore, the ESPT rate helps to determine the protein conformation. Further, the ESPT reaction has been suggested as a source for generating protons[8]. Since the absorption of light radically changes the acid properties of some molecules, ESPT can create local regions of high acid or base strength. This process is known as the laser pH jump technique. This proton source may be applied to the initiation of catalytic reactions. If very fast (picosecond) laser excitation is used, then ESPT becomes a "picosecond switch" for the initiation of some other chemical event. To best apply ESPT in such schemes, to these practical uses, an understanding of the fundamental kinetics of the ESPT process is required.

Investigations of ionization reactions by themodynamic measure-

ments yield results which shed light on relationships between structure, chemical reactivity, and solute/solvent interactions[22]. Since ionization reactions involve the solvent as well as the solute, these studies can be used as an effective probe of the "structure" of water and aqueous solutions[23-28]. Initial studies of ESPT reactions focussed mainly on the importance of solute structure and reactivity. Once the ESPT phenomenon was identified, the energetics of the process were easily determined spectroscopically. However, detailed analyses of the precise interplay between the solute and solvent demands more refined techniques.

The first observations of the ESPT event by Weber[29] in 1931 were met with some confusion. It was noticed that some aromatic acids, when excited, would emit light at highly Stokes-shifted (red-shifted) frequencies. Further, the Stokes-shift was dependent on the pH of the solution. In the late 1940's, Förster demonstrated that the emission arose from the electronically excited conjugate species, even though it was not directly excited[2]. An analogous scheme may be presented for proton abstraction from water by an excited base. The following general ESPT reaction scheme was proposed:

$$ROH + H_2O \overset{h\nu}{\longleftrightarrow} ROH^* + H_2O \longleftrightarrow RO^{-*} + H_3O^+ \overset{h\nu}{\longrightarrow} RO^- + H_3O^+ \qquad \text{(ESPT)}$$

An important feature of this scheme is the existence of an adiabatic proton transfer reaction occurring on the excited state surface. Examples of such events are relatively rare[30]. Weller studied the ESPT process in many organic acids and bases and extended the theories of Förster and his treatment of the process (the Förster cycle[2a], outlined below). Weller further developed the kinetic theory and performed analyses based on steady state methods, fluorescence titrations,

Förster Cycle Thermodynamic Model

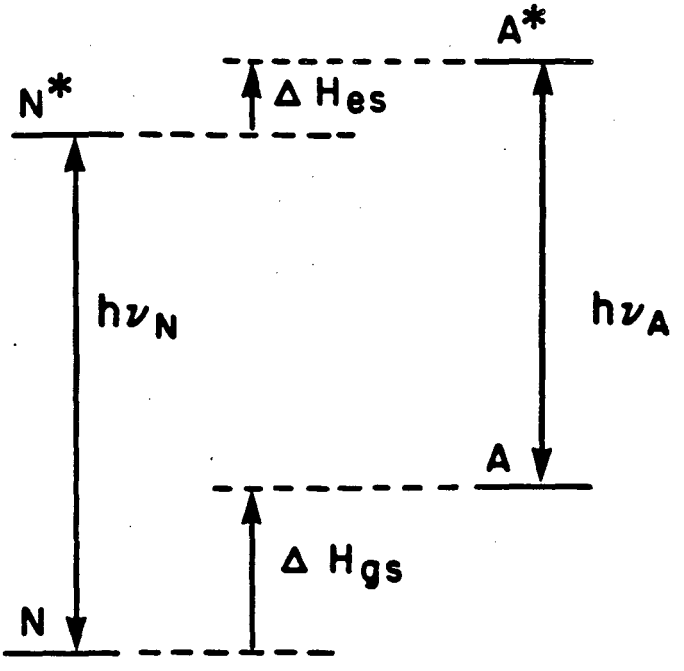

For the ESPT Reaction Process:

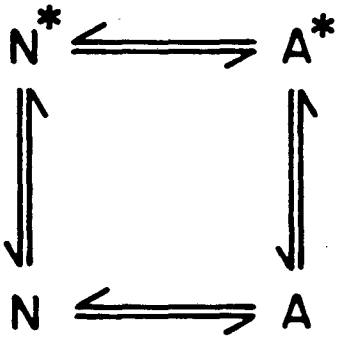

Fig. 2: The Förster Cycle thermodynamic model, as applicable to the 2-level ESPT process.

and time resolved measurements[3-5]. Since this early pioneering work, many reviews have appeared, citing numerous investigations into ESPT reactions[31-32].

The Förster cycle is a thermodynamic analysis of the ESPT process. This analysis provides a simple means to estimate the excited state pK_a (pK_a^*) based on a knowledge of the ground state acidity constant and spectroscopic measurements. The four-level scheme of the Förster cycle is shown in Fig. 2.

Two assumptions are involved in the application of the Förster cycle to ESPT reactions. The first assumption is that the 0,0 transition energy can be determined for both the protonated and deprotonated species. The 0,0 transition energy is the energy of the electronic transition between the lowest vibrational levels of the ground and excited states. These levels define the zero point energy for each state. Therefore, the 0,0 transition measures the thermodynamic enthalpy difference, ΔH, between the ground and excited states. The second assumption is that the entropy change, ΔS, for the ground state proton transfer reaction is identical to the ΔS for the excited state process. If ΔS is the same in both states, then the entropy terms cancel in the calculation of the free energy, ΔG. This simplification allows the measured enthalpy difference for the two reactions to be directly converted to the free energy difference. With these assumptions in mind, an energy cycle can be written as

$$N_o h\nu_N + \Delta H_{es} = N_o h\nu_A + \Delta H_{gs} \qquad (1)$$

where ν_N and ν_A are the 0,0 transitions between the ground and excited state for the neutral and anionic species, respectively. From basic thermodynamic considerations we have

$$\Delta G = \Delta H - T\Delta S = -2.3RT \log K_a \quad (2)$$

and

$$pK_a = \Delta H/2.3RT - \Delta S/2.3R \quad (3)$$

so that

$$\Delta pK_a = pK_a(\text{ground state}) - pK_a^*(\text{excited state})$$
$$= (\Delta H_{gs} - \Delta H_{es})/2.3RT \quad (4)$$

since $\Delta S_{gs} - \Delta S_{es}$ is assumed to be 0. Inserting Eq. 1 into Eq. 4 and rearranging gives the explicit expression for the excited state acid dissociation constant in terms of "known" quantities,

$$pK_a^* = pK_a + (N_o h/2.3RT)(\nu_A - \nu_N) \quad (5)$$

or

$$pK_a^* = pK_a + (2.1 \times 10^{-3})\Delta\bar{\nu} \quad (6)$$

where $\Delta\bar{\nu}$ is in wavenumbers and represents the difference in the 0,0 transition energies of the neutral and the anion, and T = 298 K. For ESPT reactions where the proton is transfered to the solvent, the emission from the conjugate base is generally red-shifted. For these cases the energy gap between A and A^* is less than that between N and N^* (see Fig. 2). The excited state pK_a^* is therefore smaller than the ground state pK_a and N^* is thus a stronger acid than N. Since the Förster cycle is easy to apply and requires relatively simple experiments, many systems have been analyzed by this technique. Changes in pK_a of six to seven pK_a units upon electronic excitation are commonly predicted [31]. Although the Förster cycle has been employed extensively, the assumptions necessary for this simple treatment of ESPT reactions can lead to inaccurate assessments of the pK_a^*. The determination of 0,0 transition energies is not always straightforward. Absorption and emission spectra do not provide this information directly. The

vibrational progressions apparent in gas phase spectra typically are not present in solution phase spectra. In solution, solvent interactions broaden transitions, causing spectra that are diffuse and structureless. The energies of the absorption and emission maxima are often averaged to obtain the 0,0 transition energy, but this technique is not accurate for all systems. Indeed, only when the system consists of two electronic states with no higher, interacting excited states, and only when these states are equally influenced by solvent interactions will this approximation be valid. In such cases, the absorption and emission spectra are mirror images of each other. This averaging technique fails for cases where multiple excited states or solvent reorganization is reflected in disparate absorption and emission spectra[33]. In assessing the accuracy of the pK_a^* derived from the Förster cycle method, it is important to realize that a four nanometer error in the determination of the 0,0 transition energy will result in an error of one pK unit in pK_a^*.

The assumption that the two ΔS's of the ground and excited state reactions will have the same sign is reasonable. In both reactions an uncharged species, N (or N^*) forms two charged species, H^+ and A (or A^*). The magnitude of the entropy change, however, would be expected to be unequal for the ground and excited states. The different electronic structures should lead to solvent organizations that will be substantially different around the ground state and excited state species. The quantitative effect of this assumption is difficult to assess and will certainly vary from system to system.

A more informative analysis of excited state proton transfer would be obtained from direct, time resolved measurements. The same

thermodynamic pK_a^* can be determined from the ratio of the forward and reverse ESPT reaction rates. In addition, more information is obtained because the two rate constants are uniquely determined. The effects of solute structure or solvent interactions may be explored in relation to the forward and reverse rates. Also, no assumptions are made about entropy effects, and studies of the ESPT rate constants as a function of temperature can yield the entropy change for the ESPT reaction.

In order to obtain a complete kinetic analysis of ESPT reactions the technique of fluorescence titration is coupled with lifetime measurements[28,31]. Fluorescence titration is a steady state method developed extensively by Weller[3]. Steady state means that the system is continuously excited into a quasi-stationary state or dynamic equilibrium. The fluorescence is collected over time to give the relative quantum yields for the two excited state species. The technique is called fluorescence titration since measurements of the relative fluorescence yields are determined as a function of the pH. Under favorable conditions and with the proper fluorescence lifetimes, the desired forward and reverse rate constants are found. The details and the exact form of this analysis are presented in Chapter three.

B. ESPT in 1-Naphthol

The 1- and 2-naphthol isomers, Fig. 1, make an ideal comparative system. The 2-naphthol molecule has been extensively studied and provides the model system for the description of the fluorescence titration technique[31]. For 2-naphthol, a Förster cycle calculation gives an excited state pK_a of about 2.8, matching the value determined from both fluorescence titration[15] and by complete time dependent[14]

analyses. In fact, all excited state pK_a measurements for 2-naphthol reported in the literature fall within ~0.5 pK units[31] of each other. The exact reaction scheme for the 2-naphthol system has been presented in various forms[15]. Nonetheless, the pK_a^* shows little deviation. The reason for this agreement is twofold. First, the system does not deviate from the proper four state model shown in Fig. 2. As a well-behaved system, 2-naphthol is relatively unaffected by solvent interaction. Intense emission is observed from both of the excited species. Second, the lifetimes and formation times for the excited state species can be measured with nanosecond techniques.

ESPT in 1-naphthol would be expected to be similar to 2-naphthol based on the similarity of the two structures. Many experiemnts have been performed on 1-naphthol[6, 7,33,35]. As in 2-naphthol, the emission from the excited conjugate base (the 1-naphtholate ion, hereafter termed the anion) is intense. The intensity of the signal stems from an equally long lifetime and efficient ESPT process as in 2-naphthol. All of these previous studies suffer from a serious problem, however. The emission from excited 1-naphthol (hereafter termed the neutral) is either absent or extremely weak in aqueous solution[4,16]. Many explanations have been proposed for this lack of signal including: proton quenching[13,16], solvent quenching[32,35,43], electronic/structural features[7,38,39], excited state level crossing[33,38,40-42], and remote quenching (quenching by protons at the aromatic ring)[36-38]. Previous to this study, no accurate kinetic measurement of neutral had been made. Without this information, many of the above explanations are purely speculative.

This work investigates the "peculiar" nature of 1-naphthol. The

focus of the work is the resolution of the anomalous kinetic behavior of 1-naphthol by the application of time resolved detection and steady state emission techniques. Both time resolved and steady state measurements with sufficient sensitivity to detect accurately the presence of the neutral have been made. Temporal and quantum yield measurements have been performed as a function of solution pH to better understand the relative importance of the various kinetic processes in the ESPT reaction. The nature of the analysis is outlined in Chapter three. Also, studies have been performed to elucidate isotope effects and solvent interactions. These experiments include: the effects of 5,8 di-deuteration of the aromatic ring[37a], the full kinetic study in D_2O, the use of mixed solvents (ethanol or acetonitrile with water), the changes due to added inorganic salts, and the study of the ESPT reactions at high pressure.

The ring deuteration study probes the possibility of diabatic quenching of the aromatic nucleus, as suggested by Weller[36]. From molecular orbital charge density calculations, NMR studies, and photochemical methods, the 5,8 positions are known to be photolabile[37b]. The question, then, becomes: does proton attack at these positions provide an additional, non-radiative decay channel to the ground state? Such a decay route is not manifest in 2-naphthol[38]. A secondary isotope effect in the diabatic quenching rate would support this mechanism.

The other investigations address the role of the solvent in the ESPT reaction. Deuteration of the solvent affects any hydrogen (or deuterium) bonding, especially in relation to proton abstration[44]. Solvent quenching will also be different in D_2O. The mixed solvents

and salts cause restructuring of the solvent, in this case the water, network. Thus, the overall entropy, caging, hydrogen-bonding, and water quenching will be altered[45,46]. Finally, pressure modifies the water structure without changing the solvent or introducing additional solutes[26,47]. The results of these experiments and a discussion of their implications are presented in Chapter four.

In all of these studies, the small quantum yield of the neutral suggests exceedingly short lifetimes. The picosecond time resolved emission apparatus used in these studies is capable of measuring weak signals on short timescales. Chapter two describes the details of the picosecond apparatus and experimental techniques employed in this study. The results in Chapter four demonstrate the necessity of using picosecond techniques for analyzing the ultrafast ESPT reactions in 1-naphthol.

Chapter Two

Experimental Apparatus and Techniques

A. Introduction

Advanced techniques are often required to understand basic chemical phenomena. Chemical events in solution typically occur on the timescale of molecular collisions.[19,20] Picosecond laser techniques expand our knowledge of chemical dynamics by probing these fundamental events.[18] Since the laser and detection apparatus are such an important tool, this chapter is devoted to the description of the picosecond laser apparatus and the experimental techniques used in this work.

The basic goal in the investigation of an ultrafast process is the direct observation of chemical the event. Laser light is a useful tool to monitor these fast molecular reactions. Tunable laser light often allows specific events to be singled out. A second requirement for direct observation is measurement on the timescale of the event. The picosecond laser system in our laboratory meets these requirements.

Traditionally, kineticists have depended on the interactions of two competing reactions. Kinetic information was achieved by comparison of the product distributions between a reaction with a known rate and the unknown reaction. Later, reaction rates began to be measured, not only by competing chemical processes, but also by direct spectroscopic techniques. Kinetic information has also been derived via Fourier transform of the spectral linewidth. These measurements required high spectral sensitivity. Also, inaccuracies occur due to the difficulty in sorting out the contributions of the homogeneous and inhomogeneous components of the linewidth.

The theory and the goals of time resolved laser spectroscopy are the same as these earlier techniques. By using the absorption of light, a process which occurs on a timescale of 10^{-15} seconds, to initiate a chemical process, it is possible to directly measure the time evolution of the subsequent chemistry. It is important that the initially excited species or state be formed in a time short compared to the rate process of interest.

Two extremes in the preparation of an excited state can be considered: continuous wave excitation (CW) or delta-function pulsed excitation. CW excitation refers to the continuous input, or pumping, of light energy into a system. The result is a dynamic equilibrium between the laser light and the evolving state. Only by transforming the spectral response can any temporal information be obtained. The sample is constantly absorbing and emitting photons such that the resulting spectrum measures a complex average of many processes. Conversely, delta-function pulses are light pulses which are infinitely short in time. These pulses produce an excited, reactive state in a single instant in time. The state evolves and emits in time as a function only of chemical and physical processes. For a state that emits, the emission intensity is directly related to the population in the excited state. Therefore, its kinetics can be measured. With such initiation methods, direct measurements can be made without complications due to continuous perturbations by the excitation field. In reality such infintely short pulses are not achievable. Instead, pulses of finite width are used. This condition forces a limitation on the rates of processes that may be studied to those reactions that occur on a timescale that is long compared to the pulse width. As pulses become "short"

relative to the reaction time, they approximate the delta-function excitation process. Data obtained from "long" pulse excitation require a mathematical treatment to remove the pulse response. The optimum situation requires the use of the shortest possible light pulses as the excitation source. Unfortunately, shorter pulses result in smaller numbers of photons for a given power density. A threshold exists which limits the maximum useable power density either to the damage threshold of the material in the experiment or to a level where the onset of any undesired, non-linear optical effects occur. Therefore, weak signals are almost an inevitable problem in ultrafast spectroscopy.

In addition to a fast excitation source, direct measurements of ultrafast emission processes require a detection system that can measure the time-evolving emission of the state on an appropriately short timescale. A detector must be able to analyze very rapidly rising or falling emission intensities. The ability to produce a state in an exceedingly short time is useless if the rates of the resulting reaction cannot be measured. The detector must also be sufficiently sensitive to measure the low signal levels inherent in ultrafast experiments.

Ultimately, the energy resolution achieveable with short laser pulses is limited by the Heisenberg uncertainty principle. Simply put, the uncertainty principle requires that the product of the temporal duration and the spectral range be a constant. Therefore, as pulses become shorter in time they become less certain, or broader, spectrally. In a laser cavity there is a limited gain bandwidth or allowable spectral width that can be supported. Pulse durations from any laser cavity cannot be shorter than the inverse bandwidth of that cavity. Very short (15 fs, fs = 10^{-15} seconds) pulses have been generated by the

interaction of short laser pulses with fiber optic pulse compressors that allow for further spectral broadening and therefore shorter pulses. Of course, some of the utility of the laser pulses may be diminished by the spectral broadening.

Similarly, detectors have their own limitations. The two important processes in many laser spectroscopy experiments are emission and absorption. In emission, the emitted light intensity is proportional to the population of excited species. Time resolved emission monitors how the population of the state decays in time. Ultimately, these photon signals are converted into electrical responses by some sort of photodetector, typically either a photomultiplier, or a photodiode. This conversion from photons to electrons is generally very fast (less than a few ps) except in the photomultiplier. Photomultipliers are multi-element devices whose response is a function of the geometry of the elements and the electron-accelerating voltages. Typically, the response times of photomultipliers are many hundreds of picoseconds. Presently, the major limitation in most of these devices is the speed at which the electrons travel in the circuit, and the timing jitter of the electronic components. A single foot of electrical cable with one ohm internal resistance and twelve picofarads of capacitance will convert a delta function electronic signal into a twelve ps response. Similar broadening occurs in all circuits. The timing jitter of an electrical signal is important in applications where chemical changes are mirrored in electronic signals which are measured relative to each other in time. This type of jitter results in variations in measurements and broadening of signals of at least tens of picoseconds. Some techniques minimize the inaccuracies due to jitter and broadening by

determining the average total response including jitter. A mathematical means of removing this broadened response is performed in a manner similar to that for broad laser input pulses. In fact, it is generally the total response function of both the laser and the detection system, in the absence of any chemical or physical event, that is measured. This response function is removed from the actual data by mathematical means (deconvolution). At best, rate processes which are no faster than one tenth the time of this response signal can be accurately determined.

This chapter will detail the active/passive, modelocked Nd:YAG laser and the streak camera detection system developed and operated in our laboratory[52]. Illustrative comparisons to the widely used "sync-pump" dye laser with single photon counting detection will help point out the features sought in both the laser and the detection system[48-51]. Many examples of other experiments carried out on this system will further demonstrate its utility in the study of a variety of primary, chemical events. Standard steady state measurements that are important to a more complete picture are described. The sample preparation techniques used in this work are also described in this chapter.

B. Experimental Apparatus

1. Picosecond Laser System

The laser (Quantel YG400) used in these experiments utilizes a solid-state, Neodymium-doped, Yttrium/Aluminum/Garnet (Nd:YAG) crystal as the gain medium. The active element, Nd^{+3}, emits at its fundamental wavelength of 1064 nm. An important feature of this laser is the ability to generate high-powered, short-duration (20-25 ps) pulses. These

pulses occur due to the "modelocking" process which results from the design detailed below. The uniformity and stability of the pulses are functions of the laser cavity elements and alignment.

The laser cavity (see Fig. 3) consists of the laser head, active and passive modelockers, apertures, and optics. Lasing occurs when a larger fraction of excited Nd^{+3} atoms exist relative to the non-excited species (population inversion). This population inversion is driven by the absorption of light from two, three-inch-long Xenon flashlamps pulsed at 10 Hz by a high-voltage, pulse-forming network at 1.1 kV. Relaxation is sufficiently rapid that separate lasing events occur on each firing of the lamps. For stable operation it is important to maintain a constant temperature in the laser head. This temperture control is accomplished by flowing cooling water (28°C, Neslab recirculator) around the lamps. The optical arrangement produces a stable cavity configuration for the generation of the laser light. The optical components are: a rear reflector (99+% reflecting, +75 cm radius of curvature); an intracavity dispersing lens (f= -30 cm) that acts in conjunction with the curved rear mirror as a compensator for any thermal lensing in the laser rod; and an output mirror (70% transmitting at 1064 nm) to couple out a fraction of the intracavity light without causing too much loss in the laser. All the optics are high quality and appropriately coated (CVI Corp.).

The 0.07" ceramic apertures are placed approximately at beam waists of comparable diameter in the cavity. These apertures limit the possible spatial modes, or transverse electronic modes (TEM), to TEM_{00}. TEM_{00} has no spatial nodes in the beam cross-section. A TEM_{00} beam approximates a Gaussian intensity profile normal to the laser

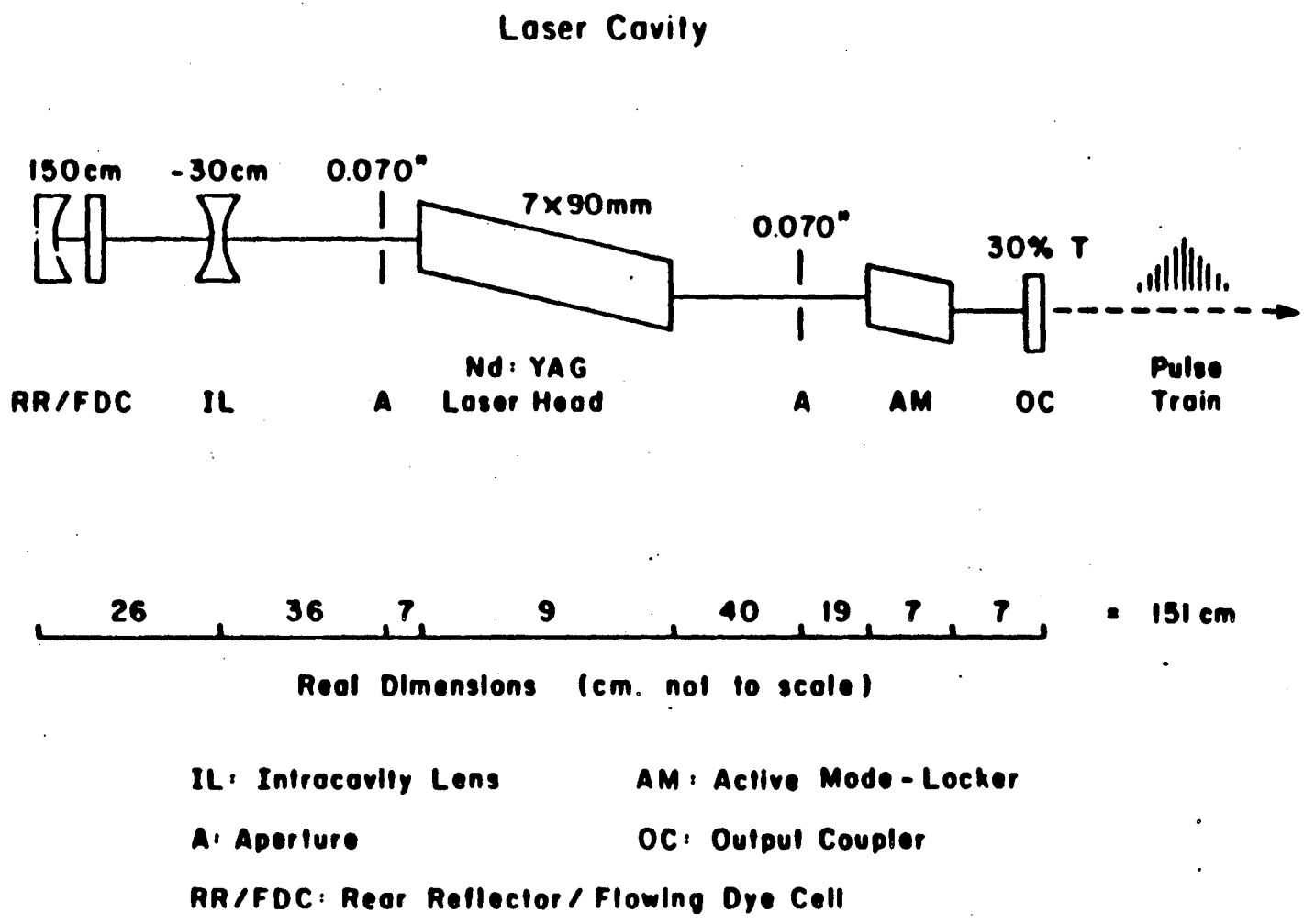

Fig. 3: Diagramatic representation of the laser cavity. The elements are not shown to scale but the actual dimensions are given below the drawing.

propagation direction. This mode has the best characteristics for interactions with other elements. There are no "hot spots" as the intensity is well distributed and homogeneous.

The actual generation of short duration pulses is a result of the interaction of the laser light with the modelockers. The passive modelocker is responsible for most of the pulse shortening and part of the pulse formation. Specifically, this modelocker consists of a short-pathlength (100 μ), flowing dye cell that is in contact with the rear reflector to minimize losses from optical surfaces. The dye (Kodak Q-switch dye #9740) is dissolved in 1,2-dichloroethane and acts as a Q-switch and saturable absorber in the modelocking process. Initially, the dye cell passes only a single photon-packet that has sufficient intensity to bleach the dye. The generation of such pulses is a random process that occurs in the laser head during excitation. This single pulse repasses through the laser medium, increasing in intensity by stimulated emission. This one pulse is further shortened in each subsequent pass through the dye. The dye is then acting as a saturable absorber. Intensity is removed from the "wings" of the pulse, thus shortening the temporal duration. The active modelocker (Intra Action #ML-505-Q) operates mainly to form and stabilize the pulse. It allows only for the propagation of a pulse or wave packet that is in phase with the acoustic wave in the crystal. Simply, a radio-frequency (RF) transducer establishes a standing wave in a quartz crystal. Five watts of 45.870 MHz RF are absorbed by the crystal. This absorption induces an acoustic wave in the crystal which generates a time dependent index of refraction. The index change deflects (by diffraction) any laser light which is out of phase and passes the in-

phase light. Therefore, only this single mode is allowed to propagate through the cavity. This selectivity results in considerably enhanced intensity stability by reducing the propagation of "noise" pulses. This device must also be carefully aligned, temperature-controlled, frequency selected, and cavity-matched. Only certain standing waves can be established in a crystal, given by the crystal length and temperature and is determined by maximizing the absorption of the RF signal. Cavity-matching means that the length of the cavity (and therefore the transit time of a photon) is such that the frequency of the appearance of the photon at the crystal matches the frequency of the standing wave in the crystal. The cavity matching equation is given as

$$2F = c/(2L)$$

where F is the RF (Hz), c is the speed of light in air (3.0×10^{10} cm/sec), and L is the cavity length (cm). For the frequency used here a cavity length of approximately 1.6 meters is optimum.

The output of the laser (Fig. 4) is a train of pulses. Each pulse in the train represents one round trip passage of a single pulse. The separation of the pulses is given by the cavity round trip time (2L/c). The round trip time for this cavity is 10.9 nanoseconds (ns). The intensity of the pulses is a complex function of the laser parameters, but, in general, follows the intensity profile of the exciting lamps. Under optimum conditions, identical pulse trains would result for every firing of the lamps.

For the experiments described here, only a single pulse is selected from the train. The next task is the amplification and propagation of this single pulse to the sample and detector, Fig. 5.

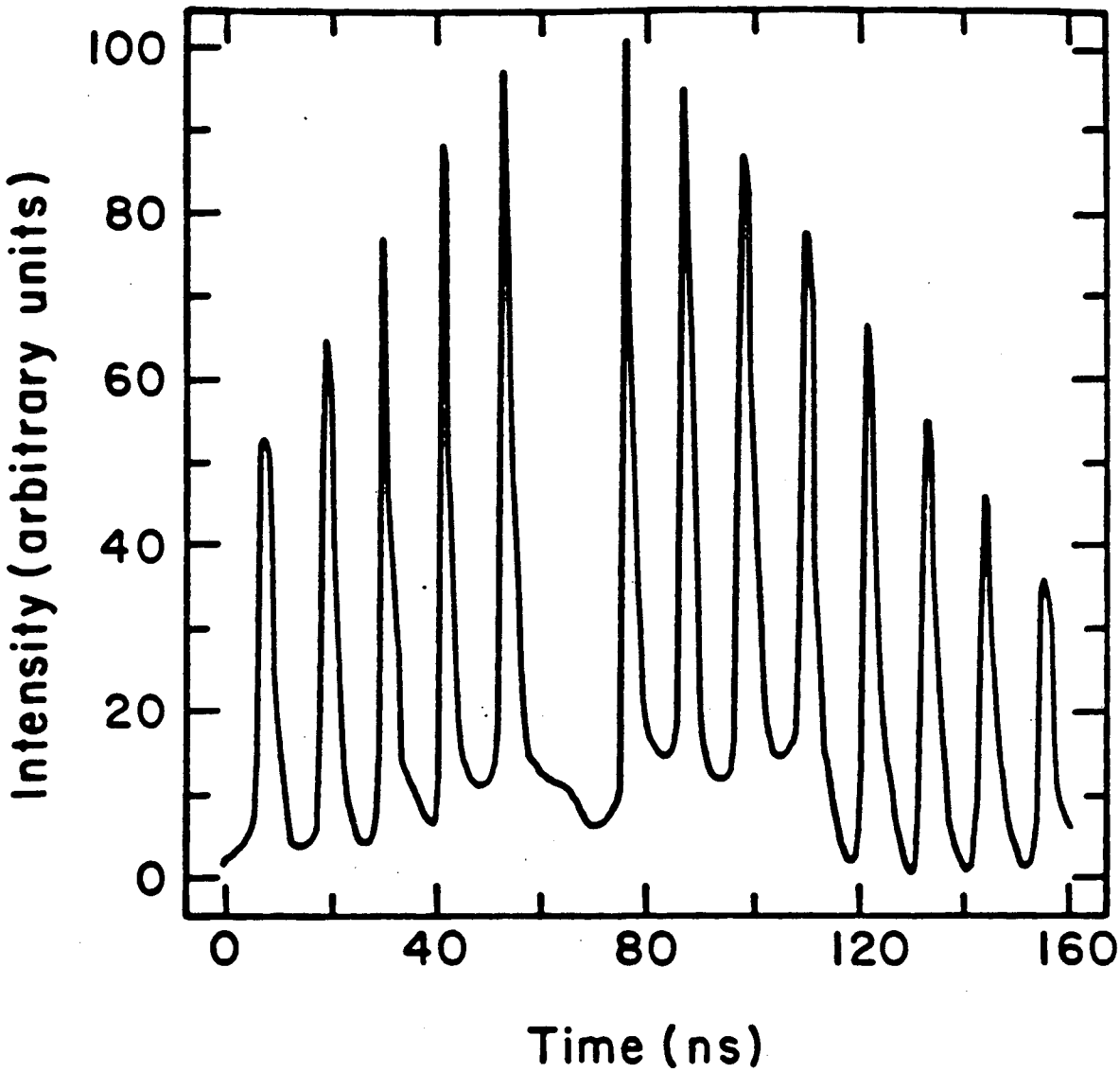

Fig. 4: Typical output from a modelocked, Nd:YAG laser showing the train of picosecond pulses (about 20 to 25 ps in duration). The figure depicts the unused pulses after single pulse extraction (removed in this case from the center of the train). Note the time scale in nanoseconds, with pulses appearing at the round-trip time of the laser cavity of about 10 ns.

Fig. 5: Diagramatic representation of the time resolved emission apparatus. SHG - Second harmonic generator (KDP crystal); DM - Dichroic mirror; FHG - Fourth harmonic generator (KDP crystal); BS - Beam splitter; F - Filter; GT - Glan Thompson polarizing prism; L - Lens.

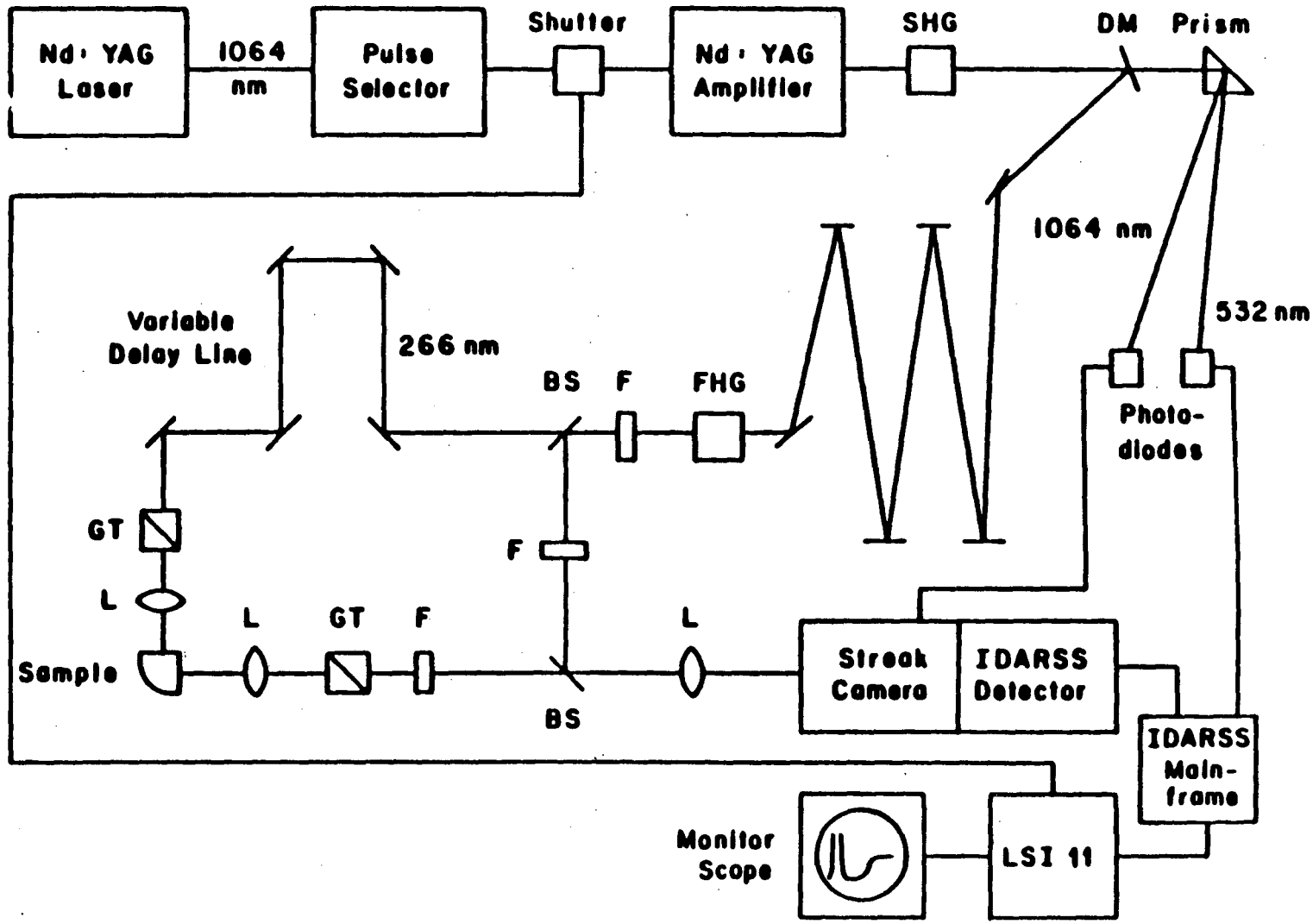
Nd: YAG Laser
1064 nm
Pulse Selector
Shutter
Nd: YAG Amplifier
SHG
DM
Prism
1064 nm
532 nm
Photo-diodes
Variable Delay Line
266 nm
BS
F
FHG
GT
L
Sample
L
GT
F
F
BS
L
Streak Camera
IDARSS Detector
IDARSS Main-frame
Monitor Scope
LSI 11

Fig. 5

Single pulse extraction is accomplished by a Pockels cell (Quantel, PF 302). A Pockels cell works using the optical properties of KDP (potassium dihydrogen phosphate). An applied potential across a crystal of KDP causes it to act as a waveplate (by electronically-induced birefringence) to rotate the polarization of light passing through it during the applied electronic signal (the Pockels effect). Since the output pulses of the laser are horizontally polarized, the Pockels effect can be used to selectively rotate the polarization of a single pulse from the train of pulses. A voltage ramp on the crystal during the passage of a single pulse results in that pulse being rotated to vertical polarization. Once a single pulse is perpendicularly polarized relative to the other pulses, it is a simple matter for a Glan polarizer to pass specifically that pulse. The triggering of the voltage ramp is initiated by a previous pulse from the train. At the beginning of an experiment, the sensitivity of the trigger is adjusted to select a pulse from either the center of the train or late in the train, depending on the application. The most intense pulses are found in the center of the train, while shorter pulses can be selected later in the train.

The single pulse is expanded 1.75 times through a collimating telescope and amplified in a second laser head. Amplification is achieved by stimulated gain in a Nd:YAG rod which is pumped by 4" flashlamps at between 1.5 and 1.8 kV. The gain is between 10 and 30 times for this voltage range, producing single pulse energies of 3-6 mJ.

Depending on the application, harmonics of the fundamental at 532 nm or 355 nm are generated after the amplifier. These new wavelengths are formed by non-linear optical mixing in angle-tuned, type II, KDP

crystals. In this manner two photons of 1064 nm are added to make the 532 nm light (frequency doubling). Similarly, a 532 nm photon can be summed with a 1064 nm photon to form the third harmonic at 355 nm (frequency summing). The residual IR and a fraction of the green (532 nm) beam are used to activate photodiode triggers (H.P. #5082-4220) for the streak camera and the readout array of the detector, respectively. These two beams, originally collinear through the crystals, are separated by a dispersing, Pellin-Broca prism. The IR beam is further shortened and temporally filtered (by removing any satellite pulses) to ensure a sharp leading edge for triggering.

The desired color, either green or UV (355 nm), is propagated along a fixed optical delay to allow time for the triggers to activate the detectors. The last leg of the delay line contains a reducing telescope (2X) and, when desired, additional non-linear crystals. A type I KDP doubler for the generation of the fourth harmonic (266 nm) can be placed in the green line as is the case for this study of 1-naphthol. In other studies, a pair of KDP crystals are put in the 355 nm beam to function as an optical parametric source (OPS). The OPS forms tunable light in the visible (450 - 640 nm) and IR (760 - 1640 nm) by the decomposition of a 355 nm photon[57]. The chosen frequency is split into a major and minor fraction. The minor fraction is used as a marker pulse (see below). This pulse is suitably attenuated, diffused, and focussed onto the slit of the streak camera. The major fraction is appropriately delayed with respect to the marker pulse, and sent through a Glan polarizer, to ensure vertical polarization. The pulse is cylindrically focussed onto the front edge of a magnetically-stirred, 1 cm square cuvette containing the sample solution.

For the fluorescence experiments used in this study, the first 1 mm of the sample fluorescence is collected with a lens (at f2) at right angles to the excitation beam. The fluorescence is passed through a second Glan polarizer (24x24 mm in size, but apertured to allow through only a 20 mm dia. beam) which is mounted in a rotary stage for setting the detection polarization. The signal is filtered using 10 nm band-pass interference filters, recombined with the minor fraction, and focussed onto the slit of the streak camera via a 1:1 imaging telescope.

2. Streak Camera System

A streak camera is an ultrafast, optical-signal measuring device which determines photon intensity as a function of time. The active element in the camera is a photocathode which converts a photon beam into an electron current. This current is an exact analog of the photon emission from the sample as it evolves in time. The electron beam is dispersed horizontally by a deflecting voltage ramp at a fixed and measurable rate. The temporally spread beam strikes a phosphor screen that converts the electrons back into photons. It is this "streak image" that is analyzed. The streak image provides a direct measurement of the light intensity from the sample in time. Throughout the process of photon-electron-photon conversion, care must be taken that saturation of the signal does not occur. Saturation manifests itself in two ways in the camera. First, the normal problem of saturation is the loss of a linear correlation between the signal in and the signal out. This non-linearity causes a distortion in the data which is difficult to distinguish from a real response. The second problem is more subtle. As more electrons are formed at the photocathode per

short time interval, the electrons will spread out due to space-charge repulsion. This spatial spread appears as a broadening of the signal in time. To avoid these problems, operation at low input intensity is preferable. The outcome is a reduced signal-to-noise ratio. It is therefore necessary to average many shots. Repetitive operation has been a prime goal in the development of the system. The details of the operation of the streak camera used in the present system are described below.

The streak camera is a Hadland Photonics Imacon 500. This camera has a quoted temporal resolution of 2 picoseconds. In this work the camera was operated at the firing rate of the laser (10 Hz). The workings of the detection system are described as follows. The electrons at the photocathode are swept in time as determined by a timebase switch on the camera which ranges from 0.02 to 34 ns/mm across the phosphor. The electron signal is intensified using microchannel plates by a factor of up to 1000 times prior to its striking on the final phosphor screen. The streak image is lens relayed to an intensified, 1024 channel, photodiode array (Tracor-Northern, IDARSS) and the information from the array is stored in a microprocessor-controlled mainframe (Tracor-Northern 1710). The 1:1 coupling of the entire streak camera phosphor to the array yields a maximum time window for a given streak speed. The disadvantage of maximizing the time window is distortion effects that occur at the edges of the detector due to the non-uniform deflection of the photoelectron beam (pin cushion distortion). These distortions require correction.

The array mainframe, like the camera, is triggered by the laser pulse. The operation of the mainframe is controlled by a DEC LSI 11/73

minicomputer. Sets of seven scans, where each scan is a single laser shot consisting of the marker pulse and fluorescence decay signal, are accumulated in the mainframe and then transfered sequentially to the computer. The computer controls the laser pulse rate by opening and closing a shutter situated before the pulse selector. The pulses are accepted at the maximum processing capability of the computer. Effective data collection rates of nearly 3 Hz are presently obtained. In this manner, the accumulation of at least 500 shots, with all the corrections explained below, is routine.

C. Analyses, Calibrations, and Corrections

The specific operation of the computer and the photodiode array signal detector is as follows. A short program is run on the detector mainframe which acquires and saves an averaged, negative, dark trace into 1/8 of the memory buffer. This spectrum serves as a correction for dark counts in each of the data scans. By transfering the negative of the dark trace to the seven areas for each scan (1024 channels per area) a dataset is automatically background-corrected when the signal is summed into its memory spot. Once the dark spectra are in place, the array is enabled and ready to accumulate the seven laser shots (or scans for the fluorescence in time). Each scan is made up of five "reads" of the 1024 channels of the diode array. The array is read five times in order to accurately integrate the signal from the phosphor screen.

The LSI 11/73 program analyzes each laser shot based on user-supplied parameters. The information to be supplied includes: a correction dataset (see below), the time window (or range) for the marker

pulse, the acceptable minimum height of the marker pulse, and the position of a time window where no signal is to be found (a null region). The marker pulse (pre-pulse) sets limits on the electronic jitter which occurs on a shot-to-shot basis. An acceptable scan is one in which the marker pulse and the fluorescence signal are roughly centered on the array. Time jitter sometimes causes either the prepulse or the fluorescnece to partially miss the detector. Generally, at least 750 channels are maintained for the signal. The limit on the acceptable height of the prepulse determines whether a laser shot of sufficient energy was registered. Variation in laser power per shot causes some pulses to be too weak to generate a useable amount of signal from the sample. This restriction also eliminates the possibility of a noise "spike" being counted as a prepulse. Establishing a null signal area has two functions. First, since no signal should exist in this region, a pulse appearing there often signifies an unwanted satellite pulse which may distort the fluorescence signal. Second, the jitter of a particular scan may cause the emission signal to fall in the prepulse window. If the signal is sufficiently intense, it can be confused as a prepulse. This condition would result in signal in the null area and the scan is rejected. Since only the prepulse establishes both acceptability and the time reference for signal averaging, small signals that are correlated to this pulse can be correctly accumulated.

The acquisitions are started once the parameters for the experiment are set and the number of scans are entered. The computer sends a signal to open the shutter. A 16 bit, addressable ADAC 1664 ATTL board generates this control signal. After the seventh data scan has been taken the computer closes the shutter and begins the transfer of

the data from the array mainframe to the computer. The data is tested, corrected, and summed. The summed output is displayed on a monitor scope via a DT 2771 D/A point plotter with Direct Memory Access. The cycle reinitiates with the signal that opens the shutter.

Due to the timing jitter, each dataset must be shifted so as to be referenced to the same "time-zero" point. The center of the marker pulse serves as this reference point. However, the response of the detector system is not uniform from channel to channel in either time or intensity. Therefore, the corrections explained below must be applied to each unshifted dataset, and not simply to the final, composite data.

Temporal calibration of the detection apparatus requires some standard with a known time response. The calibration technique must cover time ranges from 300 picoseconds to thirty nanoseconds (i.e. the time windows of the fastest and slowest streak speeds, respectively). Calibrations are performed using etalons. Etalon traces are the signals produced when a single pulse is reflected between the surface of two, opposed, partially-reflecting mirrors. Similar to the laser cavity which produces a train of pulses separated by the round trip time, these mirrors also function to create a series of pulses separated by the time it takes the input pulse to traverse the mirrors. Each peak is the fraction of the pulse which is transmitted through the final mirror. Specifically, a pulse enters the air-gapped, pair of mirrors and some fraction of the pulse passes through both mirrors. The major fraction of the light, however, reflects internally between the two mirrors. At each mirror on each pass another fraction of the light is transmitted. Therefore, the signal from an etalon is a series

of peaks separated in time by a known amount (2L/c) with an exponentially decaying intensity as a function of the mirrors' reflectivity. By setting and measuring the air-gap between the mirrors and then recording the signal produced at the detector, the time per array element is calculated. This procedure can be performed at each streak speed of the camera.

Two considerations must be followed regarding the construction of the etalon. First, the mirror surfaces must be absolutely flat and arranged perfectly parallel to each other. In practice these conditions cannot be met and the result is that the beam will eventually "walk-off" itself, especially as the air-gap is increased. This walk-off determines how many peaks may be focussed onto the slit of the streak camera. Second, the total reflectivity should be high (at least 80% reflecting) to maximize the number of etalon pulses of measurable intensity. Too small a reflectivity will result in too large an exponential decay of the peak-to-peak intensity. Too high a reflectivity means that little light will escape per pass of the mirrors and the whole etalon trace will be of low intensity.

In the analysis of the raw etalon traces, several critical observations are made. From the physics governing the etalon formation, etalon peaks with a constant spacing and an exponential decay of intensity are expected. Instead, peaks are found which vary in separation and decays are observed which are neither exponential nor exactly alike in successive acquisitions. These observations demonstrate both the non-uniform temporal and intensity responses of the detector system. These inconsistancies, due to shot-to-shot fluctuations, are eliminated after averaging even a few scans. However,

the need for the time and intensity corrections remain.

The rationale for the construction of the correction set goes as follows. First, a temporal uniformity must be established across the entire time window. Once the timing is correct, then the intensity can be normalized to give an equal response for an equal number of photons/ unit time/channel. This combined time/intensity correction scheme is applied to each dataset prior to signal averaging. Only by making the corrections can experimental fluorescence decays be accurately obtained.

The time base correction is generated from the analysis of several etalon traces at each streak speed. A plot is made of etalon separation versus the mean channel position for that separation. Figure 6a shows such a plot for the fastest streak speed. No net time can be created or destroyed by the correction function. Therefore, the correction redistributes the same total time (average time/channel times the number of channels) of the raw uncorrected data into a more uniform arrangement. This redistribution is done, essentially, by rearranging the intensity/channel by borrowing from or donating to adjacent channels. For example, an uncorrected channel may represent a larger-than-average amount of time. This channel would have a correspondingly larger signal intensity for a given input than an average channel. Therefore, by removing some fraction of the intensity and donating it to some channel with a smaller-than-average time window, the amount of time/channel will become equivalent across the array. A channel contains more than the average amount of time if it has a smaller than average etalon spacing (points below the line in Fig. 7). The effectiveness of this correction can be seen in Fig. 6b. Here, the same set of etalon traces were summed, one with correction (Fig. 6b)

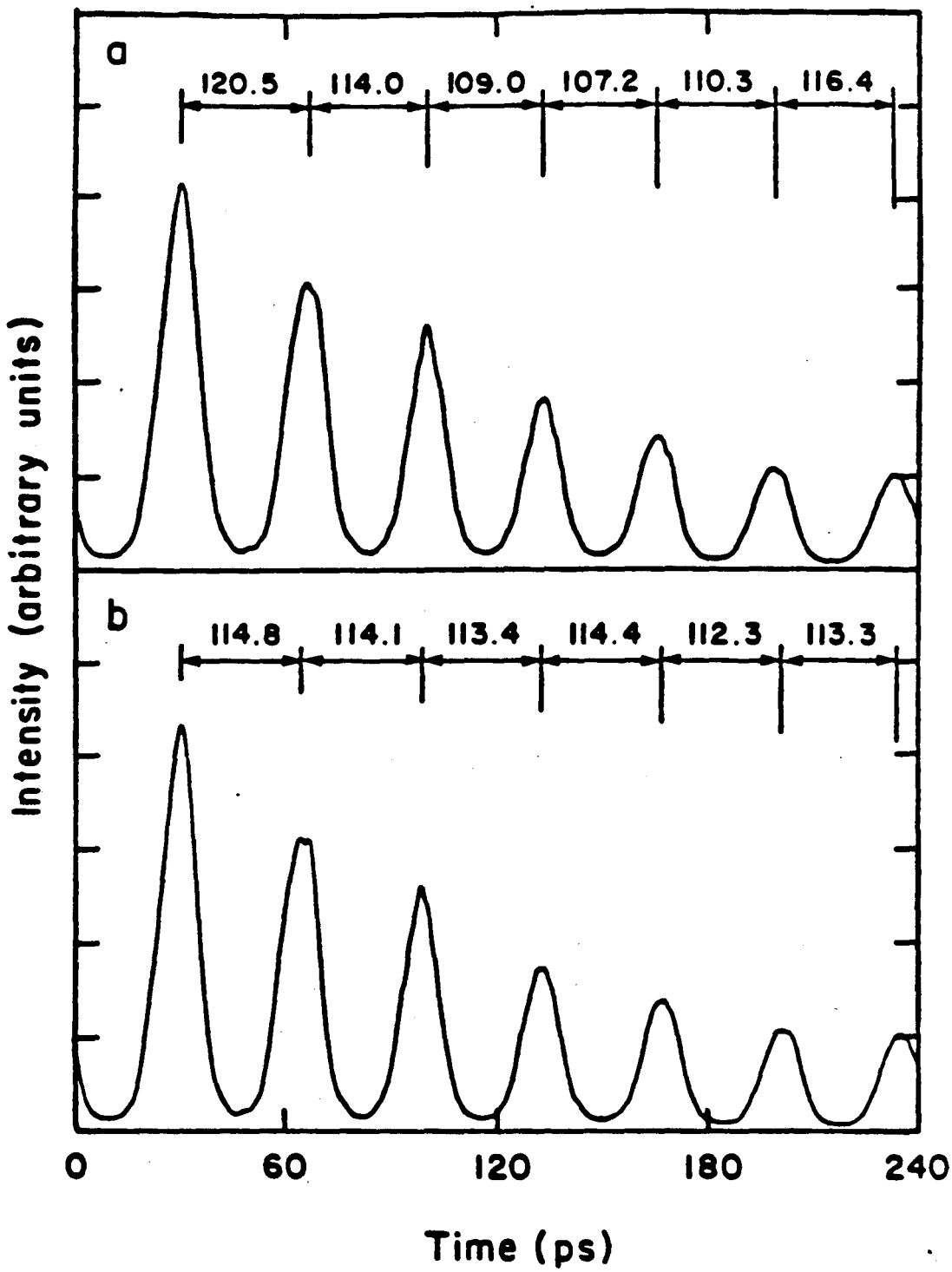

Fig. 6: Etalons generated for temporal calibration of the streak camera. The upper trace, a, presents the directly measured series of reflected, single pulses formed by multiple reflections between two mirrors. The lower trace, b, gives the corrected version of the same series of etalons. Spacing between the pulses are: a) 113 ± 5 channels and b) 114 ± 1 channel, yielding (for the known mirror spacing) 0.31 ps/channel.

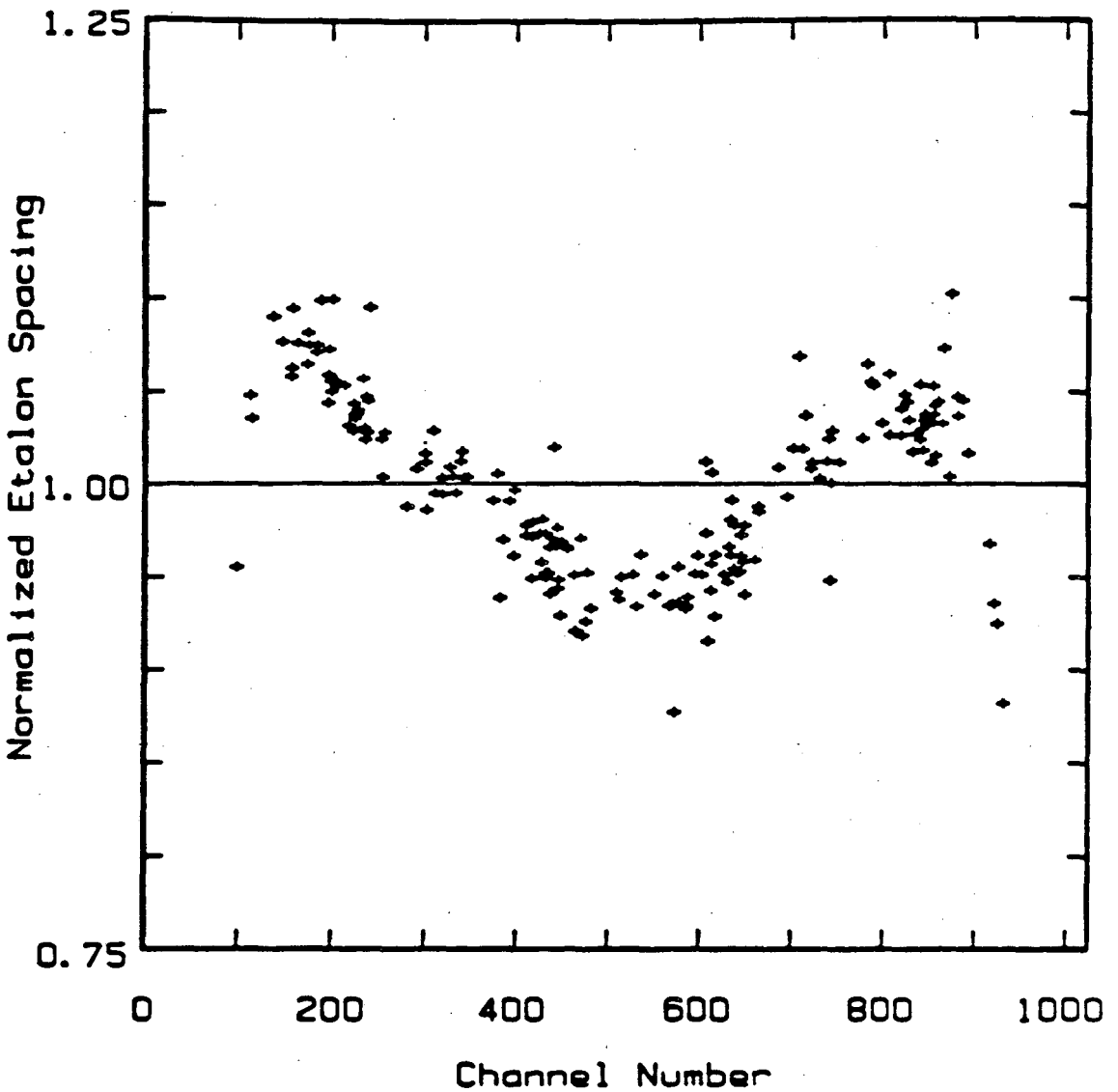

Fig. 7: The normalized, etalon spacing as a function of the position on the detector. The figure shows the non-linear temporal response of the detector due to a variety of effects (see text). A "perfectly" uniform time-response would give equal spacing between etalon peaks across the detector and is shown as the straight line with a value of 1.

and one without (Fig. 6a). The reduction in the standard deviation of the separation is considerable in the corrected set. An important outcome is that the average spacing is not affected (less than 1% change in this case) by the correction, only the uniformity of the spacing is improved. Further, both Figs. 6a and 6b show that the averaged scan resembles a good exponential decay. This is not always the case in the individual scans that made up these averaged etalons.

The time base correction is fixed by the geometry of the streak camera screen and the photodiode array. As long as this arrangement is unchanged, the calibration, which is rather tedious and time consuming, need not be retaken. Such a situation is not true for the intensity correction. The channel-to-channel, intensity non-uniformity is dependent on the input geometry of the fluorescence into the streak camera. The geometry necessarily changes as the alignment of the sample fluorescence is changed for each new experimental set-up. Therefore, new intensity corrections are taken at the beginning of each day's experiment or whenever changes are made in the sample collection geometry. Fortunately, this correction procedure is relatively simple.

Emission scans are accumulated and temporally corrected at the same streak speed and alignment geometry of the experiment. Corrections are performed using a fluorescing species whose lifetime is known to be "long" with respect to the streak speed. A typical calibrant used in this laboratory is ruthenium tris(bipyridine) dichloride, whose radiative lifetime is nominally 600 nanoseconds (in water). This lifetime is much longer than the time window of even the slowest streak speed (34 ns)[53]. Such a calibrant should produce a uniform intensity across the detector, since little decay occurs over the time

of the measurement. Instead, some deviation is found due to irregularities in the intensity response. The correction factor is the multiplicative inverse of the response. This correction factor is combined into the time base correction to create the final complete correction set which is called by the main operating program.

The completely corrected datasets are saved, if desired, for analysis of the decay kinetics. Two types of analyses are performed. For long time (relative to the pulse width), single-exponential, decay measurements, logarithmic plots are fit by a linear least squares' routine to yield the lifetime. These lifetime determinations are often used as fixed parameters in the more involved kinetic calculations which are explained next. Kinetic analyses of more complex decays are based on a best fit of the data either to a model kinetic scheme or to the simplest scheme of exponentials necessary for a proper match to the raw data. Fits are determined by minimizing the sum of the squared residuals of the raw data and the kinetic expression. By varying the exponential and pre-exponential factors, and minimizing the difference between synthetic spectrum and the raw data, the computer iterates to the best fit. The synthetic spectrum also incorporates the instrument response function by convolution. All fits are performed on a VAX 11/780 for speed of calculation.

An extension of the time resolved emission technique is the construction of time-evolving spectra. Fluorescence spectra can tell many things about the state of the emitting species. A spectrum, as it changes in time, describes how a state or transitory species evolves over the course of a reaction. An example of a state evolution process of interest in this laboratory is the interaction of a

solute with the solvent. How the solute is affected by hydrogen-bonding, dielectric relaxation, and viscosity of the solvent are important questions. Here, not the solute alone, but the solute/solvent complex changes in time. In the excited state the solute/solvent complex shifts to a new equilibrium orientation to accommodate its new electronic configuration. This re-equilibration is manifest by a spectral red-shift, as in Fig. 8. Besides this type of process, spectra in time can indicate whether an excited state reaction is occuring. An excited state reaction would result in one excited species producing another. These two species would normally have two, different fluorescence spectra. By observing the decay of the spectrum from the initially formed species, and the appearance of a second spectrum, information is gained about the coupling between these two emitting species. Direct coupling is signaled by an isobestic, or isoemissive, point in the time evolving spectra.

Time-evolving spectra are measured by the following procedure. Time resolved scans are taken at individual, 10 nm bands throughout the fluorescence region of interest. This series of scans is fit by the normal computer analysis to create a series of "deconvoluted", single-wavelength, fluorescence decays as a function of time. Next, the total fluorescence signal for each band is normalized to the corresponding fluorescence yield under the equivalent wavelength band in the steady state spectrum. Finally, individual time cuts which give the intensity at a single point in time are taken from each wavelength dependent scan. These intensities create an intensity versus wavelength plot at that particular time. These spectra are necessarily crude since the wavelength resolution is determined by

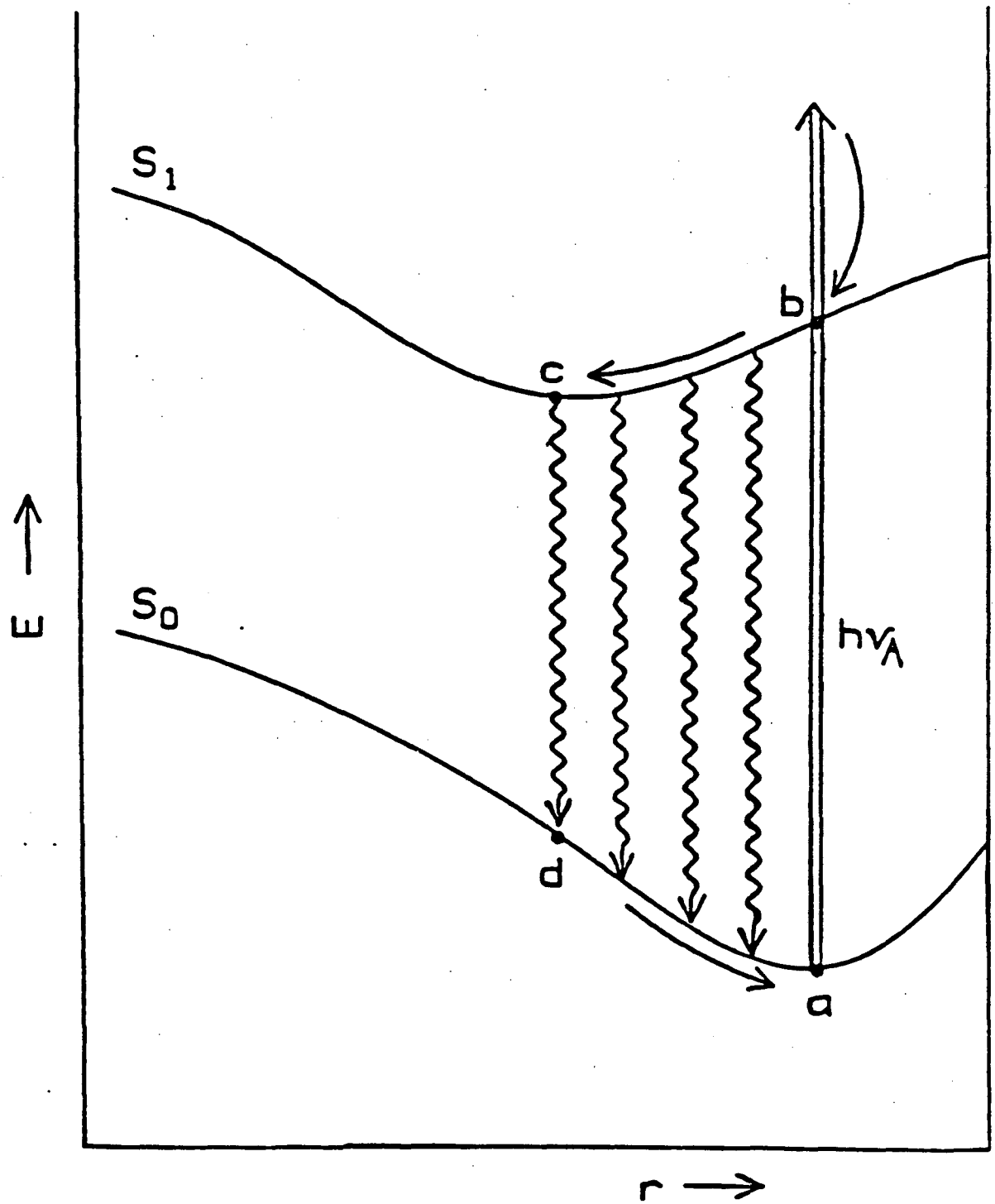

Fig. 8: Schematic representation of the ground and excited state potential surfaces for a system (solute/solvent state) undergoing re-equilibration. Initial excitation and rapid, vibrational relaxation (points a to b) produces a high-energy, non-relaxed complex which adiabatically relaxes to the S_1 minimum potential well (c) while fluorescing. Points d to a represent the same process on the ground state surface.

10 nm band pass filters. Nonetheless, valuable information is obtained from these plots.

D. Comparative Features of the Laser and Detection System

Some features of the Nd:YAG laser system are worth comparing to high-repetition rate systems. The points to consider are: power, output frequency range, laser repetition rate (or, more importantly, data acquisition rate), and pulse width. The central feature in the system described here is the large peak power—several hundreds of microjoules per 25 ps pulse. This power is easily boosted by the addition of any number of Nd:YAG amplifiers (10-30 times per amplifier) to tens or hundreds of milijoules. High power is important since it can be traded off for tunability and/or temporal width.

Tunability is accomplished with various combinations of non-linear optics. Both the generation of the laser harmonics or the tunable light from the OPS result from the use of KDP crystals. An additional feature of the OPS is the pulse narrowing which shortens pulses to between 1/2 to 1/3 their original width. Temporal narrowing may be achieved for the fundamental frequency as well. Saturable absorbers, dye solutions similar to the passive modelocker, are used in the beam prior to amplification for this narrowing. Power levels after these schemes of frequency conversion or temporal narrowing are still substantial, being in the range of at least a few to tens of microjoules.

The repetition rate of the Nd:YAG, 10 Hz, is slow compared to many other lasers and the combined data acquisition rate is presently detector/computer limited to <3 Hz. These conditions can be contrasted to high-repetition-rate systems. These systems produce pulse widths of a

couple of picoseconds which are tunable only over narrow wavelength regions, determined by the laser dye. Repetition rates up to tens of megahertz are obtained, but data rates often two orders of magnitude slower are normal. Finally, the high repetition rate means low power levels, usually in the nanojoule range.

Two major characteristics can be compared in a streak camera system versus, for example, single photon counting (SPC)[48,50,51] or other[54-56] detection systems. They are: 1) the signal-to-noise ratio which determines the reliability of the analysis of the data and 2) the temporal resolution. The signal-to-noise ratio is superior in high repetition rate systems (MHz data collection rates) where very large statistical averages can be made (SPC is an example that requires high averaging). However, the temporal resolution of the streak camera is between one and two orders of magnitude better than in SPC experiments.[8,51] Fitting techniques often allow measurements down to 1/10 of the instrument response function which is typically hundreds of picoseconds for SPC versus about twenty five picoseconds for the system described here.

For complex, multiple exponential signals, analyses based on computer fits to the data with minimized, randomly distributed residuals are the most accurate and unbiased. This method of analysis is best performed on data with high signal-to-noise ratios that have been statistically averaged. This streak camera system, though not commensurate with the signal-to-noise of SPC data, is capable of averaging at least 500 shots routinely. This averaging considerably improves the signal, especially as compared with other streak camera systems which often accumulate, at most, tens of shots. Obtaining an absolute

measurement of multiexponential decays is nonetheless difficult from streak camera measurements and subject to some judgement. However, this camera measures single-exponential picosecond rise times more precisely than other methods. This ability stems from the high time resolution, low jitter, and accurate corrections (for the irregularities in the response). Few examples of reliable, rapid rise times exist in the in the literature from SPC data. This lack of results is due mostly to the temporally-large, instrument response function. Other two-photon correlation methods, such as pump/probe absorption or fluorescence upconversion techniques, also yield good multiexponential fall times. However, they suffer from artifacts such as coherence spiking and pulse-to-pulse variations which must be precisely understood and carefully controlled if accurate, rise time measurements are to be made.[51]

E. Applications

This laser/streak camera apparatus has been applied to a variety of experiments ranging from simple pulse diagnostics to complex biological systems. When properly calibrated and corrected, events on timescales ranging from the pulse width (about twenty ps) to several nanoseconds can be observed without complications from the instrument response function. With computer fitting, responses down to a few picoseconds have been achieved. A brief description of the types of experiments already performed on this system will demonstrate its versatility and the range of chemical phenomena which can be studied.

The direct observation of individual laser pulses allows for the immediate characterization of laser/optical conditions.[58-60] Such

single pulse measurements, when combined with simultaneous, spectral measurements, yield direct evidence for transform-limited pulses. Also, the conditions necessary to produce the shortest pulses can be studied. The effect of intracavity pulse compression by self-phase modulation has been studied by determining the temporal widths of pulses extracted from various positions in the pulse train, Fig. 9.[60] Pulses down to a few picoseconds in width and near the transform-limit were found under certain conditions.

The large peak powers of the laser permit the generation of tunable light via non-linear crystals. This tunability can be used in investigations of the effect of excess excitation energy in excited electronic states. Such an experiment was performed on rhodamine 6G to ascertain the effect of excited state vibrations on the rotational lifetime and the rotational anisotropy. The importance of vibronic distortion of the excited state emission dipole and the effect of local solvent heating are evaluated.[61] Since the excitation-laser light is linearly polarized, a prefered distribution of excited states is produced due to the alignment of the absorption dipole with the laser. This non-random distribution is a unique state which decays to the normal, polarization-scrambled excited state as a function of the reorientation time of the emitting dipole. By observing polarized emission, a measurement of the rotational reorientation time is possible. Rotational effects are monitored by the proper selection of excitation and emission polarizations through the setting of Glan polarizers. Parallel and perpendicular fluorescence polarizations are shown in Fig. 10 for rhodamine 6G. The intensities have been normalized at long times relative to the rotational reorientation

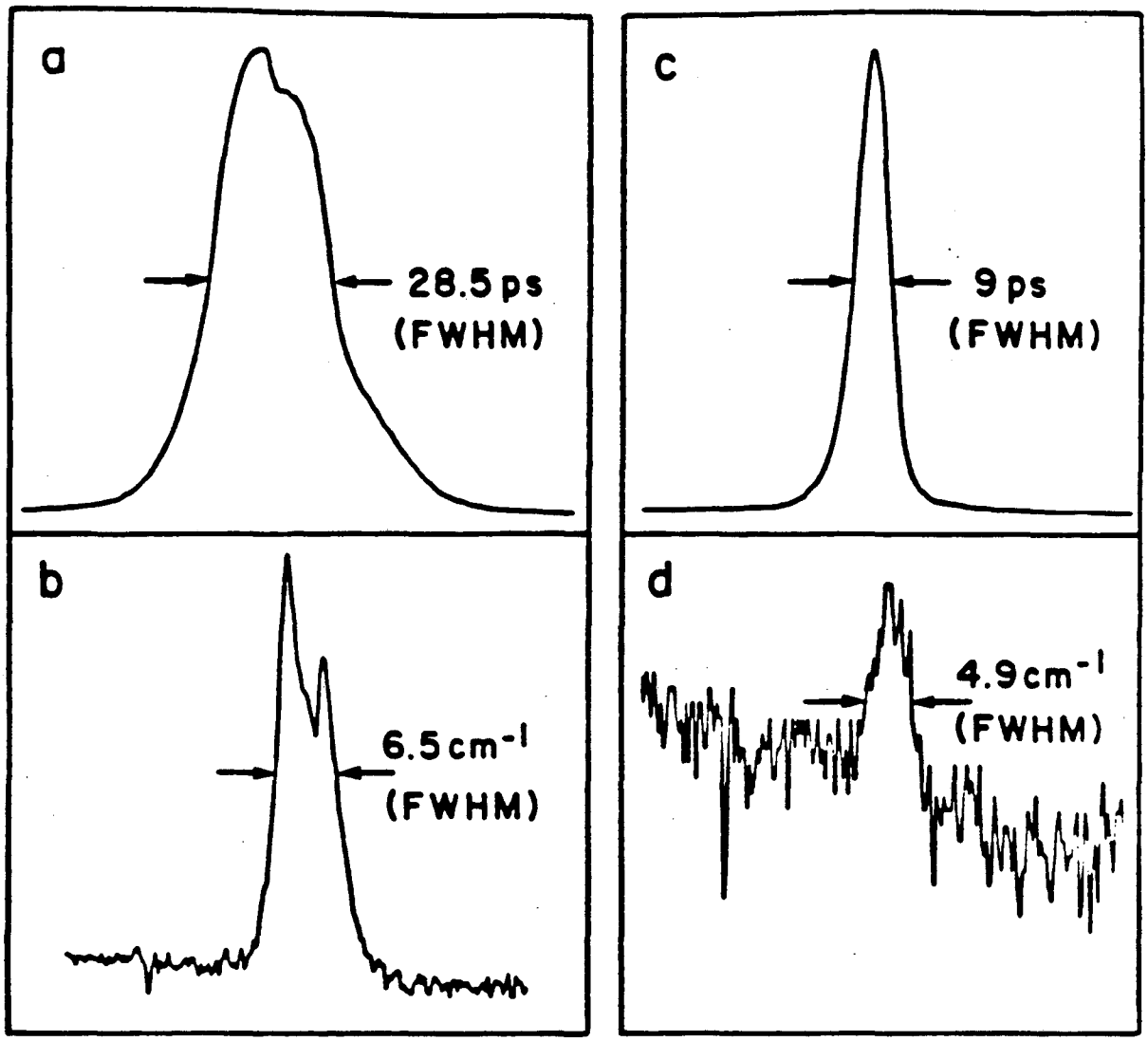

Fig. 9: Simultaneous, spectral/temporal measurements of a pulse as a function of position in the pulse train. Traces a (100 shot average) and b (single shot) represent the temporal and spectral response, respectively, of a pulse taken from the middle of the modelocked train. Traces c and d were similarly measured from a single pulse taken nine pulses past the middle of the train (approximately 1/50th of the power of a,b).

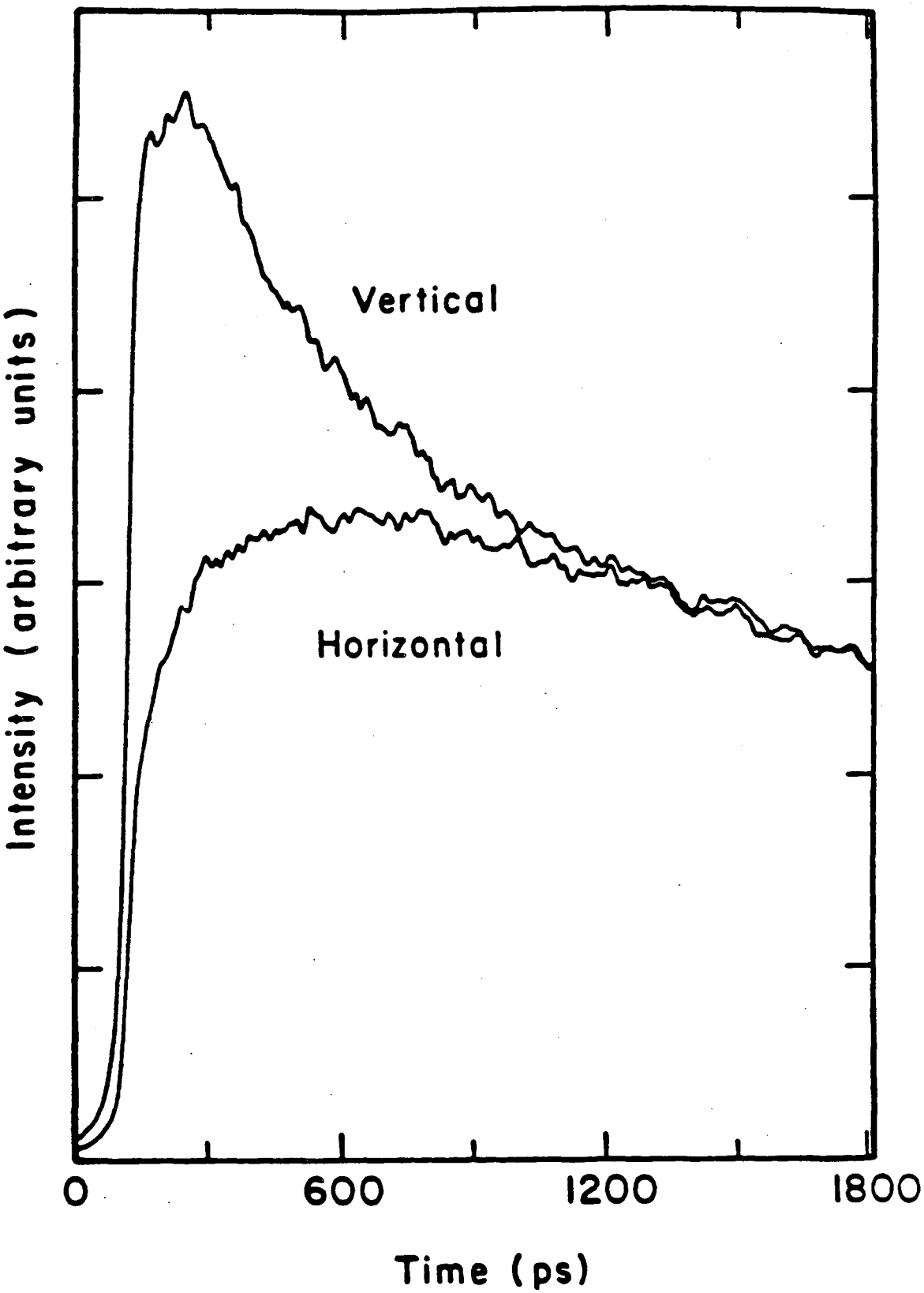

Fig. 10: Vertical and horizontal components of the fluorescence decay of rhodamine 6G in ethanol with 476 nm excitation. The two sets of data were tail matched over the last 100 ps depicted in the figure.

time (i.e. tail-matching[62]). No dependence was found on either the rotational time or the anisotropy due to the excess vibrational energy (Figs. 11 and 12). The implication is that rapid, vibrational relaxation and energy dissipation occurs in this system.

Since the sensitivity of the system is high, emission measurements ulilizing narrow, 10 nm bandpass interference filters are possible, even in the case of weakly emitting or very dilute samples. Time-evolving spectra with 10 nm resolution can give insight into solute/solvent reorganization, as explained above. Such studies are being tried on 4-aminophthalimide in various hydrogen-bonding solvents, Fig. 13, to test what effects dominate the excited state re-equilibration.[63] Many solvents have been studied. A good correlation has been found between the dieletric relaxation time of the solvent and the rate at which the emission spectra shift in time.

One of the most important features of this apparatus is the ability to average hundreds of shots accurately and efficiently. Signal averaging makes possible low intensity experiments. This point is dramatically depicted in Fig. 14 for the light-harvesting units of algae and cyanobacteria called phycobilisomes. In this figure the need for signal averaging (Fig. 14a) is apparent. In fact, these data were taken at approximately 1000 times higher intensity than normal. Under attenuated conditions the need to signal average is even greater. The attempt to compensate for the lack of signal by increasing the input power is often inappropriate. The result can be additional, undesired, excited state processes such as the exciton annihilation depicted in Fig. 14 or stimulated emission.

Once the excitation conditions were established, a study to find

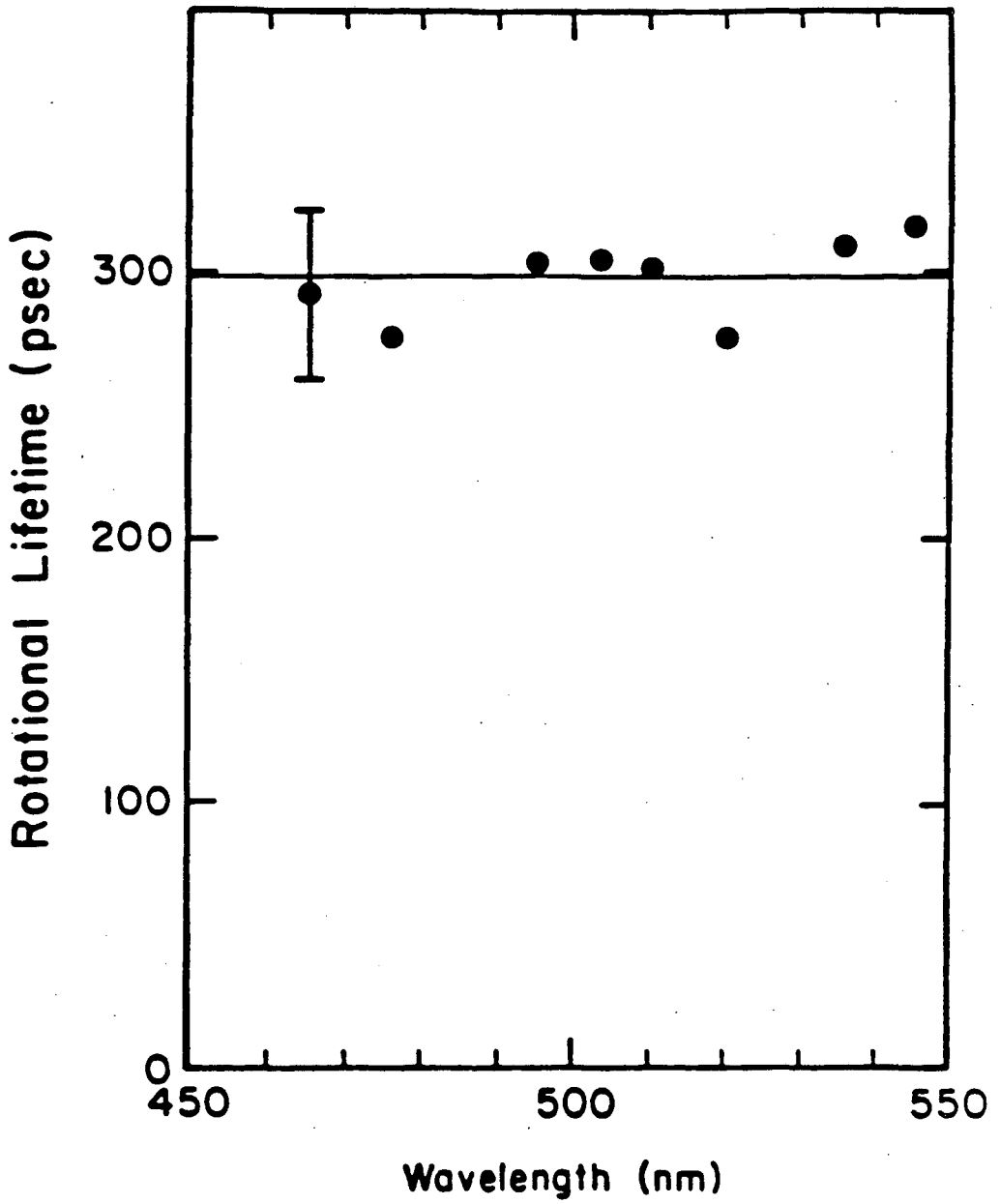

Fig. 11: Plot of τ versus excitation wavelength. The error bars represent systematic as well as random uncertainty in the data.

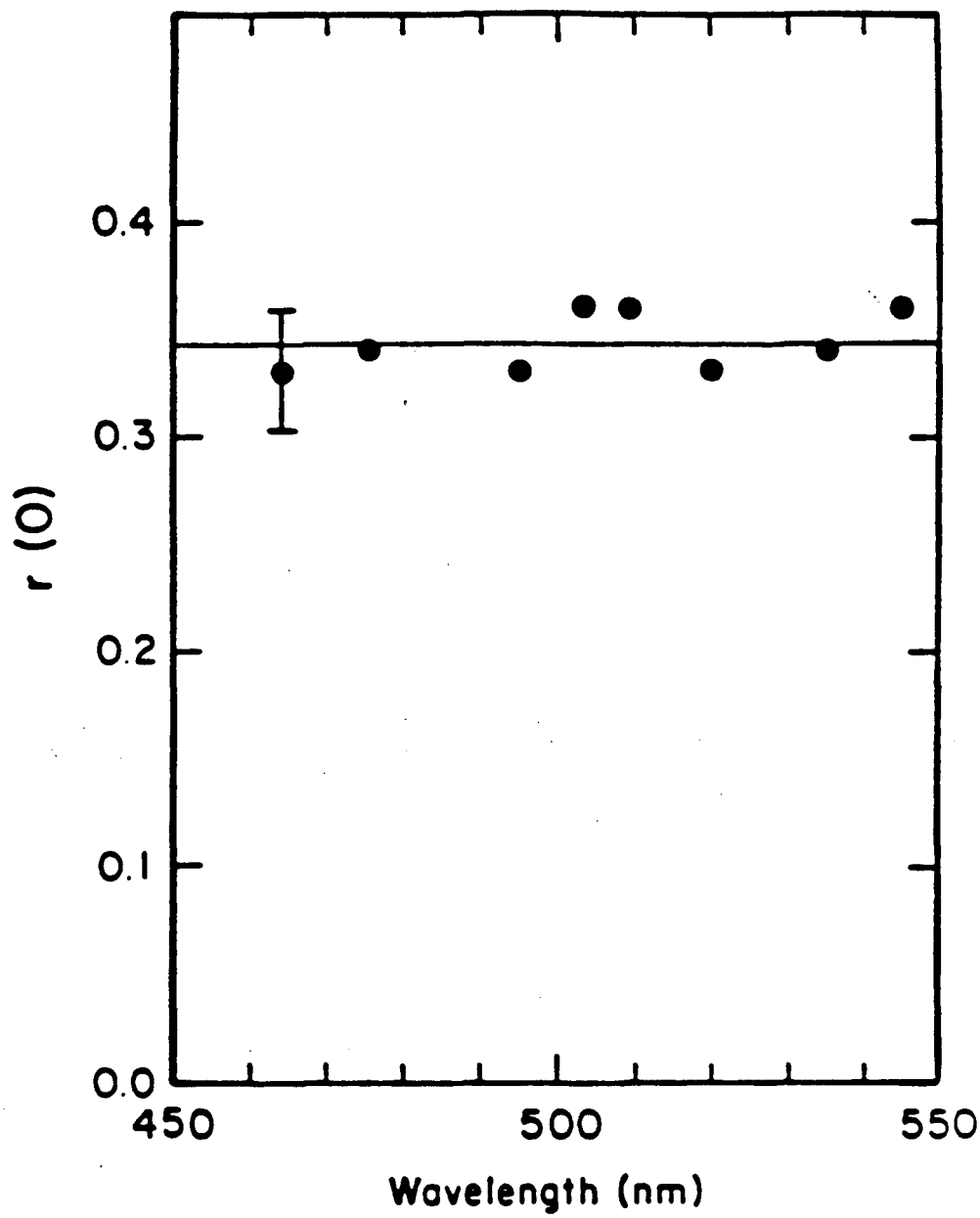

Fig. 12: Plot of r(0) versus excitation wavelength. The error bars represent systematic as well as random uncertainty in the data.

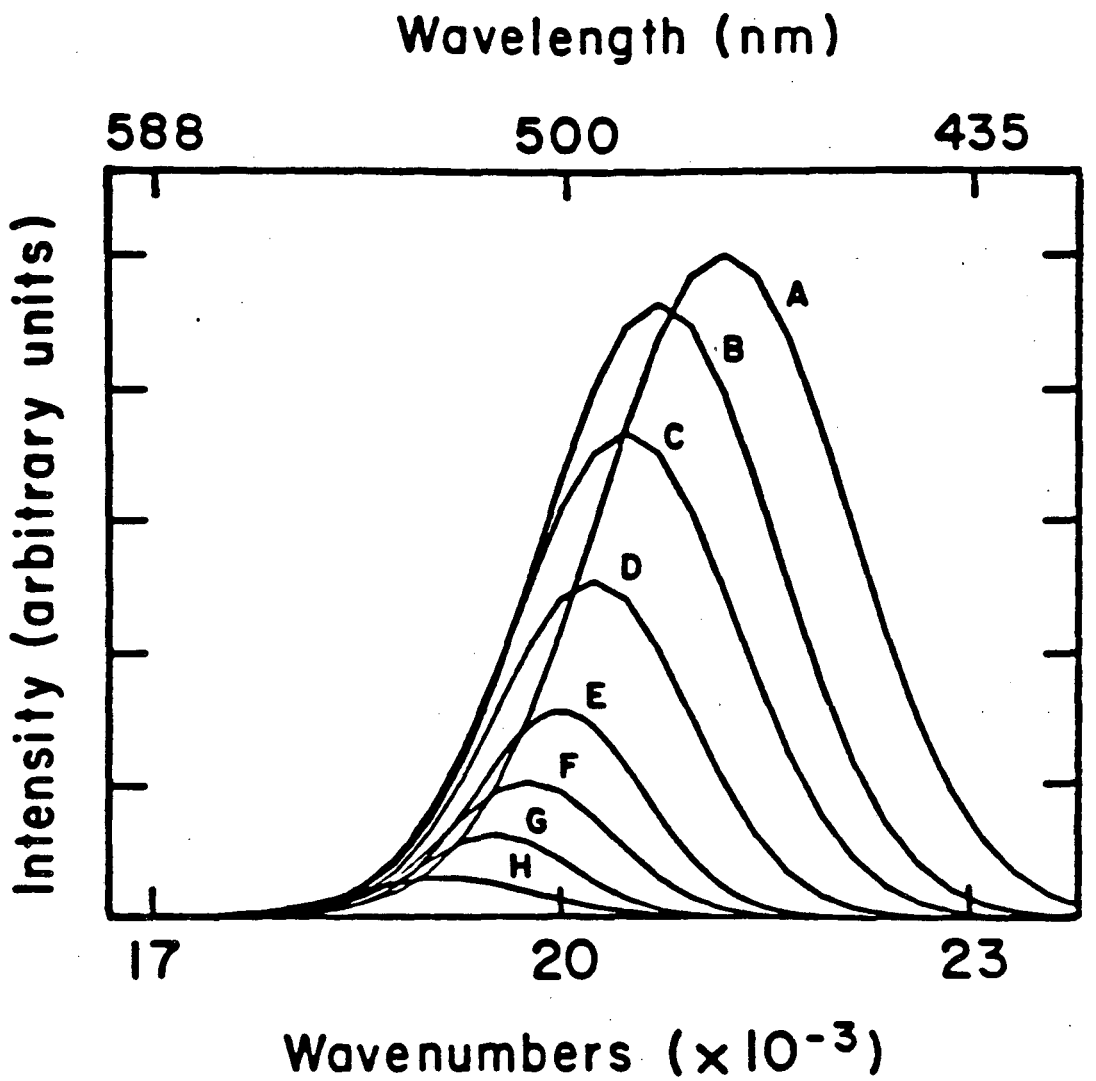

Fig. 13: Time-evolving spectra of 4-aminophthalimide in propanol. The traces show the smoothed, Gaussian-approximated spectra of the solute/solvent state as a function of time. Spectra A through H represent time slices of: 10, 50, 100, 200, 400, 600, 1100, and 1900 ps, respectively.

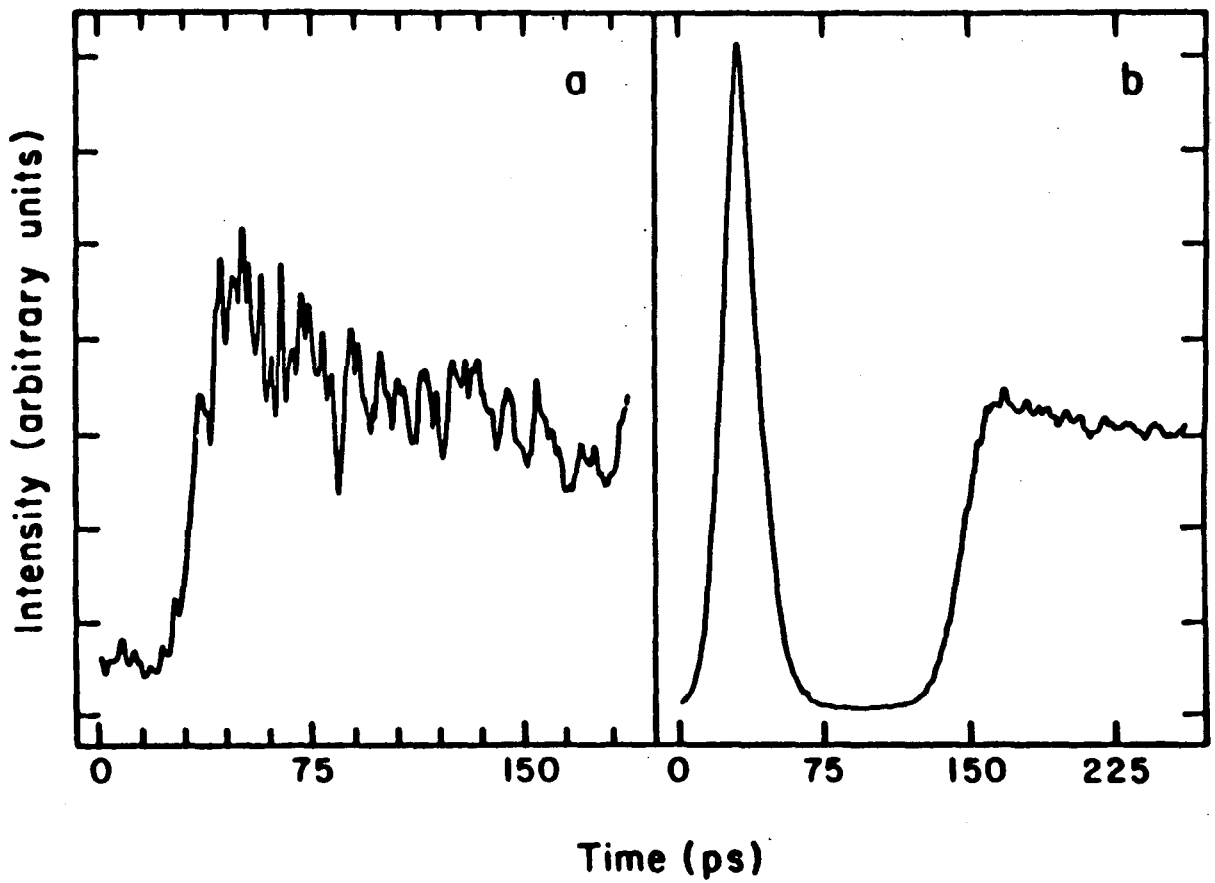

Fig. 14: Signal averaging and laser power dependence on the measurement of fluorescence from two different phycobilisomes, P. cruentum (a) and WT 6701 (b). Trace a shows the sum of 31, unattenuated laser shots (532 nm line) taken at the 680 nm emission peak of the terminal emitting unit of the phycobilisome. Trace b is a comparable bacterium excited and detected as in (a) but the sum of 200 shots. In both cases the use of unattenuated laser light causes prompt emission due to exciton anihilation, the build-up of self-quenching excited states and other non-linear optical effects. The properly attenuated signals (about 1000 times) show the energy transport times as the excitation is passed to the terminal emitter (as seen by a rise time to the fluorescence). Such weak signals require even greater signal averaging.

how energy flows in phycobilisomes was performed.[64a] Phycobilisomes are made up of many macromolecular units (or disks) which are further composed of multitudes of chromophores. Thus, the energy transport important for photosynthesis in these systems is complex. The application of overly intense excitation distorts the kinetics of this system away from the processes that occur naturally. A two-fold experiment was designed to measure the inter-disk energy transfer between two specific structural units, called phycoerythrin and phycocyanin, in the phycobilisome, WT 6701. One experiment[64b] involved the comparative use of a WT 6701 mutant, CM 25. The object was to discover the difference in the rise time, which describes the energy transfer time to the terminal emitter in each phycobilisome. Since the mutant lacked phycoerythrin, a shorter path for excitation transfer to the terminal emitter exists in this phycobilisome. The shorter path in the mutant was reflected in a faster rise time of the emission from the terminal acceptor. An analogous experiment involved the analysis of the wild-type phycobilisome, WT 6701. The experiment used tunable excitation to bypass the phycoerythrin units. This experiment is equivalent to the mutant study but relies on a single phycobilisome. Similar results were found and determined the transfer time to be 25 ps for transfer between these units.

The application of the tunable OPS and the use of reliable rise time data were also required in a similar study on the energy flow <u>within</u> a particular phycobilisome unit, phycoerythrin. These experiments showed "instantaneous" rise times of the emission independent of the absorbing chromophore. This result suggests very rapid internal energy transfer. These two types of experiments helped establish that

the rate-limiting step in the energy transfer process in phycobilisomes is inter-disk rather than intra-disk energy transfer.

In addition to the solution work described above, this laser system and the time resolved emission technique have been applied to a wide range of other experiments. Studies have been performed on solids, both doped films and single crystals, and on gas phase species. Also, solute/solvent interactions are presently being extended by investigating the effect of temperature on the excited state solute/solvent reorganization process. Also, studies have been performed to examine the role of pressure in chemical processes.

Analysis of a transition metal complex, ruthenium tris(bipyridine)$^{++}$, in aqueous solution elucidated the nature of the photophysics of its excited state. Insight was gained concerning the role of spin-orbit states in heavy atom molecules[53]. For this molecule, the degree of localization of the electron with respect to the ligands in the charge-transfer excited state was debated. Another issue was whether the observed emission was from the excited singlet or triplet. Picosecond Raman experiments, coupled with nanosecond Raman studies from the literature, resolved the charge localization debate. This study showed that a localized state with the electron residing on a single bipyridine ligand was formed within the 25 ps pulse width. The question of the spin multiplicity of the emitting state arose from the long (hundreds of nanoseconds) decay time. This decay time was longer than expected for a singlet state. Therefore, the triplet state had long been hypothesized as the emitting state. Questions were raised as to what happens to the initially formed singlet state. Does it emit? The fluorescence rise time (Fig. 15) was analyzed with respect

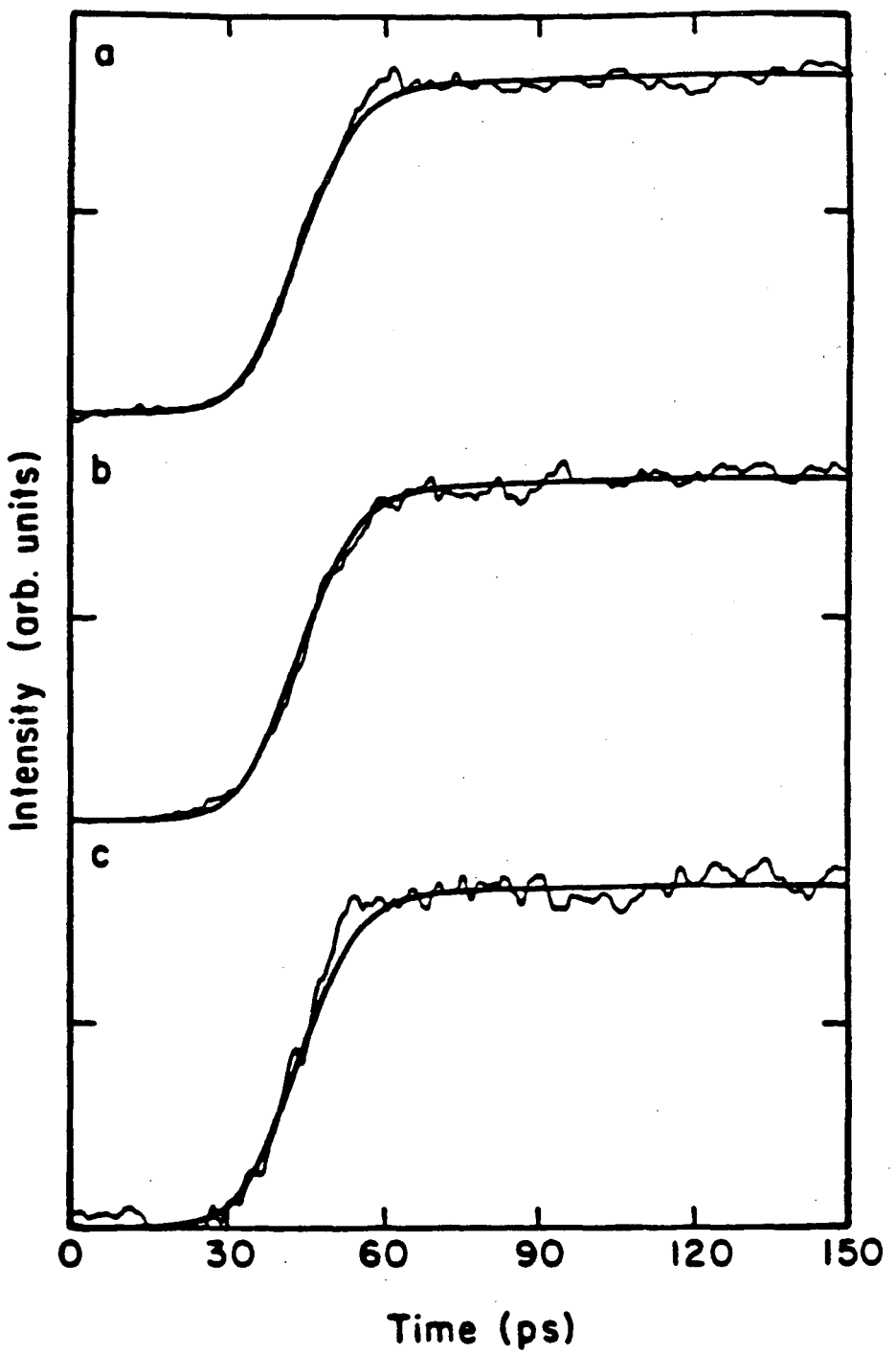

Fig. 15: Time resolved emission spectra of Ru tris(bpy)$^{++}$. a) 355 nm excitation with detection through a 600 nm band pass filter. b) 355 nm excitation with detection through high pass cutoff filter (> 570 nm). c) 532 nm excitation with detection through high pass cutoff filters as in b). All three sets of data are shown with the same computer generated fit to the data. The computer fit has a rise time of 0.041 ps and a fall time held at 600 ns.

to a two-state, singlet and triplet model. A prompt rise time for excitation at both 532 nm and 355 nm proved that the emitting state was formed instantaneously without signal from a second state. The rapid intersystem crossing time implied by these results suggested that the heavy ruthenium atom couples the spin-orbit singlet and triplet states.

A unique opportunity in liquid studies was afforded by the adddition of a high pressure cell developed in this laboratory. This apparatus made possible solution phase studies in the picosecond regime at pressures of up to seven kbar (approximately 7000 atm)[65].

Considerable interest has been generated regarding the effect of the solvent on solute dynamics. Since the inception of the Debye-Stokes-Einstein (DSE) equation, which relates the bulk property of solvent viscosity to solute rotation, numerous theories modifying the DSE equation have evolved to describe how solvent viscosity alone can account for the observed solute/solvent interactions. These theories treat the solvent as a continuous medium characterized by its viscosity. This medium provides a frictional force on the motion of the solute. By knowing the parameters of the solute size and shape, predictions are made relating molecular reorientation to solvent viscosity. As previously mentioned, rotational reorientation times can be determined via spectroscopic methods by proper selection of excitation and emission polarizations. Studies in the past relied on solvent variation or temperature changes to bring about changes in the viscosity. These methods can change the solute/solvent interactions and/or intramolecular potentials. Pressure effects, while changing solvent viscosity, cause unique perturbations in terms of these interactions. Studies on rhodamine 6G (Fig. 16) in a linear alcohol series and a

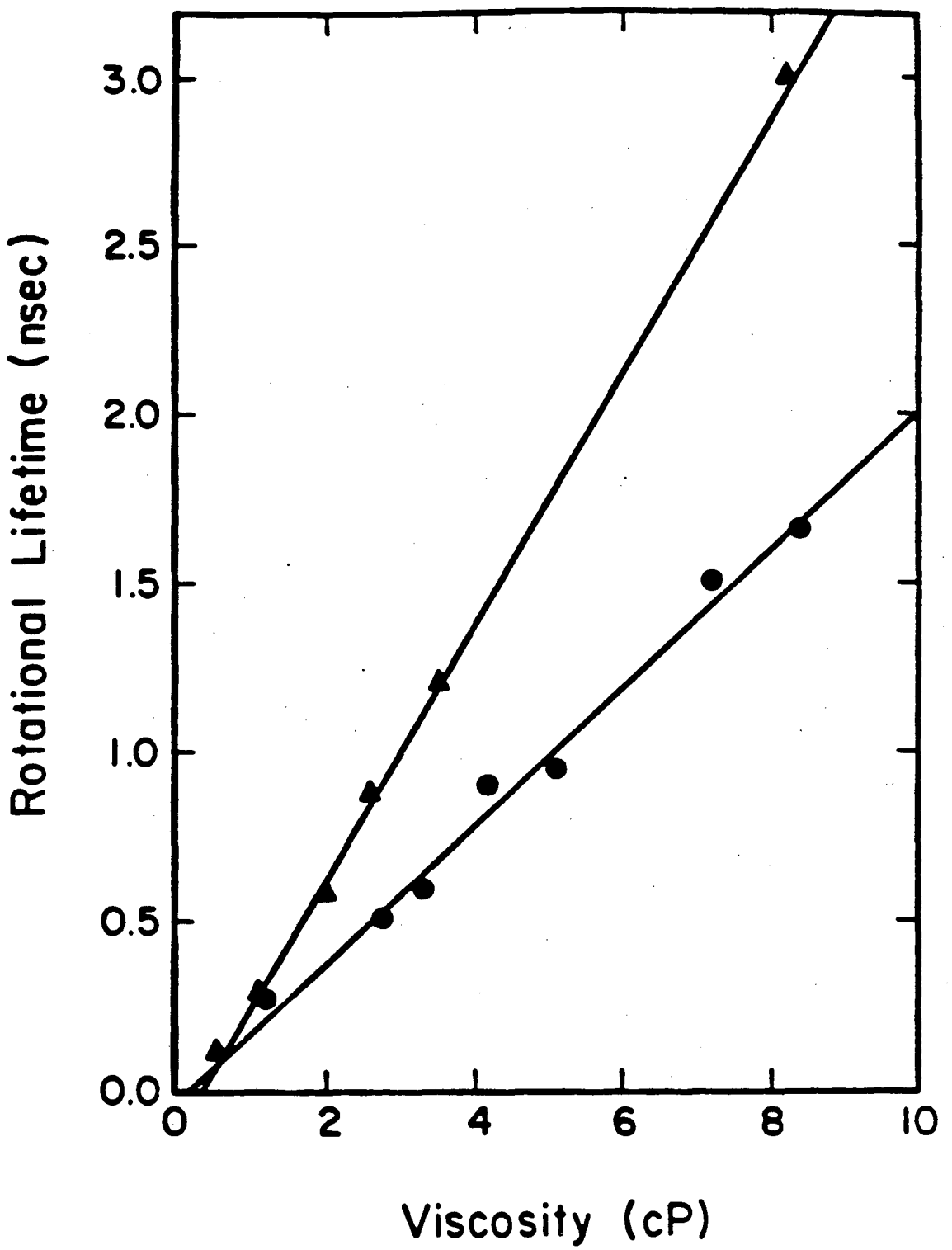

Fig. 16: Rotational reorientation lifetime for rhodamine 6G vs. viscosity: linear alcohols (triangles) vs. ethanol under pressure (circles). The two plots show a linear dependence on viscosity but with differing slopes indicative of the presence of additional processes other than pure viscosity which determine the rotational lifetime.

pressure series showed that different rotational reorientation times are observed under isoviscous conditions when hydrogen bonding between the solute and solvent is possible[47]. Such dramatic differences are not found for less interacting solutes[66].

All these investigations prove the utility of the system. Many of the experiments would be difficult or impossible to do with other laser or detection systems, especially where tunability or accurate rise time information is required. Certainly measurement of these fundamental processes without time resolved techniques would be much more difficult and subject to more ambiguities.

F. Sample Preparation and Steady State Methods

In spectroscopic studies and in particular these investigations that require the measurement of fluorescent signals, impurities which emit in the region of interest must be avoided. Also, undesired side reactions must be eliminated. In picosecond experiments, impurities which fluoresce with a long time constant with respect to the process of interest can be mathematically removed from the fluorescence signal if they are not too large. Generally, only low quantum yield, fluorescing impurities can be tolerated.

The most careful procedure used in the time resolved, picosecond measurements of 1-naphthol as a function of pH was as follows. The 1-naphthol was HPLC purified and stored in sealed vials under nitrogen (L.C. Labs). Solutions of water (steam distilled, Alhambra) and concentrated HCl (AR grade, Baker) were freeze-pump-thawed for at least three cycles to remove any dissolved oxygen. All sample concentrations were then measured by dilution to between 10^{-3} to 10^{-4} M, pH adjusted

1 cm quartz cuvettes, all while inside a glove bag under nitrogen. The solution pH was determined on a pH meter for solutions between pH 2 and 10 and titrated against a standard for those outside this range.

Identical results were found following a simpler, modified procedure. Recrystallized (from hexane) and sublimed 1-naphthol was used at approximately 10^{-4} M. Solutions were of the same quality but were degassed when necessary by purging with nitrogen. This degassing step was also found to have no bearing on the measured kinetics. In all cases, solutions were prepared and run on the same day. Highly basic solutions were run within a few hours of preparation, since these high pH solutions discolored after several hours.

Non-aqueous solutions were made up in the following manner. For the deuterium study 100 atom % D_2O (Aldrich gold label) was obtained. The pD was adjusted with DCl and NaOD (Aldrich gold label). A glove bag and sealed cuvettes were used to avoid water contamination. The pH meter was calibrated by a sodium acetate-d_3/D_2O buffer. The 1-naphthol was recrystallized and sublimed. Ethanol (Gold Shield, 95%) and acetonitrile (spectral grade) were obtained without further purification for the mixed solvent studies. Solution mixtures were prepared on a per cent volume basis. For the salt studies all salts were analytic reagents and used directly. All pH measurements were uncorrected for these additional species.

Absorption measurements were taken on a spectrometer (Beckman Model 25) and referenced to a water blank. Full absorption spectra were determined for each of the samples used in the steady state measurements. Beer's law plots for the neutral (1-naphthol) and the anion (1-naphtholate) showed linear behavior to at least 5×10^{-5} M,

the concentration used in all the steady state analyses. The excitation wavelength, 266 nm, was selected for compatability between the laser and steady state measurements. This wavelength is not a good analytic wavelength for absorption, since it is not at an absorption maximum.

Steady state determinations were performed on a Flurolog II Spectrofluorimeter (Spex Industries). The excitation source, a 150 W Xenon lamp, was intensity-corrected by a concentrated rhodamine 6G quantum counter and photomultiplier. The overall response was calibrated via normalization to a standard lamp spectrum (Optronix 245). Both pairs of excitation and emission slits were maintained at 2 mm. Sample fluorescence was collected at right angles from the dilute solutions, 5 x 10^{-5} M, to minimize any geometry-dependent responses. Scans across the entire output range were measured at 1 nm steps with an integration time of 1 sec/nm. Intensity was read as photon counts on a cooled photomultiplier and single-photon-amplifier-discriminator. For the excitation spectra of the H_2O sample, emission was monitored at the peak of the anion fluorescence (485 nm) for both pH 7 and pH 12 solutions.

All the data were stored on a computer (VAX 11/780) for later analysis and plotting. For extraction of the weak emission signals from the neutral species, normalization and subtraction of the anion signal were performed. The "pure" anion signal was obtained from the spectrum of a pH 12 solution. Easilly identifiable and quantifiable signals were thereby obtained for the emission from neutral 1-naphthol. Normalized excitation spectra were generated by digitizing the corresponding absolute absorption spectra and dividing them into the excitation spectra. All of these measurements are presented in Chapter four.

Chapter Three

Theory

A. Introduction

Since the initial identification of the excited state proton transfer reaction by Förster[2a], much work has gone into the development of schemes to quantitatively analyze the kinetics and thermodynamics of such processes. Most notably, Weller derived the integrated rate equations for the coupled, two-state, ESPT process, as shown in Fig. 17. Weller also developed a system of analysis based on the measurement of relative emission quantum yields, henceforth refered to as the steady state method[4]. The general methods for the time dependent analysis are easily deduced from these same integrated rate expressions. A detailed derivation of the equations used in both the time dependent and steady state methods is given in the Appendix. Equations from the Appendix will be utilized throughout this chapter and will be identified by the format: (A#). The goal of this chapter will be to outline the procedure used to determine the rate constants for the ESPT reaction in 1-naphthol. A simpler but similar scheme has been used previously in a completely time dependent analysis of the ESPT reaction in 2-naphthol by Laws and Brand[14]. A reasonably complete (and comlex) analysis based entirely on steady state results has been carried out by Selinger and Harris for 1-[16] and 2-naphthol[15].

The analysis presented here makes use of both steady state and direct time resolved results. The advantage of using both methods of analysis is two-fold. First, the more information there is available to describe a system, the better and more reliable the analysis. Second, knowledge of both the temporal and steady state responses of

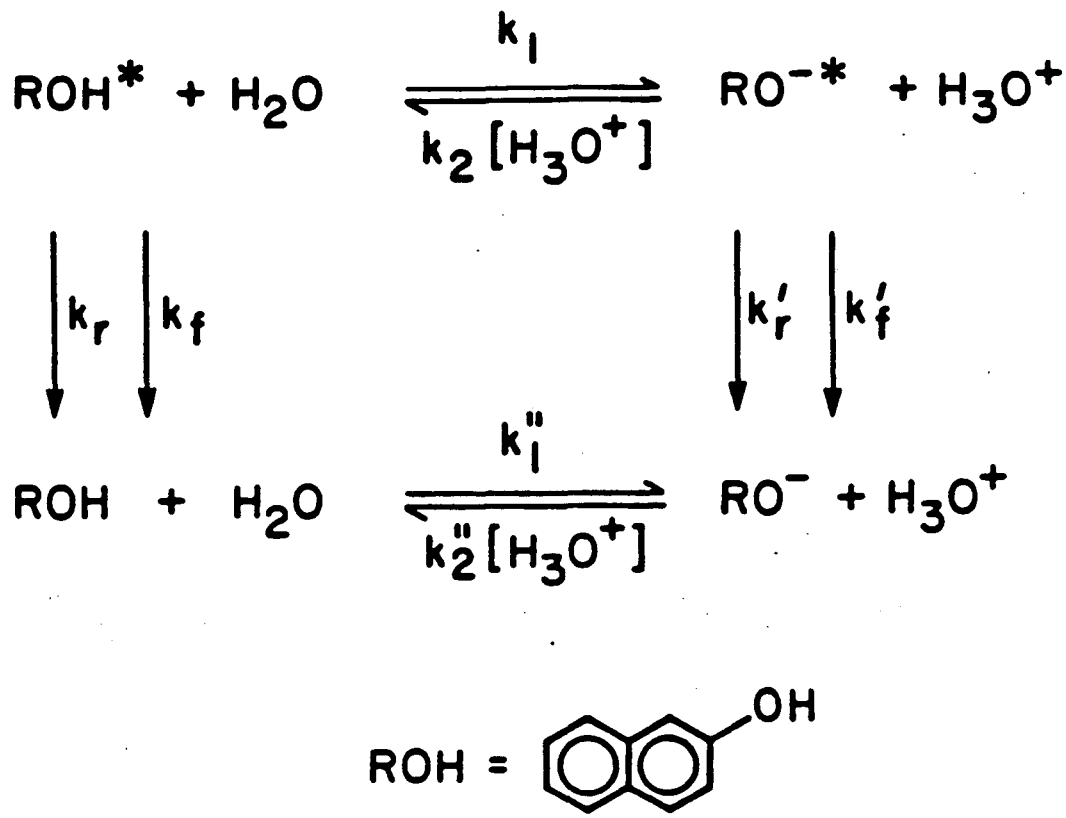

Fig. 17: The ESPT reaction scheme for 2-naphthol. This model employs the minimum number of rate processes required for a general description of ESPT in 2-naphthol molecule. The rate constants are: forward proton transfer (k_1), fluorescence and radiationless decay (k_f + k_r are defined as k for the neutral, k_f' + k_r' are defined as k' for the anion) , and reprotonation $k_2(H_3O^+)$.

the system will often allow for a more complete evaluation of a given model, an evaluation which might not be possible using time resolved measurements alone.

The goal of this approach is not simply to develop a model to be fit with rate constants, but rather to analyze all of the existing data to assess the validity of a given model. Two results may occur. First, the data may fit the model correctly, in which case the rate constants obtained will provide insight into the relative importance of each of the individual molecular processes that determine the overall ESPT reaction scheme. The second possibility is that the model is not entirely consistent with the data, implying that the model does not provide a complete description of the important processes. Of course, conditions may exist where a particular model is applicable, but only over a selected range of conditions.

A model is desired that consists of a reaction mechanism that predicts the interactions of the various rate constants as a function of the solution pH and provides an adequate fit to the data. Once the scheme of analysis has been developed, it will be demonstrated that various modifications to the scheme must also be considered. Since data is taken as a function of the solution pH, all effects other that those resulting explicitly from the hydrogen ion concentration must be further accounted for. The rationale behand these corrections will be presented separately, following a description of the basic model and the associated scheme of analysis. This should help minimize any confusion surrounding the basic model. It will be seen that these corrections to the basic model do alter the kinetic model that will be presented, but do so in a straightforward manner. Further, it will

be demonstrated that the exact nature of the corrections is not yet precisely known. A totally unambiguous selection of the proper corrections is not yet possible. A detailed discussion of this matter is given below.

Since a model will be presented and appropriate rate constants will be determined, a comparison of the complete results to the raw data is possible. A computer program was written to perform such a comparison. The general features of the program will be described. The quantitative evaluation of the model and the conclusions that can be drawn from such an analysis, along with the pertinent experimental data will be presented in Chapter four.

Many rate constants are necessary for a complete description of ESPT in 1-naphthol. In addition to the six fundamental rate constants shown in Fig. 18, there are many algebraic combinations of these fundamental rate constants that, for simplicity, will be given their own symbol. All these terms are defined and derived in the Appendix. It is suggested that the most rigorous reader will find it useful to read the Appendix before reading the next section. For the more casual reader, it is perhaps sufficient to realize that a given rate constant, k_n, can be distinguished as belonging to a process involving the excited neutral species if it is unprimed, while a primed constant refers to a process involving the anion.

B. Theoretical Models and Methods

The establishment of a model is a necessary step in understanding the results of any experiment. A "simple" model is often easy to apply and may yield general and far-reaching conclusions. However,

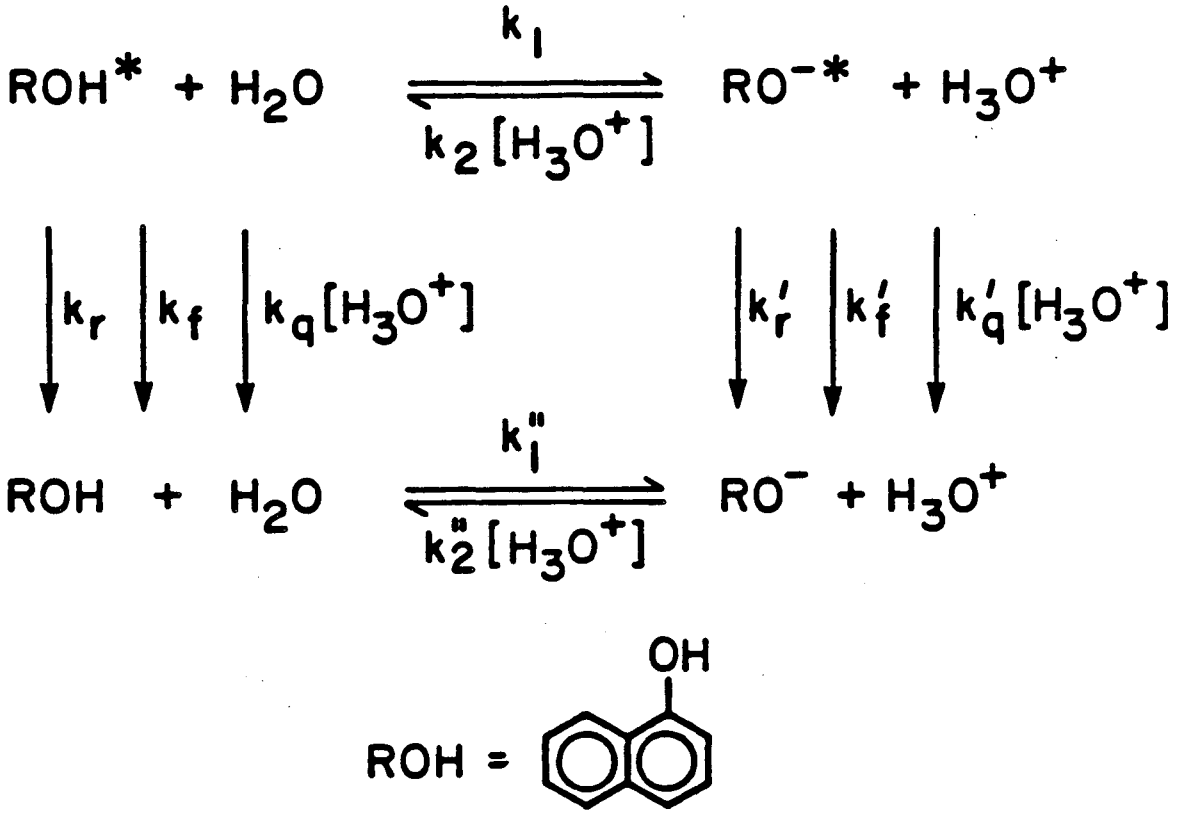

Fig. 18: The ESPT reaction scheme for 1-naphthol. This model, as contrasted with the simple 2-naphthol case, has the added proton dependent, bimolecular quenching rate constants given by k_q and k_q' for the neutral and anion, respectively. All the other rate constants are as given for the 2-naphthol case.

except for equally simple systems, such models can be severely limited in their range of application. Conversely, a "complex" model that can account for all the data often becomes tedious to apply and may not be applicable to a broad range of other systems. Another "feature" of a model is its inflexibility. Once chosen, a particular model predicts only certain occurances and cannot account for any anomolous behavior. Further, evaluating the differences between a faulty model and "noisy" data can be a difficult task. The approach taken here is to strike an appropriate compromise between simplicity and complexity so as to devise a reaction scheme that is sufficiently complex to accurately fit the data yet still general enough to apply to other systems. Determination of this middle ground will depend on the system(s) and the degree to which a "match" between the model and the data is judged acceptable. For the 2-naphthol system, much has been learned by the fitting of various kinds of data with various models. The increased complexity of the 1-naphthol system provides a stringent test of any model of ESPT.

The general model for ESPT is given by (A1) and is depicted in Fig. 17. This reaction scheme shows the possible existence of adiabatic equilibrium between the two excited state species. For the 1-naphthol case, Fig. 18, this model includes six rate constants as given by (A3) and (A4), where $k_f + k_r$ are defined as k, and $k_f' + k_r'$ are defined as k'. The constants k_r and k_r' refer to any process or sum of processes which diabatically and non-radiatively depletes the neutral and the anion, respectively. These processes may include, for example, crossing to the triplet or internal conversion to the ground state. Such processes are assumed to be pH and solvent independent.

As shown in the Appendix, there are only certain circumstances for which an ESPT equilibrium is established. In general, methods that are independent of equilibrium thermodynamics will therefore be needed. The model presented here is independent of equilibrating excited states but requires certain other conditions. First, all the rate constants are unimolecular, pseudo-unimolecular, or bimolecular (with protons always acting as one of the species). Second, the pseudo-unimolecular rate constants are treated as if they were strictly unimolecular, that is, the solvent is considered a continuous medium with no orientational or structural properties. Lastly, all the rate constants are assumed to be independent of the solvent over the full range of pH studied. Both the time dependent and steady state analyses meet the requirement of being independent of equilibrium conditions.

The time dependent method directly follows the rates of reaction as given by (A18) and (A19). The rates are found from the change in excited state populations. These populations are determined by monitoring the intensity of various fluorescence signals as a fuction of time using the picosecond time resolved emission technique described previously. Each integrated rate equation consists of the sum of two exponentials. In addition to the exponential terms, the pre-exponential factors also contain kinetic information. In practice the extraction of reliable information from pre-exponential terms is difficult. Both of these expressions, (A18) and (A19), have identical exponential terms. The neutral species shows a double exponential decay, while the anion has one rising term (evidenced by the negative pre-exponential factor) and one decaying term. Each of the exponential factors, G_1 and G_2, represent a complex combination of the six

rate constants and are explicitly pH dependent. A measurement of these exponentials at several pHs will then distinguish the various rate constants.

The steady state method relies on a measurement of the relative emission yields as a function of pH. These measurements reflect a competition between all the rate constants. They are independent of a maintained, excited state equilibrium since it is this very competition which essentially thwarts the establishment of the equilibrium. Further, as shown in Section C of the Appendix, the steady state method is similar to the summation of many pulsed experiments. Both studies provide kinetic information. As the solution pH is changed, a new distribution is established among the excited state species. This distribution is determined by the various competing rates. Spectroscopic integration of the individual signals from each excited species measures these competing kinetic rate constants, as given by (A46) and (A47). Equations (A46) and (A47) may be used directly if the spetroscopic measurements provide absolute quantum yields. However, the form of these equations requires a knowledge of the natural lifetimes, k_f and k_f'. By making relative determinations of the quantum yield, the effect of the natural lifetimes is eliminated as given by (A65a) and (A65b).

Implicit in this quantum yield analysis is that, in the absence of quenching, the sum of the relative quantum yields from the neutral and the anion at any pH will be 1. This result is the outcome of the definition of the normalizing quantities, ϕ_N' and ϕ_A'. These quantum yields account for the fluorescent and non-radiative rates. Therefore, at any pH where there is no additional quenching, the only processes

remaining in the model are the ESPT rate constants, k_1 and k_2. Since these rate constants are adiabatic, they do not reduce the total quantum yield by maintaining the same total population on the excited state surface.

The techniques for the application of the ESPT model are summarized as follows. For the time dependent analysis, an exciting pulse creates a single excited state species, which in these examples is the neutral, 1-naphthol molecule. This excited species will evolve in time by decaying to other, non-emissive states or by deprotonating and forming the excited 1-naphtholate anion. These events can be monitored by detecting the fluorescence intensity from either species as a function of time. Since the emission spectrum of the anion is considerably red-shifted from that of the neutral (see Figs. 20 and 21) both species fluorescence may be observed independently. Observation and analysis of either fluorescence signal will yield the desired kinetic parameters, as given by the exponential and pre-exponential terms. These terms are then related via a series of experiments at different solution pH, distinguishing the proton dependent from the proton independent rate constants. Unless quenching effects are small, all of the rate constants cannot be determined solely by time dependent methods without measurements of the pre-exponential factors. Equation (A18) may be solved for the ratio of the two pre-exponential terms to yield a_1 as shown below:

$$N_1/N_2 = (a_1 - G_2)/(G_1 - a_1) \qquad (7)$$

or

$$a_1 = [G_1(N_1/N_2) + G_2]/(1 + N_1/N_2) \qquad (8)$$

where N_1 and N_2 are the pre-exponentials for the G_1 and G_2 exponential terms, respectively, and a_1 is given by (A2) and (A3). The term

"a_1" can be calculated from Eq. (8) if the exponentials G_1 and G_2 are known. A plot of of a_1 versus hydrogen ion concentration will result in $k_1 + k$ from the intercept and k_q from the slope. The problem then reduces to the case where the quenching of the neutral is ignored (explained in the Appendix). However, experimental techniques are often not able to assess accurately the pre-exponential factors. Other techniques are better suited to gain this same kinetic information.

The steady state measurements reported here were designed to provide reliable quantum yields. The quantum yields can be obtained simply from the peak intensity of the emission for each species. The model assumes that the intensity at any point in the emission spectrum of each species is dependent only on the kinetic rate law, (A46) and (A47). Therefore, each wavelength of the emission mirrors the same excited state and the same reactive rates. Peak responses are chosen since they give the maximum dynamic range. Of course, shifts in the peak maximum or changes in the shape of the emission curves are not accounted for in the model. Their occurance shows that the real system may be deviating from the model. Unlike the time dependent analysis, the steady state method is unable to determine the various rate constants. The steady state method can, however, relate the various rate constants to one another. However, an absolute, temporal measurement must eventually be made. Normally, the individual rates of decay of the two excited species in the absence of proton transfer are determined. In the absence of ESPT these states are decoupled and the kinetics are simplified. These temporal measurements are usually easy to perform and display simple, single exponential kinetics. All that is required experimentally are two liquid solutions. One solution,

at a pH much less (two or more pH units) than the pK_a^*, is used to determine the time resolved emission from the isolated neutral species. The other solution, at a pH much greater than the pK_a, is selected for the determination of the anion. As discussed in the Appendix, the assumption is that these solutions do not introduce new decay channels (which changes k and k') nor are the other rate constants affected by these pHs. If those assumptions are all true and if the lifetimes are known, then all the rate constants may be determined from the steady state analysis.

C. Method of Analysis

Both time dependent and steady state methods may be used independently under favorable circumstances to analyze all the processes which occur in an ESPT reaction. In many real systems like 1-naphthol, the model consists of complex kinetics. Also, the data is too difficult to be obtained reliably in any one set of experiments. The most informative method is to combine the features of both techniques. This section will describe the specific equations used in the the analysis.

The starting point of the analysis is obtaining the data. For the 1-naphthol system the rapid kinetics demand the use of picosecond methods to obtain reliable, time resolved fluorescence data. This combination makes possible the determination of the exponential decays, G_1 and G_2, from either the neutral, or the anion, or both. A sensitive spectrofluorimeter with low dark counts and high sensitivity is also required for this particular molecule. Since the natural lifetime, $1/k_f$, is much longer than the decay time, $1/\Sigma k_i$, for the neutral species, the quantum yield of fluorescence is very small. This small yield, coupled with the sizable emission from the anion, means that

differentiation of the two species will be difficult, even though their respective emission maxima are well separated. Evaluation of the fluorescence intensity of each species at several pHs will yield steady state quantum yields according to Eqs. (A46) and (A47).

The most useful solvent condition to begin the analysis of the data is at neutral pH (pH 6-7). In this region some important considerations prevail. First, since the solution pH is less than the ground state pK_a (9.2), only the neutral is excited, as required by the initial conditions of the model. Second, since the solution pH is greater than the excited state pK_a*, ESPT will occur. (The pK_a* may be estimated using the Förster cycle to be less than 3.[4,6,33]) Thirdly, the most important aspect of this pH region is that the bimolecular processes which are dependent on the proton concentration will be negligible compared to the other rates. The third point suggests that the kinetics will be much simplified at this pH. The reciprocal of the anion lifetime at this neutral pH gives the first rate constant, k'. Since quenching is negligible, the model requires that the sum of the relative quantum yields is 1 (see the arguements leading up to Eq. (A64)). The relative quantum yield of the anion is obtained by a measuring the ratio of the fluorescence maxima at this pH relative to a high pH (much greater than the pK). The individual spectra are first normalized to the absorbance and lifetimes as given by (A53)-(A55). The relative yield of the anion and the fluorescence spectrum of the neutral at pH 6-7 will give the quantum yield of that species in the absence of proton transfer and quenching, ϕ_N' (A59). The values for the relative yields at all the pHs can then be determined for both species. Kinetic information is obtained by the use of Eqs.

(A65a) and (A65b). Moreover,

by combining (A65a) with (A69) we obtain, at neutral pH:

$$\phi_A/\phi_A'(\text{pH } 7) = k_1k'/D_7 = k_1/(k_1 + k) = k_1/G_1(\text{pH } 7) \qquad (9)$$

The determination of G_1(pH 7), obtained from the time dependent analysis of the fall time of the neutral or the rise time of the anion, will give two more rate constants, k_1 and k. A reasonable estimate for the excited state pK_a^* is now possible. Since most reprotonation rates, k_2, lie between 10^{10} and 10^{11} $M^{-1}sec^{-1}$, therefore, within a single pK_a unit range, the pK_a* is given by: $-\log (k_1/5x10^{10})$.

No conclusions can yet be drawn about the quenching rates nor the exact size of the reprotonation rate at this pH. To find these rates, additional analyses are needed. However, the analysis schemes vary depending on the degree of quenching in the model. What is described below is a method which considers the quenching of both the neutral and the anion by protons.

Two steady state and two time dependent plots can be made as functions of (H^+): equations (A71),(A66b) and (A72),(A73), respectively. The plot of (A71) versus (H^+) gives the ratio, k/k_1 (intercept), and the sum, $k_2 + k_q'$ (slope). This calculation is possible because k' has already been determined. Equation (A66b) yields direct information about the quenching terms. The lefthand side of Eq. (A66b) is plotted versus $[1 + (k_2 + k_q')(H^+)/k']$. Since the ratio, k_1/k, and the sum $(k_2 + k_q')$ are known from (A71) and k' is known, k_q' (intercept) and k_q/k (slope) can be determined. Using the value of k measured at neutral pH, Eq. (9), all the rate constants are calculable. Equation (A66b) is dependent on accurate values from

(A71) and is prone to large scatter of the plotted points. Equation (A72) and yields rate constants similar to those from Eq. (A71). A plot of $G_1 + G_2$ versus (H^+), with k' known, gives $k_1 + k$ (intercept) and $k_2 + k_q + k_q'$ (slope). Equation (A73) can be rewritten as

$$G_1 * G_2 = [k_1 + k + k_q(H^+)][k' + (k_2 + k_q')(H^+)] \qquad (10)$$

and then redefined as

$$G_1 * G_2 - k_3 k_4 = -k_1 k_2 (H^+) \qquad (11)$$

The values for k_3 and k_4 come from a combination of the other three equations. This equation, like (A66b), is more involved and is dependent on previous results. In addition, it consists of products and differences of very large numbers. Nonetheless, this plot does give a direct measure of k_2 (slope) if k_1 is found by other means (Eq. (9), for example). All together these calculations should provide the best possible average. The accuracy of these equations can be checked by the calculations performed on the numerical model (described in Section E). First, the corrections which must be applied to the hydrogen ion concentration are discussed.

D. Calculations of the Acid Strength

Two types of corrections must be considered for ionic solutions, such as HCl dissolved in water. First, the proton concentration must be converted to activity. Second, Weller[4] has shown that a correction must be made for the ionic screening effect if the derived kinetic parameters are to be independent of the ionic strength of the solution. This screening effect is important only for rates involving ionic species, namely the processes involving the anion and protons. These two effects are somewhat related and an exact and appropriate

treatment of them has not been previously carried out. In this study corrections were made for all the solutions to reflect the hydrogen ion activity, (H^+). A second factor, $F_\pm$, as defined by Weller, was used to correct for the ionic screening and was applied to these activities. The form of each of these corrections is explained below.

The activity coefficient, $\gamma_\pm$, was calculated from Eq. (12) for the thermodynamic activity as derived empirically by Harned and Owens[68]:

$$\log\gamma_\pm = \frac{-0.502\sqrt{c}}{1+1.409\sqrt{c}} + 0.1312c + 0.0063c^2 - \log(1+0.03604m)-0.0004 \qquad (12)$$

where c is the concentration in moles/liter and m is the molality, given in terms of the concentration by

$$m = (-0.998 + \sqrt{(0.998)^2 + 4(0.018)c}\,)/2(0.018) \qquad (13)$$

This correction was used for all the titrated solutions (below pH 2). Since a properly calibrated pH meter reports activities directly, solutions measured by it need not be further corrected by an activity coefficient[69]. Equation (12) is reportedly valid to 4 M solutions of HCl.

The corrected concentrations were next used to determine the effective, ion-independent concentrations by the Debye equation[69] used by Weller:

$$-\log F_\pm = AZ_i^2\sqrt{I} \;/\; (1 + Ba\sqrt{I}\,) \qquad (14)$$

where the coefficients A, Z, B, and "a" refer to thermodynamic and stoichimetric quantities which were taken from Weller[4] to give:

$$\log F_\pm = -1.02\sqrt{c} \;/\; (1 + 2\sqrt{c}) \qquad (15)$$

where c is now the hydrogen ion activity. The range over which Eq.

(15) is applicable is not known. In Chapter four, these corrections are explicitly used by plotting versus $(H^+)*F_\pm$ rather than just (H^+). The ionic screening is therefore eliminated in interactions between the anion and protons (reflected in the rate constants, k_2 and k_q'). However, these plots would over-correct the interaction between the neutral and protons (given by the constant, k_q) by the factor $F_\pm$. Therefore in the Appendix, expressions containing k_q should be read as $k_q/F_\pm$ and (H^+) should be read as $(H^+)*F_\pm$.

This ionic screening term is explicitly dependent on the hydrogen ion concentration. Therefore, this correction factor introduces a non-linear proton dependence. By incorporating this factor into the hydrogen ion activity in the plots, the non-linearity is removed. The isolation of this non-linear factor is possible for each equation except Eq. (A72), which is explicitly written as

$$G_1+G_2 = (k_1+k+k') + (k_2 + k_q/F_\pm + k_q')(H^+)*F_\pm \qquad (16)$$

Equation (16) is explicitly non-linear in proton concentration. Thus, a plot of $G_1 + G_2$ versus either (H^+) or $(H^+)*F_\pm$ cannot yield a straight line. However, Eq. (16) will be plotted as a linear equation, neglecting the effect of the factor, $F_\pm$. The accuracy of this approximation will be verified by the assessment of the linearity of the computer plot for this equation.

E. Computer Modelling

Exact solutions exist for both the time dependent and steady state analyses for the ESPT reaction scheme. Therefore, calculations based on the model can be compared to the real data. This comparison

establishes the pH regions and the kinetic conditions where the model is appropriate. Two types of information will be generated for comparison: 1) simulated data and 2) numerical plots.

The simulated data follow Eqs. (A18) and (A19) for the generation of time resolved traces, as would be found from time dependent analyses. Since the important aspect of these time resolved spectra are the shapes and not the intensities, they can be scaled to match the of the raw data. For direct comparison to the raw data, these fluorescence traces are convolved with a model excitation pulse (see Chapter two for the details of the convolution technique) and are plotted on the same time scale as the streak camera data. Simulated data plots of both the neutral and the anion relative quantum yield versus pH were made based on Eqs. (A65a) and (A65b). Thus, these plots are also directly comparable to the plots based on the raw data.

The graphical plots follow the equations specified in Chapter three, Section C. By definition these plots must be linear, except in the case of Eq. (16). The absolute numbers from the simulated data can be dirctly compared to the experimental values.

The only information supplied to make both the simulated data and the graphical plots are the six rate constants specified by the ESPT model. A comparison of the simulated and experimental data thus provides a test of this ESPT model. The results of these comparisons are presented in the next chapter.

Chapter Four

Results and Discussion

A. Introduction

It has long been known that adiabatic proton transfers can occur on exited potential energy surfaces[2]. The details of the dynamics of this general class of photochemical reactions may be understood on many levels. From Förster cycle calculations to multicomponent kinetic analyses, increased awareness is gained as the full scope of the many processes involved in ESPT reactions are developed. Much has been learned by observing the ESPT process as a function of the solute structure or the conditions of the solvent environment. The possibility exists to probe these interactions by observing the changes that occur in the forward proton transfer rate constant, k_1. This rate can be measured directly if it is the dominant process in the ESPT reaction. Measurements of the lifetime of the initially excited species determine the proton transfer rate in these cases and serve as the probe of structural and environmental effects. Since the ESPT reaction can act as a very rapid "stop watch", fundamental processes whose interaction times are very short may be observed.

There is, as yet, little information on how to predict, a priori, ESPT rate constants. Similarly, little is known about the relative importance of the various ESPT rates, especially the forward proton transfer rate. If the lifetime of the initially excited species can be isolated, then k_1 can be determined. The rate constant k, is then derived from the lifetime of this species at neutral pH (assuming, of course, that $pK_a^* \ll pH\ 7 \ll pK_a$). In the special cases where the

proton transfer quantum yield is approximately equal to 1 (see Eq. (A74)), k_1 is the dominant rate (relative to k) and may be directly measured. In either case, isolation of k_1 from the other processes can be made in any experiment at neutral pH conditions.

This study has focussed on the ESPT reactions of 1-naphthol for three reasons: 1) prior to this work, the precise relationship between all of the rate processes was not known, 2) historically, the molecule showed anomalous behavior compared to similar molecule 2-naphthol, and 3) the fast forward ESPT rate has the potential for being a fast "stop watch" with which to investigate solute/solvent interactions. In order to ascertain the details of the ESPT process in 1-naphthol and to evaluate the validity of the model, the full kinetic scheme was determined for 1-naphthol in H_2O and D_2O. The three sections of this chapter present the results obtained in this investigation and a discussion of their significance. These sections give the details describing: 1) the general observables from the experimental measurements, 2) the analysis according to the model scheme, and 3) the investigations of solvent structure via ESPT in 1-naphthol.

B. Experimental Observables

As has been generally observed for molecules undergoing ESPT[2], the absorption and emission spectra of 1-naphthol reveal important information regarding the various ESPT processes. The absorption spectra of 1-naphthol in H_2O and D_2O, Fig. 19, point out the very different spectral properties of the two ground state forms of 1-naphthol: the neutral (1-naphthol), and the anion (1-naphtholate). The anion absorption spectrum taken at pH (pD) > 12 is both signifi-

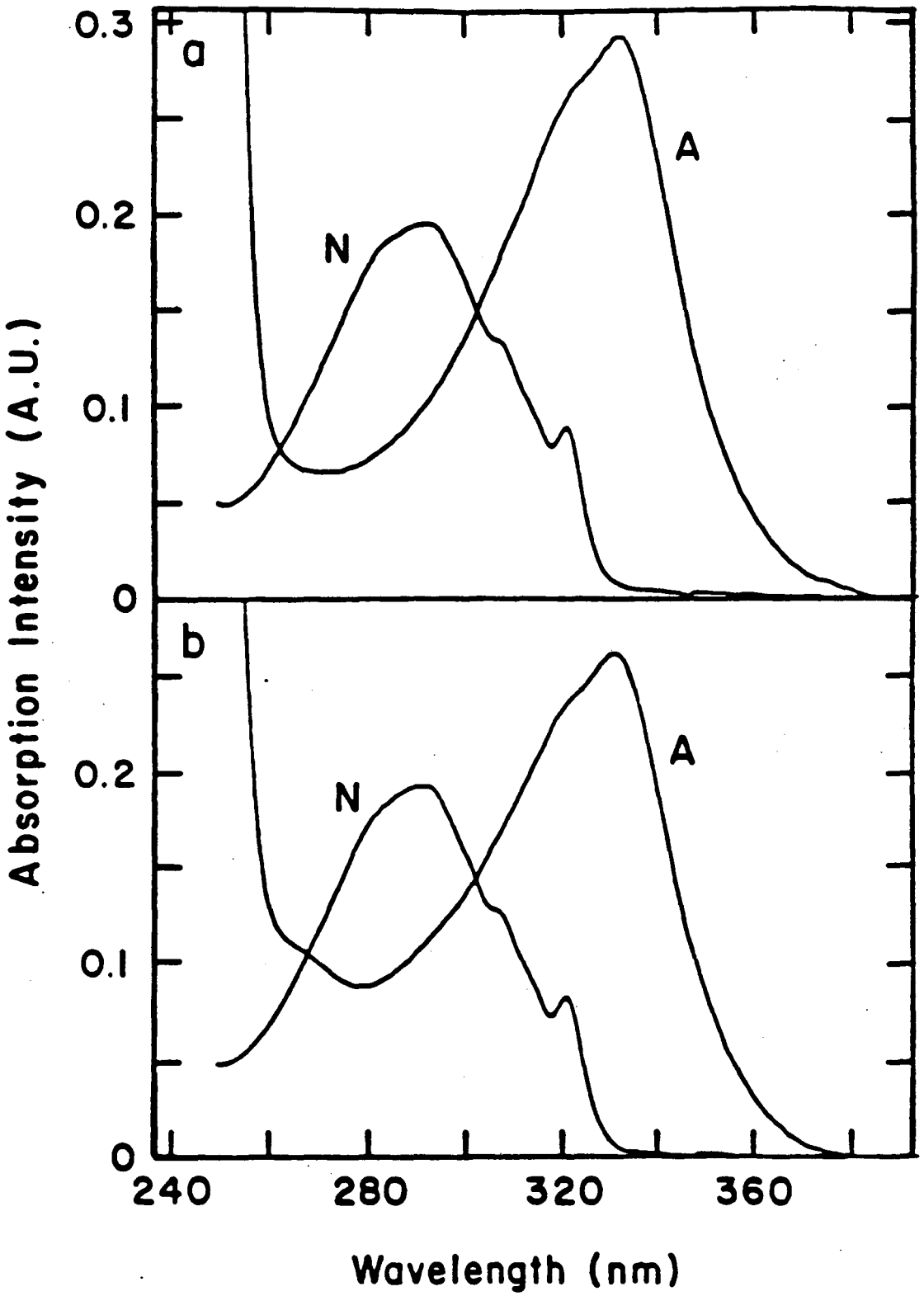

Fig. 19: Absorption spectra for the neutral (N) and anion (A) in H_2O (trace a) and D_2O (trace b). The traces show that the absorption isosbestic points for both solutions occur at approximately 303 nm.

cantly red-shifted and more diffuse (less structured) than that of the neutral taken at pH (pD) = 7. In comparison to the neutral, these features in the anion spectrum are generally indicative of a higher degree of solvent interaction[28,43]. Such differences are expected, when comparing an ionic and an uncharged species in solution. The difference between the absorption maxima is expected to be reflected in an equivalent separation in the emission spectra. Finally, in the ground state no difference is apparent in the interactions between 1-naphthol and either of the two solvents.

The emission traces, Figs. 20 and 21, demonstrate the result that was puzzling to investigators in the 1930's and 1940's. Later these traces were recognized as the characteristic spectral signature of an excited state proton transfer. Each trace in the figures was taken at a pH well below the ground state pK_a, so that only the neutral was excited. The dominant fluorescence, however, is at 480 nm, identical to the emission found from exciting the anion directly in a pH 12 solution. In the case of 1-naphthol, the fluorescence from the anion is the dominant signal with an intensity nearly 100 times larger than the fluorescence from the neutral species. In fact, the spectra of Figs. 20a' and 21a' display all the spectral features that are usually reported at <u>any</u> pH for this molecule. The spectra on the left side of these figures show the emission of the neutral which can be accurately obtained only by subtracting out the large anion component. The spectra labeled c' (pH 1.4 and pD 1.7 for the two solvents) show both species prominently as the pH is now low enough to cause proton dependent rates to reduce selectively the signal from the anion to a level more comparable to the uncharged neutral.

Fig. 20: Emission spectra for the neutral (left) and anion (right) at various pHs in relative intensity units. The pHs (corrected) are: 5.3 (a,a'), 2.2 (b,b'), 1.4 (c,c'), 0.9 (d'), 0.4 (e,e'), -0.3 (f). The neutral spectra have been obtained by subtracting off the normalized anion signal (from a pH 12 solution). Trace a has been spline-smoothed to reduce some of the noise (no difference in the peak response). Note the different intensity scales between the neutral and the anion. Trace c' shows the neutral signal (shoulder at 380 nm) which is given in c by this subtraction method of the anion signal.

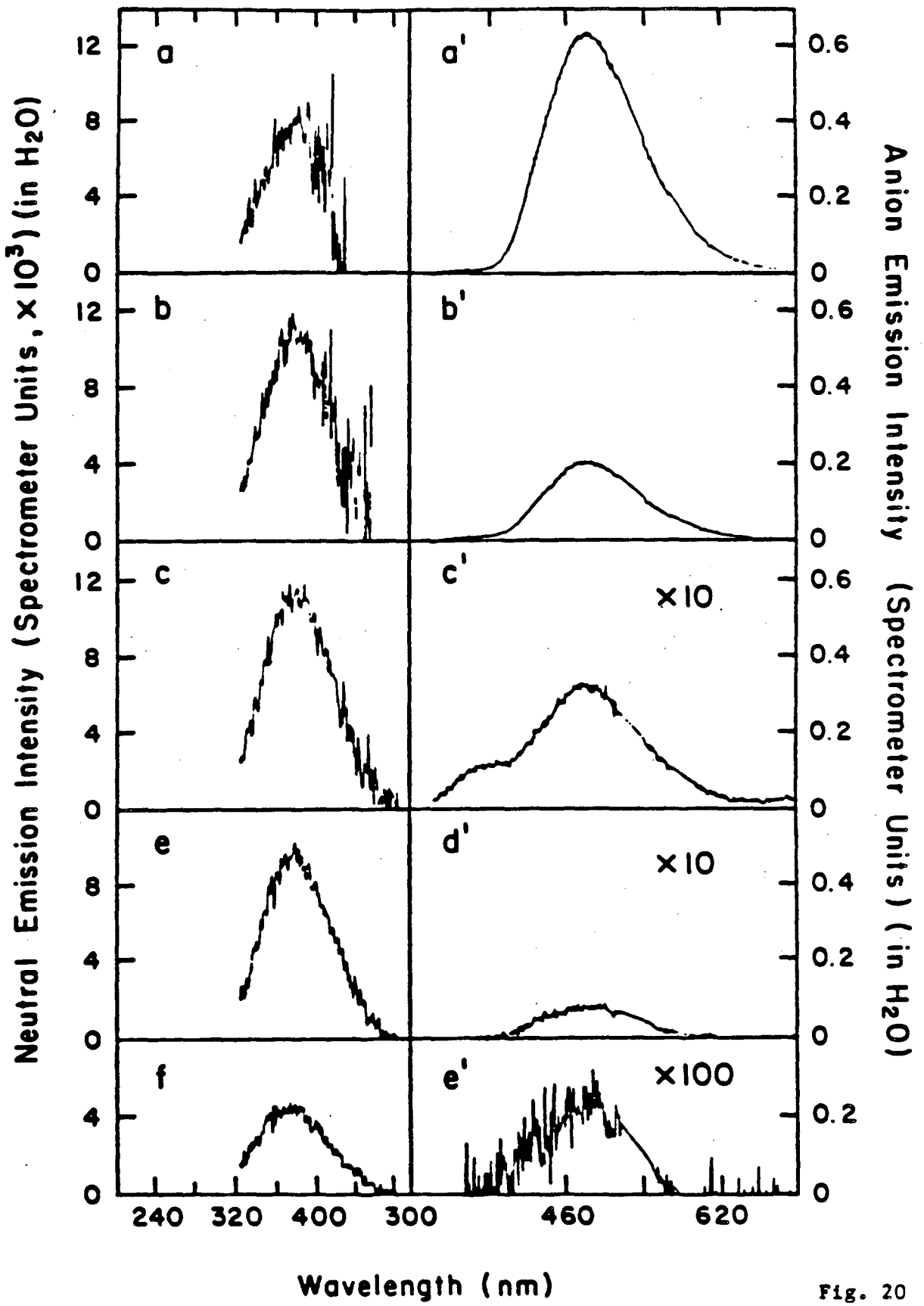
Neutral Emission Intensity (Spectrometer Units, × 10³) (in H₂O)
Anion Emission Intensity (Spectrometer Units) (in H₂O)
a
a'
b
b'
c
c'
×10
e
d'
×10
f
e'
×100
12
8
4
0
0.6
0.4
0.2
240
320
400
300
460
620
Wavelength (nm)

Fig. 20

Fig. 21: Emission spectra for the neutral (left) and anion (right) at various pDs in relative intensity units. The pDs (corrected) are: 6.5 (a,a'), 3.1 (b,b'), 1.7 (c,c'), 0.9 (d,d'), 0.4 (e,e'). The neutral spectra have been obtained by subtracting off the normalized anion signal (from a pH 12 solution). Trace a has been spline-smoothed to reduce some of the noise (no difference in the peak response). Note the different intensity scales between the neutral and the anion. Trace c' shows the neutral signal (shoulder at 380 nm) which is given in c by this subtraction method of the anion signal.

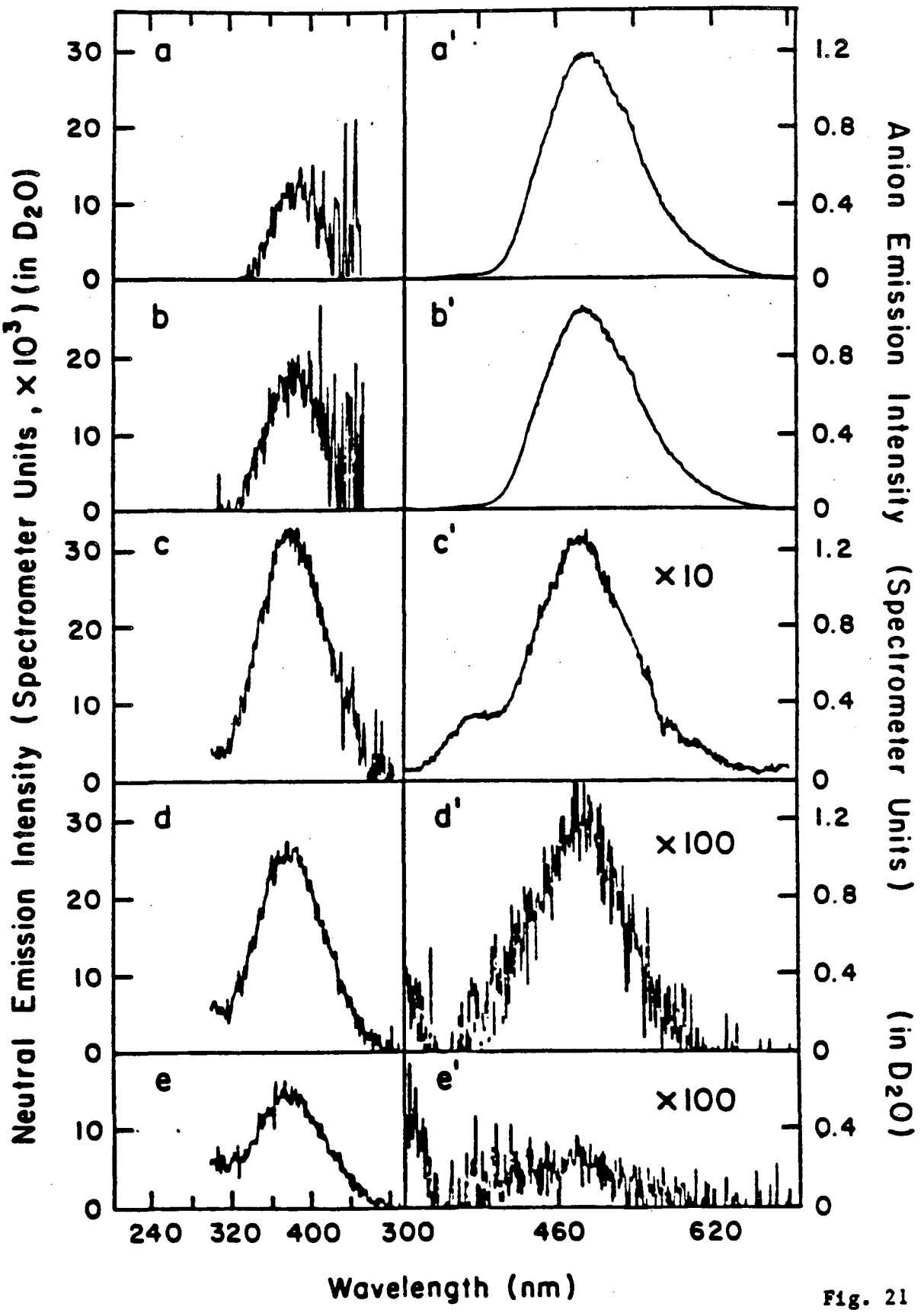
a
a'
b
b'
c
c'
×10
d
d'
×100
e
e'
×100
Neutral Emission Intensity (Spectrometer Units, ×10³) (in D₂O)
Anion Emission Intensity (Spectrometer Units) (in D₂O)
Wavelength (nm)
240
320
400
300
460
620

Fig. 21

The signal from the neutral never gets larger than 1.5 times its value at neutral pH (Figs. 20a and 21a). This small signal can be detected only with a sensitive fluorimeter. For the highly acidic solutions, the neutral response (measured in concentrated acid) has been subtracted from the anion.

The large spectral separation of the neutral and the anion (380 nm and 480 nm, respectively) can be exploited to obtain temporal measurements of each species, independently, by spectral filtering. A comparison of the time resolved emission intensities from the anion at pH 12 and pH 7, Fig. 22a, provides evidence that some additional process is occurring in the pH 7 case. The pH 12 emission from the anion displays an "instantaneous" rise within the instrument resolution, consistent with the fact that this species was directly excited. The slow rising fluorescence at pH 7 is indicative of the formation of an intermediate state(s) prior to the generation of the excited anion. Since at this pH the initially excited species is the neutral form, this rise time strongly suggests that an adiabatic ESPT process is occurring. Further supporting evidence comes from the measurement of the excited neutral lifetime at the same pH, Fig. 22b. The match (within experimental error) of approximately 33 ps for the fall time of the neutral and the rise time of the anion is direct proof that these species are coupled, as expected in an ESPT reaction. The low quantum yields for the neutral observed in the steady state spectra would predict and are consistent with the very fast decay time observed for this species.

The temporal data requires careful analysis to extract accurate kinetic parameters. The integrated rate equations, (Eqs. (A18) and

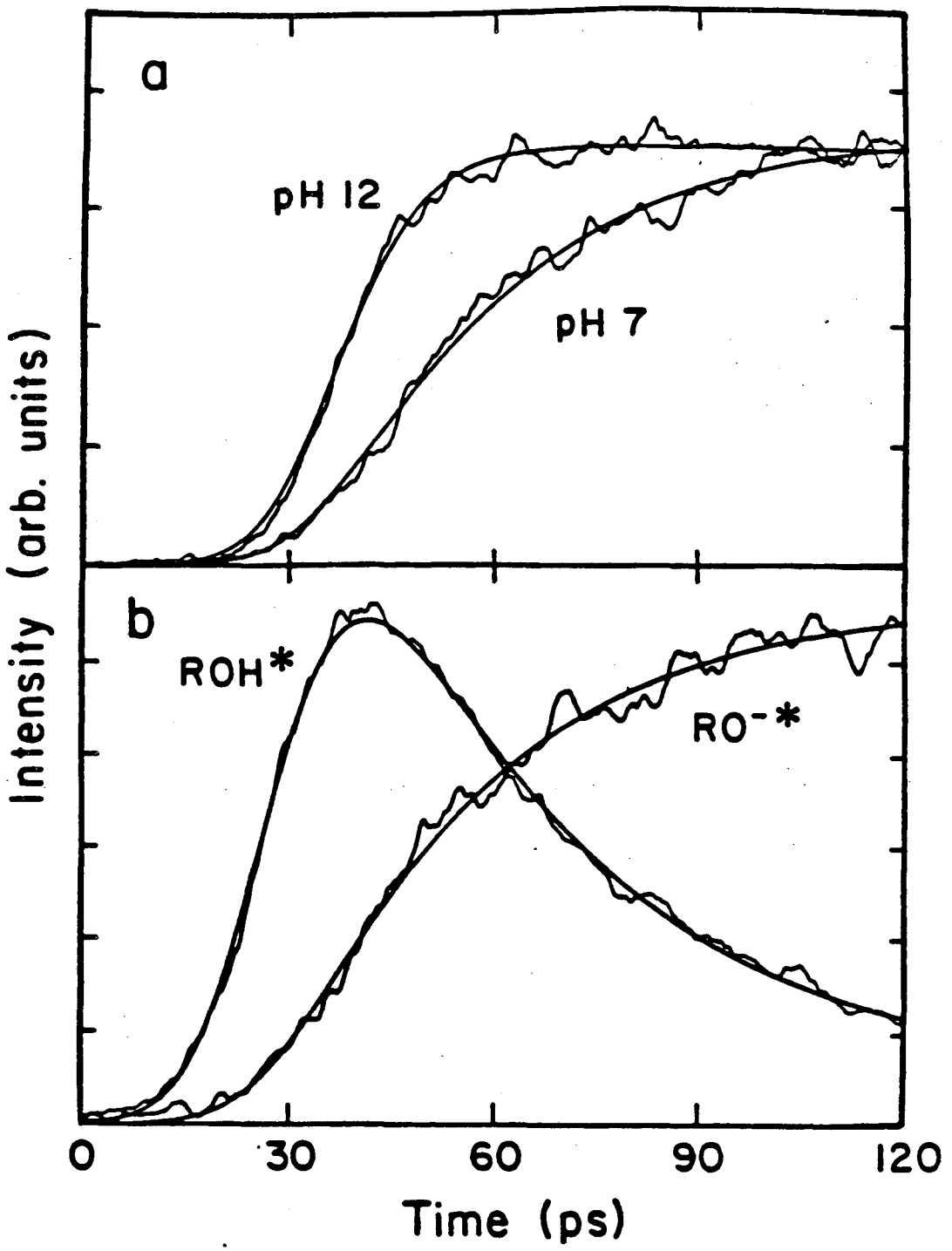

Fig. 22: Time resolved emission data for the fluorescence of the neutral and anion. Trace a presents the 1-naphtholate rise time at two pHs: pH 12 where the anion is directly excited and shows prompt emission, and pH 7 where the neutral is directly excited and produces the anion by the ESPT process. Trace b compares the emission kinetics of the neutral (ROH*, 350 nm detection) and anion (RO^-, 550 nm detection) at pH 7. Both the fall (neutral) and rise (anion) times show the same response time of 33 ± 5 ps.

(A19)) indicate that the exponential factors G_1 and G_2 may be obtained from analysis of the fluorescence lifetime of either excited species. Due to the complexity of the pre-exponential terms, analysis of the anion (only one pre-exponential term) is more accurate. Also, the signal intensity from the anion is more intense than the neutral at most of the pHs studied. Further, the anion fluorescence may be collected through a broad, high wavelength pass filter. This collection condition maximizes the emission to the detector. Increasing the signal is important for the high acid solutions where the signal is particularly weak. However, time resolved emission measurments of both excited state species provides a cross-check on the exponential factors. The longer-lived (slower rate process described by G_2 is determined from the fall time of the anion. Figure 23 shows this decaying signal and its logarithmic plot of the intensity for the anion at pH 1.1. Since the production rate, G_1, is much more rapid, the effect of this rate process on the fluorescence of the anion is negligible on this time-scale. Therefore, the anion signal displays a single exponential decay with a time constant of 320 ps.

The change in G_2 with pH, from pH = 12 to pH = 0, is dramatically depicted by the anion decays shown in Fig. 24. A least squares analysis of the logarithmic plots of these intensity versus time plots yield the value of G_2. The values of G_2 are used as fixed constants in the determination of G_1 which requires analysis at higher time resolution. Therefore, the curve-fitting routine varies only one exponential to find the best-fit value of G_1 from both neutral and anion fluorescence data such as that shown in Fig. 22b. This procedure allows for the determination of G_1 from two separate pieces of data.

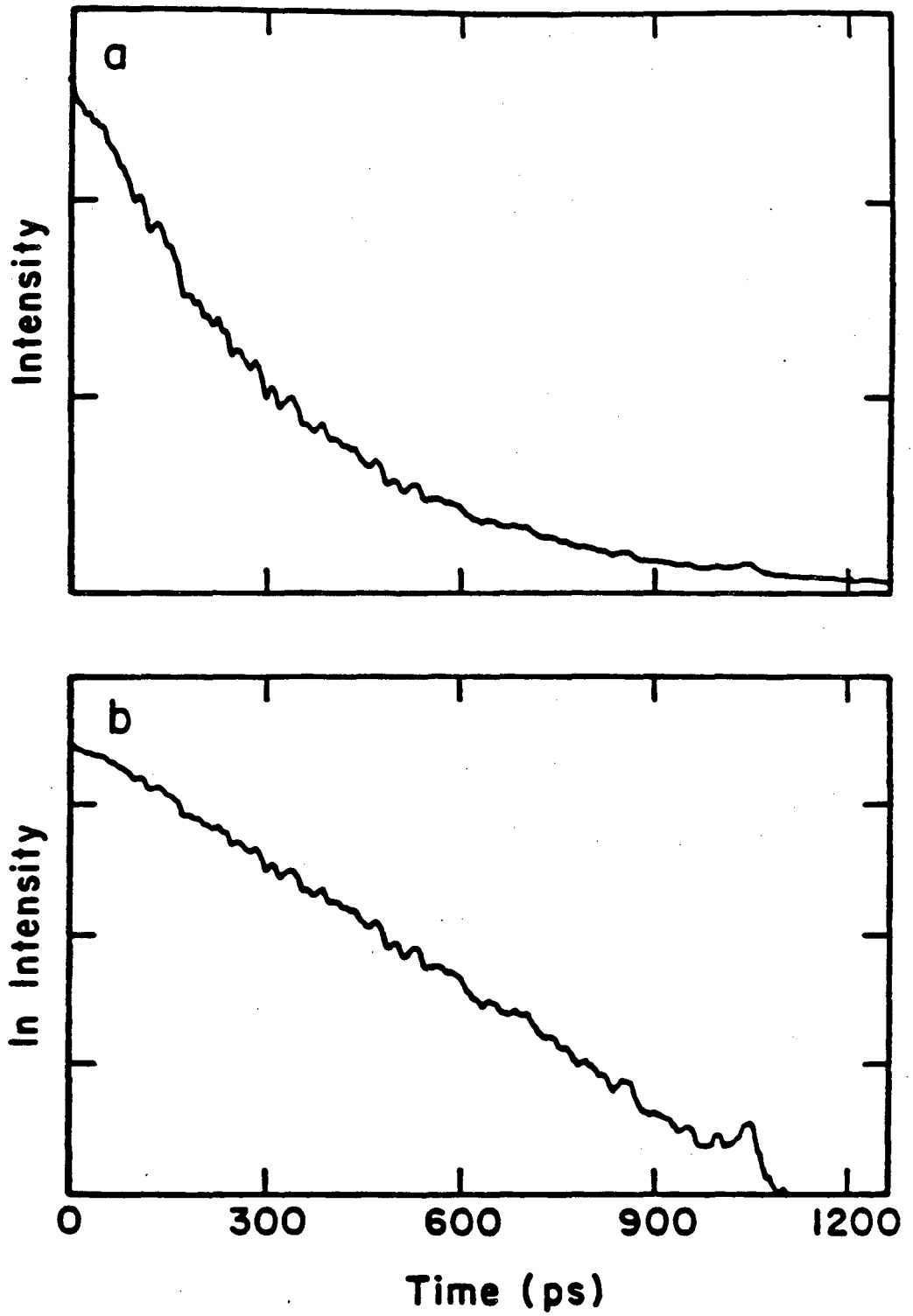

Fig. 23: Time resolved fluorescence signal (trace a) and semi-log plot (trace b) for 1-naphtholate at pH 1.1. Detection at 550 nm yields the decay of the "long lived" emission from the anion as given by $1/G_2$. The slope of the log plot determines the value for this decay as 316 ± 20 ps.

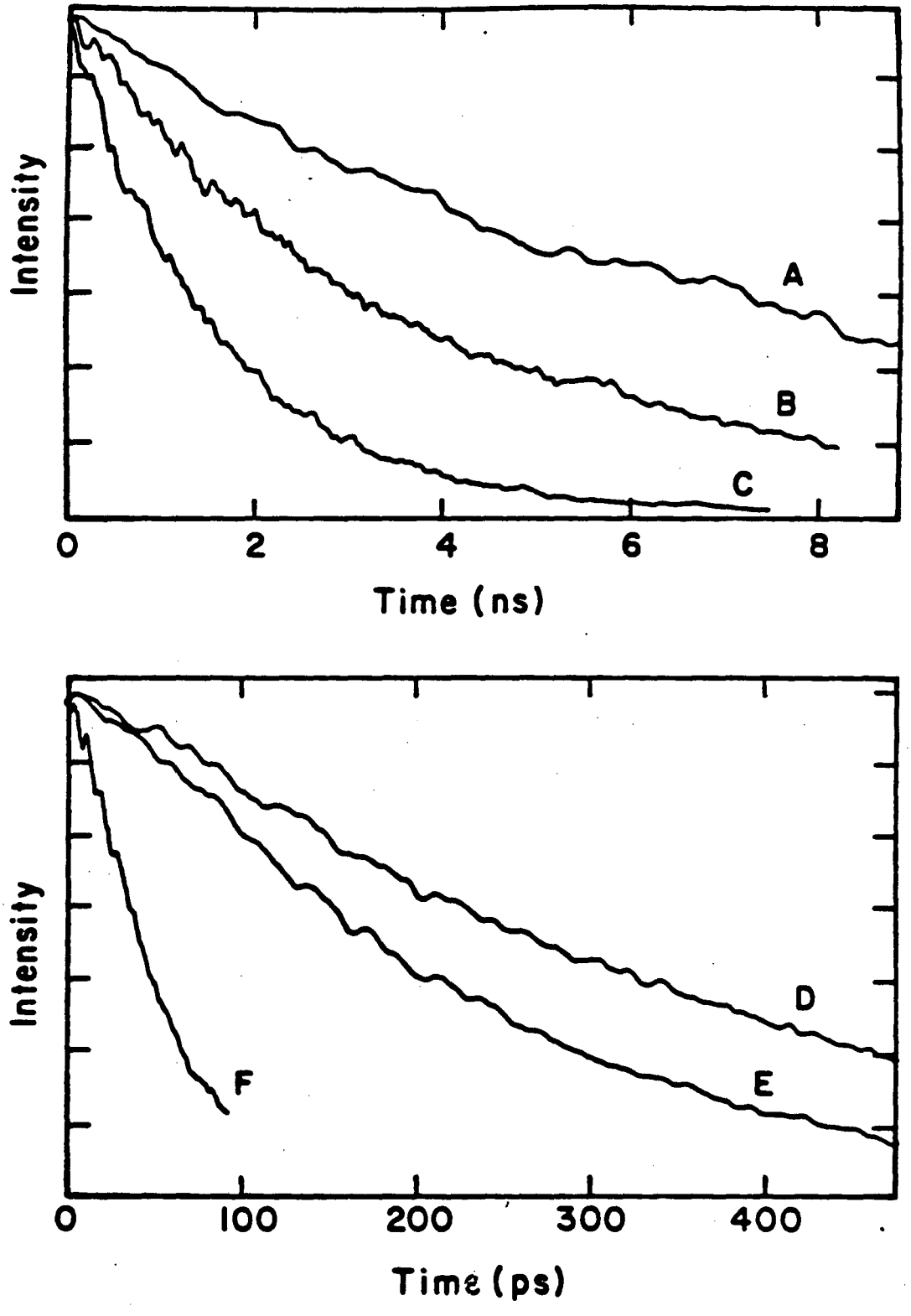

Fig. 24: Fluorescence decays of 1-naphtholate as a function of pH. The fluorescence decays A to F are the lifetimes at pH: 12, 2.8, 2.1, 1.2, 1.0, 0.0, respectively. Note the different time scales for the upper and lower plots.

An important aspect of the ESPT process is portrayed in the time evolution of the complete spectrum. At time zero, only the initially excited species contributes to the emission spectrum. The intensity of this spectrum will decay in time, as per the kinetic rate law. An additional spectrum, in this case that of the anion, will grow in at the rate of the neutral decay. Ultimately, the anion decays with its radiative lifetime, which is reflected by the decay of its spectrum. Each wavelength point in this composite spectrum is a linear combination of the spectra of the two species, dependent on the overall kinetics given by Eqs. (A18) and (A19). The amount of each component is determined by its emission intensity at that particular wavelength. At some wavelength the two pre-exponential terms for the G_1 exponential factor for anion and the neutral will be equal but opposite in sign and will cancel. The kinetics of the composite spectrum at this unique wavelength have only a single exponential term given by the decay rate G_2. This particular wavelength is called the isosbestic, or iso-emissive, point. All measurements of the intensity at this spectral point from time equal zero to times much less than the decay time, G_2, will have the same value. All other wavelengths will have intensities that change with time at a much faster rate than G_2. In fact, the composite spectra will change at the rate given by G_1. Only in a coupled, two state system will a clear isosbestic point exist. This feature can be used, therefore, for the identification of such a two state system[63].

Spectra in time, as mentioned in Chapter Two, may be generated by taking single temporal slices from a series of intensity versus time plots taken at many wavelengths. Such a series of wavelengths are shown for 1-naphthol in H_2O in Fig. 25. Time resolved spectra for

1-naphthol in H_2O, Fig. 26, and D_2O, Fig. 27, show the results of this analysis. These spectra are plotted over a time range where, except for the last time slice in each figure, the decay due to the G_2 process is negligible. Both spectra clearly show isosbestic points at 454 nm and 430 nm for H_2O and D_2O, respectively. The crude features of the spectra are due to the modest 10 nm resolution of the filters and the difficulty in analytically fitting the intensity versus time plots near the isosbestic point. Even at this low resolution the two state nature of the system is unmistakable.

C. Method of Analysis

The observations in the previous section suggest that the use of picosecond measurements can indeed enhance the understanding of ESPT reactions. In fact, picosecond time resolution is necessary for the 1-naphthol system. For a more complete knowledge of the processes occurring in 1-naphthol the full kinetic analysis, as explained in the Chapter three, is applied.

Much can be learned from the data obtained at neutral pH (Fig. 22b). Equation (9) describes the relationship at pH 7 between the forward proton transfer quantum yield and the measured rise time of the anion (or fall time of the neutral), G_1. Application of Eq. (9) requires a relative measurement of the steady state emission intensities of the anion at pH 7 and pH 12. This ratio of anion quantum yields represents the proton transfer yield. It describes the fraction of the anion produced via ESPT, relative to direct excitation of the anion. The closer this ratio is to one, the more excited state anion is being produced by the neutral species. A value of one for this

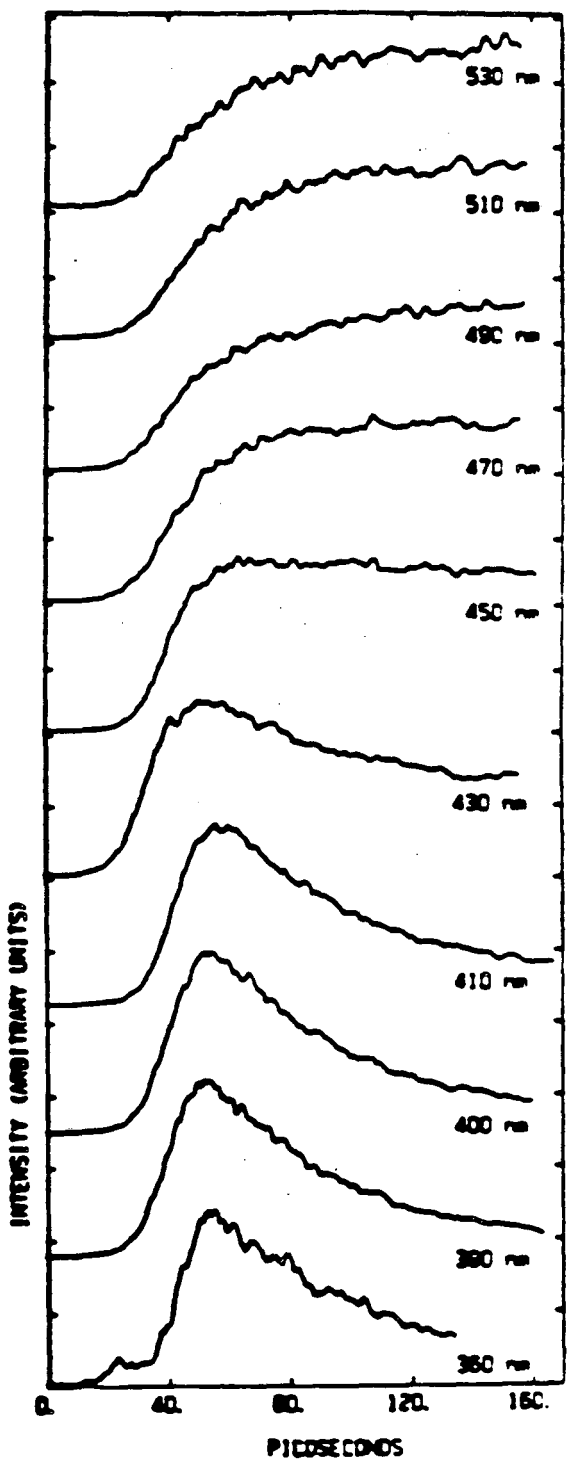

Fig. 25:
Time resolved plots of 1-naphthol at pH 6.5 as a function of detection wavelength. Ten nm interference filters select each of the fluorescence traces shown. These plots can be reanalyzed to create the time-evolving spectra given in Figs. 26 and 27.

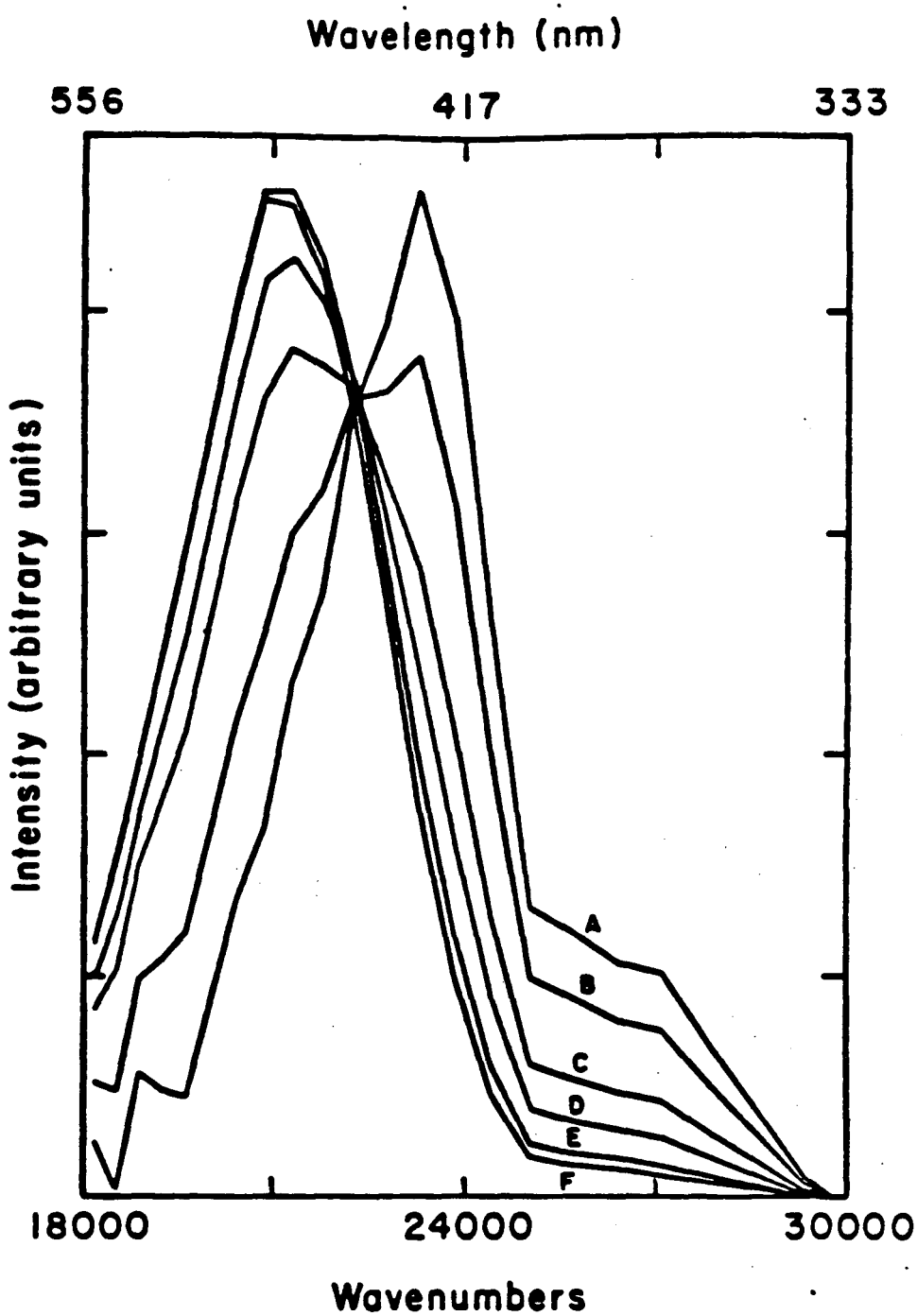

Fig. 26: Time-evolving spectra for 1-naphthol at pH 6.5 in H_2O. Each curve, A to F, represents a later time slice for the complete spectral response, which includes emission from both the neutral and the anion. Curves A to F are for the spectrum at: 0, 10, 30, 50, 90, and 400 ps, respectively. Note the clear isosbestic point (see text) at approximately 454 nm. Spectrum F misses the isosbestic point since at this time, 400 ps after excitation, a measurable degree of the excited state population, which is mostly the anion, has decayed. The spectra are plotted linearly in wavenumber (energy scale).

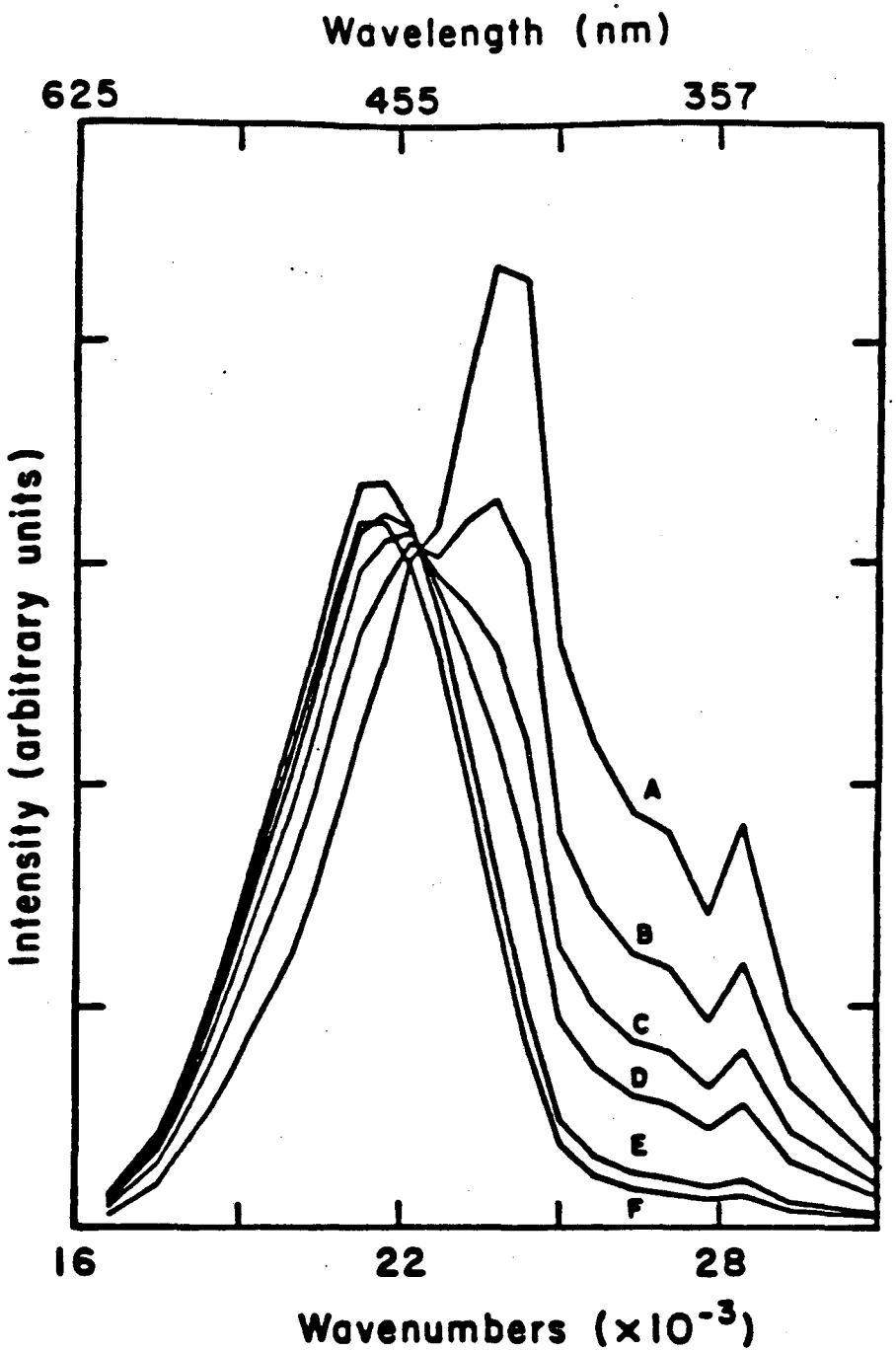

Fig. 27: Time-evolving spectra for 1-naphthol at pD 6.5 in D_2O. Each curve, A to F, represents a later time slice for the complete spectral response, which includes emission from both the neutral and the anion. Curves A to F are for the spectrum at: 50, 100, 150, 200, 400, and 1000 ps, respectively. Note the clear isosbestic point (see text) at approximately 430 nm. Spectrum F misses the isosbestic point since at this time, 1000 ps after excitation, a measurable degree of the excitated state population, which is mostly the anion, has decayed. The spectra are plotted linearly in wavenumber (energy scale).

ratio would mean that all the initially excited neutral molecules deprotonated before any other decay process occurred. The emission from the anion would then be of equal intensity at pH 7 (indirectly produced) as at pH 12 (directly excited). In all other cases, where competing processes deplete the neutral before deprotonation, the amount of anion will be correspondingly diminished. Since there are only two processes (k_1 and k) involving the neutral at pH 7, a measurement of the proton transfer quantum yield, given by this ratio of anion emissions, and G_1 will determine both of these rates (Eq. (9)).

Several procedures are possible for the determination of the relative yield of the anion emission. The most informative technique is shown in Fig. 28. Spectra a and b in Fig. 28 show the normalized excitation scans for 1-naphthol in H_2O for pH 12 and pH 6.5, respectively. These spectra have been normalized by dividing by the absorption spectra. The montitoring wavelength (excitation is scanned) is the peak response of the anion at 480 nm. According to Kasha's and Vavilov's rules[70], a single species will emit from the lowest vibrational level of the lowest excited state regardless of the initially-produced state. Thus, the expected result for Fig. 28a would be a line of slope zero. This expectation also stems from the fact that at these low concentrations, 5×10^{-5} M, the response of a spectrometer should obey Beer's law. Therefore both absorption and excitation spectra should yield the same response within a normalizing factor. This linearity is clearly not found in Fig. 28a and forewarns that instrumental discrepancies are prevalent. By the same argument, Fig. 28b would also be expected to be a line with zero slope, if the proton transfer process were wavelength independent. Within the limit of

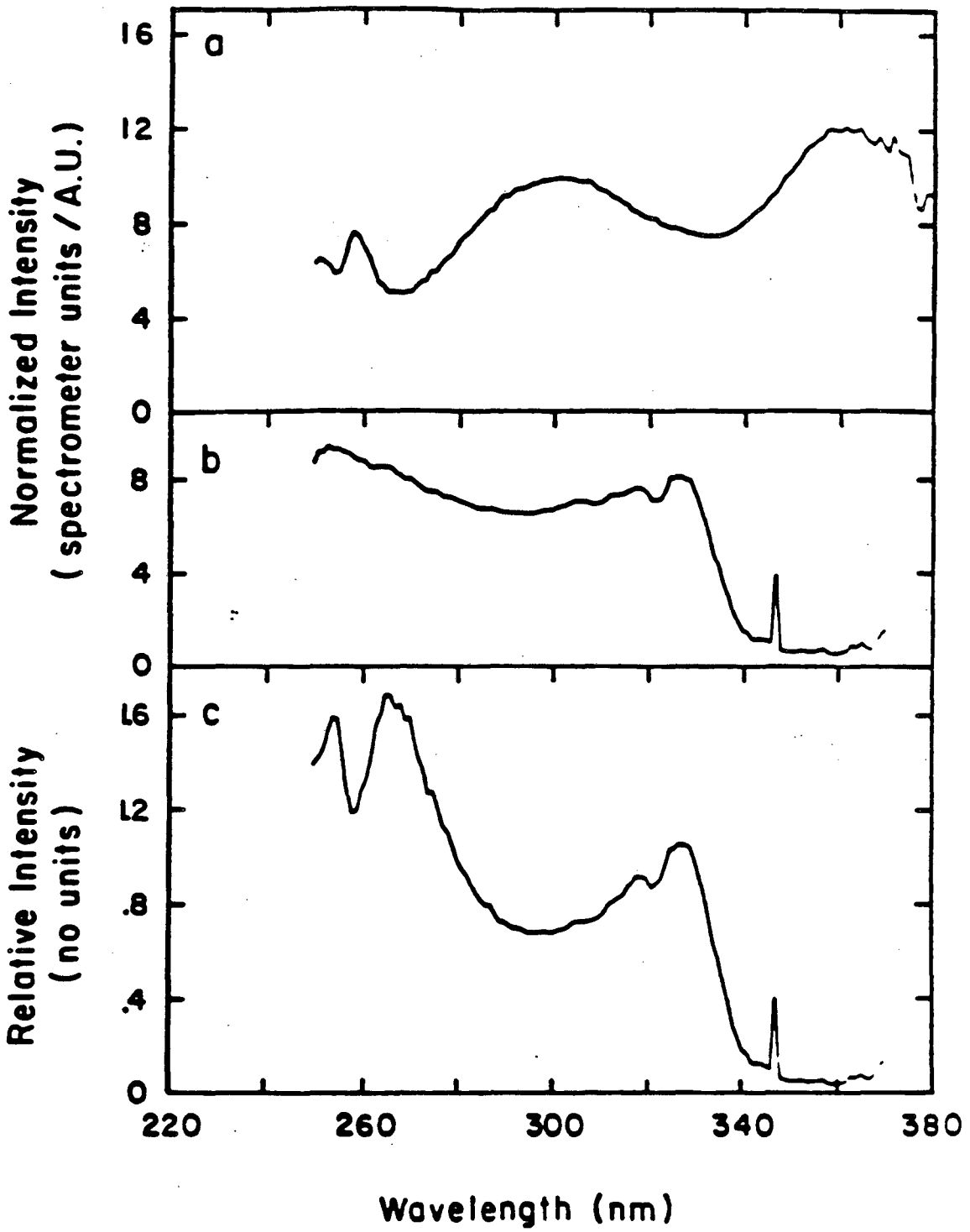

Fig. 28: Absorption normalized excitation spectra for the anion (a) at pH 12 and the neutral (b) at pH 6.5. The detection wavelength was the emission maximum of the anion at 480 nm. The ratio of these two spectra (b/a) produce the relative quantum yield for the anion which may be corrected to give the quantum yield for proton transfer (Φ_A/Φ_A'). The uncorrected value at the absorption isosbestic (303 nm) is 0.71.

the instrument the ESPT process is apparently wavelength independent (between 250 nm and 330 nm). The ratio of the spectra in Figs. 28b and 28a gives the spectrum in Fig. 28c and is precisely the quantity ϕ_A/ϕ_A'' (which is correctable to ϕ_A/ϕ_A'), but as a function of the excitation wavelength (see Eqs. (A53), (A54), and (A65a)). The plot in Fig. 28c, is also expected to be a line with zero slope, even if instrumental artifacts occur in the two other spectra. The effect of artifacts should cancel. Some cancellation is apparent but some nonlinearity remains, presumably due to intensity dependent instrumental artifacts. A small, single-valued region does exist from 285 nm to 310 nm. This region of the spectrum encompasses the 303 nm absorption isosbestic point of the neutral and the anion. Near this point the absorption and excitation intensities for the two species are most nearly equal. At the isosbestic they are identical. Therefore, the most complete cancellation of experimental artifacts will occur in this region. Therefore, the best method for the determination of the relative emission from the anion is by excitation at the absorption isosbestic[15,16].

The value for the relative anion emission intensities for 1-naphthol in H_2O, as seen in Fig. 28c, is measured to be 0.71. This ratio, ϕ_A/ϕ_A'', is not the final number but must be corrected to reflect the conditions at pH 7 (Eq. (A55)). The correction factor, τ_o'/τ_o'', is 0.94 (7550/8000) which gives the corrected value of 0.76 for ϕ_A/ϕ_A'. Using the measured rise time (or fall time) for the anion (or neutral), $1/G_1$, of 33 ps at pH 7.1 gives an estimate for k_1 of 0.023 ps^{-1} and for k (which equals $k_f + k_r$) a value of 0.007 ps^{-1} (Eq. (9)). An identical procedure for 1-naphthol in D_2O gives the following results:

absorption isosbestic ≅ 303 nm, $\phi_A/\phi_A'' = 0.66$, $\tau_o'/\tau_o'' = 17200/20000 = 0.86$, $\phi_A/\phi_A' = 0.77$, $1/G_1(pH7) = 105$ ps, $k_1 = 0.0073\ ps^{-1}$, and $k = 0.0022\ ps^{-1}$. A comparison between the two solvents is enlightening. There is little difference between the spectra in D_2O and H_2O. For example, the absorption spectra in both solvents have essentially the same isosbestic point. However, the steady state emission intensity for the anion in D_2O is greater than in H_2O, as is its lifetime. Both results are increased by nearly the same factor of two. The probability of proton transfer is essentially identical for the two, indicating that the ratio of the deprotonation rate, k_1, to the rate, k, is also unchanged by isotopic substitution. Thus, both k_1 and k must be equally perturbed by the isotope effect. The most interesting comparison is between the two k_1 values. The ratio of these two rates gives an isotope effect of about three. More about this isotope effect will be presented after the complete analysis.

These preliminary estimates portend intriguing results when all the rates are compared. Tables I and II present the pH(D)s used in the time resolved and steady state experiments with all the correction factors as explained in Chapter three. Tables III and IV list the picosecond data, while Tables V and VI present the values obtained from steady state measurements for H_2O and D_2O solutions, respectively. The steady state data in Tables V and VI have been normalized according to Eq. (A58) such that the sum of the relative quantum yields is unity at neutral pH.

Fluorescence titration curves are presented in Figs. 29 and 30. In these curves the relative quantum yield of the neutral (A) and the anion (B) are ploted verses the corrected pH. In both of these curves

Table I

$[H^+]_m$	pH	$\gamma_\pm$	(H^+)	$F_\pm$	$(H^+)*F_\pm$	pH_F
10^{-12}	12.	---	10^{-12}	---	---	---
7.9×10^{-8}	7.1	---	7.9×10^{-8}	1.0	7.9×10^{-8}	7.1
3.2×10^{-7}	6.5	---	3.2×10^{-7}	1.0	3.2×10^{-7}	6.5
5.0×10^{-6}	5.3	---	5.0×10^{-6}	0.99	5.0×10^{-6}	5.3
1.0×10^{-5}	5.0	---	1.0×10^{-5}	0.99	9.9×10^{-6}	5.0
1.0×10^{-4}	4.0	---	1.0×10^{-4}	0.98	9.8×10^{-5}	4.0
4.0×10^{-4}	3.4	---	4.0×10^{-4}	0.96	3.8×10^{-4}	3.4
1.3×10^{-3}	2.9	---	1.3×10^{-3}	0.92	1.2×10^{-3}	2.9
$2.5\times1-^{-3}$	2.6	---	2.5×10^{-3}	0.90	2.2×10^{-3}	2.7
7.9×10^{-3}	2.1	---	7.9×10^{-3}	0.84	6.6×10^{-3}	2.2
2.0×10^{-2}	1.7	0.876	1.8×10^{-2}	0.78	1.4×10^{-2}	1.9
3.2×10^{-2}	1.5	0.854	2.7×10^{-2}	0.75	2.0×10^{-2}	1.7
6.3×10^{-2}	1.2	0.820	5.2×10^{-2}	0.69	3.6×10^{-2}	1.4
7.9×10^{-2}	1.1	0.809	6.4×10^{-2}	0.67	4.3×10^{-2}	1.4
1.0×10^{-1}	1.0	0.797	8.0×10^{-1}	0.65	5.2×10^{-2}	1.3
1.6×10^{-1}	0.8	0.776	1.2×10^{-1}	0.62	7.4×10^{-2}	1.1
3.2×10^{-1}	0.5	0.757	2.4×10^{-1}	0.56	1.3×10^{-1}	0.9
6.6×10^{-1}	0.18	0.774	5.1×10^{-1}	0.50	2.6×10^{-1}	0.6
1.0	0.0	0.818	8.2×10^{-1}	0.47	3.8×10^{-1}	0.4
1.4	-0.13	0.883	1.2	0.45	5.4×10^{-1}	0.3
2.5	-0.4	1.21	3.0	0.40	1.2	-0.08
3.2	-0.5	1.49	4.7	0.39	1.8	-0.3
4.0	-0.6	1.98	7.9	0.37	2.9	-0.5
10.0	-1.0	30.4*	304.	0.32	9.7	-1.0

Table I shows the hydrogen ion concentrations, activities, and corrected values for the kinetic and steady state analyses. See the Theory chapter for the meaning of the $\gamma_\pm$ and $F_\pm$ corrections. Initial concentrations are in molarities.

* Extrapolated beyond the applicable range.

Table II

$[D^+]_m$	pD	$\gamma_\pm$ †	(D^+)	$F_\pm$ †	$(D^+)*F_\pm$	pD_F
10^{-12}	12.	---	10^{-12}	---	---	---
7.9×10^{-8}	7.1	---	7.9×10^{-8}	1.0	7.9×10^{-8}	7.1
3.2×10^{-7}	6.5	---	3.2×10^{-7}	1.0	3.2×10^{-7}	6.5
3.2×10^{-6}	5.5	---	3.2×10^{-6}	1.0	3.2×10^{-6}	5.5
2.5×10^{-5}	4.6	---	2.5×10^{-5}	0.99	2.5×10^{-5}	4.6
2.0×10^{-4}	3.7	---	2.0×10^{-4}	0.97	1.9×10^{-4}	3.7
7.9×10^{-4}	3.1	---	7.9×10^{-4}	0.94	7.4×10^{-4}	3.1
2.0×10^{-3}	2.7	---	2.0×10^{-3}	0.91	1.8×10^{-3}	2.7
2.5×10^{-3}	2.6	---	2.5×10^{-3}	0.90	2.2×10^{-3}	2.7
$5.0\times1-^{-3}$	2.3	---	5.0×10^{-3}	0.86	4.3×10^{-3}	2.4
1.0×10^{-2}	2.0	---	1.0×10^{-2}	0.82	8.2×10^{-3}	2.1
1.6×10^{-2}	1.8	0.89	1.4×10^{-2}	0.80	1.1×10^{-2}	2.0
2.5×10^{-2}	1.6	0.87	2.2×10^{-2}	0.76	1.7×10^{-2}	1.8
3.2×10^{-2}	1.5	0.85	2.7×10^{-2}	0.75	2.0×10^{-2}	1.7
5.0×10^{-2}	1.3	0.83	4.2×10^{-2}	0.71	3.0×10^{-2}	1.5
7.9×10^{-2}	1.1	0.81	6.4×10^{-2}	0.67	4.3×10^{-2}	1.4
1.0×10^{-1}	1.0	0.80	8.0×10^{-2}	0.65	5.2×10^{-2}	1.3
1.6×10^{-1}	0.8	0.78	1.2×10^{-1}	0.62	7.4×10^{-2}	1.1
2.7×10^{-1}	0.6	0.76	2.0×10^{-1}	0.57	1.2×10^{-1}	0.9
1.0	0.0	0.82	8.2×10^{-1}	0.47	3.8×10^{-1}	0.4
12	-0.06	0.84	9.7×10^{-1}	0.46	4.5×10^{-1}	0.35
2.0	-0.3	1.0	2.1	0.42	8.7×10^{-1}	0.06
5.0	-0.7	2.9*	14.5	0.35	5.1	-0.7

Table II gives the deuterium ion concentrations, activities, and corrected values for the kinetic and steady state analyses. See the Theory chapter for the meaning of the $\gamma_\pm$ and $F_\pm$ corrections. Initial concentrations are in molarities.

* Extrapolated beyond the applicable range.
† Same equation used as in the calculation for HCl.

Table III

$(H^+)*F_{\pm}$	G_1^{-1}(ps)	G_2^{-1}(ps)	G_1(1/ps)	G_2(1/ps)
10^{-12}	--	8000	---	1.25×10^{-4}
7.9×10^{-8}	33	7550	3.0×10^{-2}	1.3×10^{-4}
9.9×10^{-6}	29	7540	3.4×10^{-2}	1.3×10^{-4}
1.2×10^{-3}	25	6130	4.0×10^{-2}	1.6×10^{-4}
6.6×10^{-3}	34	3920	2.9×10^{-2}	2.6×10^{-4}
2.0×10^{-2}	35	1430	2.9×10^{-2}	7.0×10^{-4}
3.6×10^{-2}	27	800	3.7×10^{-2}	1.3×10^{-3}
5.2×10^{-2}	30	500	3.3×10^{-2}	2.0×10^{-3}
7.4×10^{-2}	25	320	4.0×10^{-2}	3.2×10^{-3}
1.3×10^{-1}	25	160	4.0×10^{-2}	6.1×10^{-3}
2.6×10^{-1}	24	78	4.2×10^{-2}	1.3×10^{-2}
5.4×10^{-1}	19	59	5.3×10^{-2}	1.7×10^{-2}
1.2	8	33	1.3×10^{-1}	3.0×10^{-2}
2.9	8	19	1.3×10^{-1}	5.3×10^{-2}

Table III presents the time resolved, kinetic results for 1-naphthol in H_2O as a function of pH, giving the best fit values to the exponential decay curves according to the ESPT kinetic model. All times are accurate to ± 10 % or 5 ps (whichever is larger).

Table IV

$(D^+)*F_\pm$	G_1^{-1}(ps)	G_2^{-1}(ps)	G_1(1/ps)	G_2(1/ps)
10^{-12}	---	20000	---	5.0×10^{-5}
7.9×10^{-8}	105	17200	9.5×10^{-3}	5.8×10^{-5}
3.2×10^{-6}	104	16800	9.6×10^{-3}	6.0×10^{-5}
7.4×10^{-4}	102	15200	9.8×10^{-3}	6.6×10^{-5}
1.8×10^{-3}	100	1200	1.0×10^{-2}	8.3×10^{-5}
4.3×10^{-3}	102	8150	9.8×10^{-3}	1.2×10^{-4}
1.1×10^{-2}	97	4200	1.0×10^{-2}	2.4×10^{-4}
1.7×10^{-2}	105	2400	9.5×10^{-3}	4.2×10^{-4}
3.0×10^{-2}	106	1300	9.4×10^{-3}	7.7×10^{-4}
5.2×10^{-2}	81	680	1.2×10^{-2}	1.5×10^{-3}
7.4×10^{-2}	85	500	1.2×10^{-2}	2.0×10^{-3}
4.5×10^{-1}	45	110	2.2×10^{-2}	9.3×10^{-3}
8.7×10^{-1}	43	83	2.3×10^{-2}	1.2×10^{-2}

Table IV shows the time resolved, kinetic results for 1-naphthol in D_2O as appropriate to the ESPT model. All times are accurate to ± 10 % or 5 ps (whichever is larger).

Table V

$(H^+)*F_{\pm}$	$\phi_N(x10^3)$	$\phi_A(x10^2)$	$\phi_N/\phi_N'^{\dagger}$	$\phi_A/\phi_A'^{\ddagger}$	$\phi_N/\phi_N'/\phi_A/\phi_A'$
$3.2x10^{-7}$	7.0	58.5	0.202	0.69	0.29
$5.0x10^{-6}$	8.3	64.0	0.240	0.76	0.32
$9.8x10^{-5}$	8.5	63.6	0.246	0.76	0.33
$3.8x10^{-4}$	8.5	56.2	0.246	0.67	0.37
$2.2x10^{-3}$	9.6	36.2	0.278	0.43	0.65
$6.6x10^{-3}$	11.0	20.4	0.318	0.24	1.33
$1.4x10^{-2}$	11.2	9.95	0.324	0.12	2.70
$4.3x10^{-2}$	11.3	3.29	0.327	0.038	8.61
$1.3x10^{-1}$	11.4	0.94	0.330	0.011	30.
$3.8x10^{-1}$	10.5	0.32	0.304	0.004	80.
1.8	7.1	0.15	0.205	0.002	114.
9.7	1.7	0.0	0.049	0.0	---

Table V gives the steady state results for 1-naphthol in H_2O. ϕ_N and ϕ_A are the absolute values (in uncalibrated spectrometer units) for the peak responses for the neutral and anion species, respectively.

† ϕ_N' is chosen such that the sum of the relative quantum yields ($\phi_N/\phi_N' + \phi_A/\phi_A'$) is equal to one at pH 5.3.

‡ ϕ_A' is chosen such that the relative quantum yield of the anion is 0.76 (corrected value, see text) at pH 5.3.

Table VI

$(D^+)*F_{\pm}$	$\phi_N(x10^3)$	$\phi_A(x10^2)$	$\phi_N/\phi_N'^{\dagger}$	$\phi_A/\phi_A'^{\ddagger}$	$\phi_N/\phi_N'/\phi_A/\phi_A'$
$3.2x10^{-7}$	12.5	118.	.22	.72	.31
$2.5x10^{-5}$	13.1	127.	.23	.77	.30
$1.9x10^{-4}$	14.9	127.	.26	.77	.34
$7.4x10^{-4}$	16.7	98.9	.29	.60	.48
$2.2x10^{-3}$	24.9	77.5	.44	.47	.94
$8.2x10^{-3}$	33.1	28.3	.58	.17	3.4
$2.0x10^{-2}$	34.1	13.3	.60	.081	7.4
$4.3x10^{-2}$	29.2	4.0	.51	.0024	21.
$1.2x10^{-1}$	27.0	1.3	.47	.0079	59.
$3.8x10^{-1}$	19.0	0.2	.33	.0012	275.
5.1	1.8	0.0	.03	.0	---

Table VI gives the steady state results for 1-naphthol in D_2O. ϕ_N and ϕ_A are the absolute values (in uncalibrated spectrometer units) for the peak responses for the neutral and anion species, respectively.

† ϕ_N' is chosen such that the sum of the relative quantum yields ($\phi_N/\phi_N' + \phi_A/\phi_A'$) is equal to one at pD 4.6.

‡ ϕ_A' is chosen such that the relative quantum yield of the anion is 0.77 (corrected value, see text) at pD 4.6.

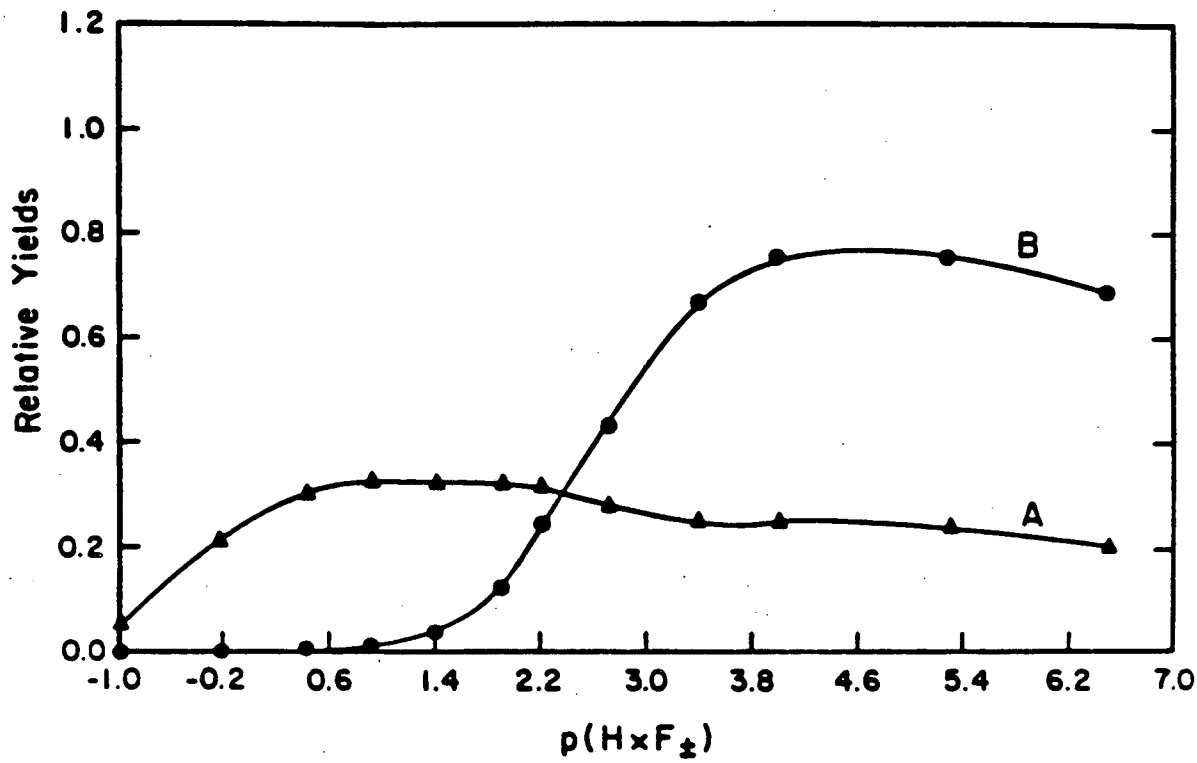

Fig. 29: Fluorescence titration curves for the neutral and anion in H_2O. Table V lists the relative quantum yields for the neutral and the anion, plotted here vs. pH (A and B, respectively). The pHs have been corrected for the ionic screening effect (see text). The relative yields were obtained by requiring the sum of both the relative yields of the neutral and the anion to equal one at pH 5.3.

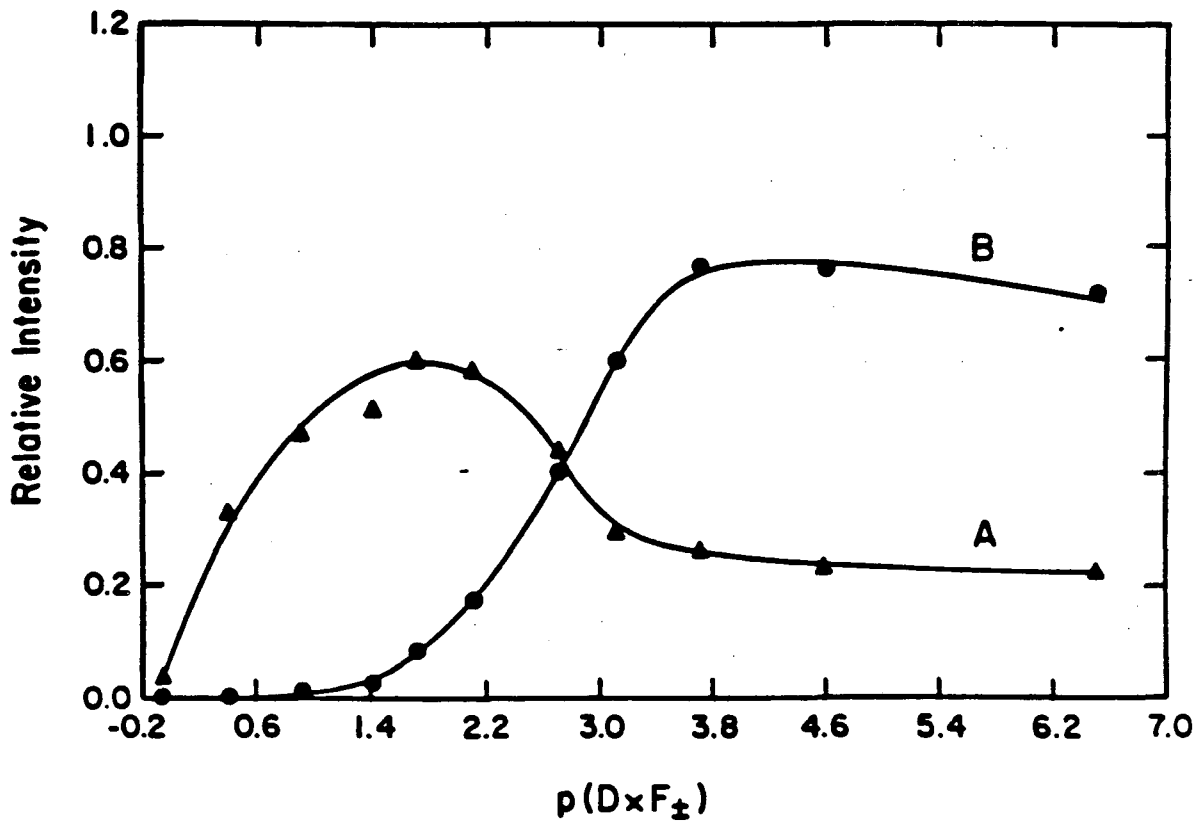

Fig. 30: Fluorescence titration curves for the neutral and anion in D_2O. Table VI lists the relative quantum yields for the neutral and the anion, plotted here vs. pD (A and B, respectively). The pDs have been corrected for the ionic screening effect (see text). The relative yields were obtained by requiring the sum of both the relative yields of the neutral and the anion to equal one at pD 4.6.

the appearance of some quenching mechanism, especially in strong acid, is apparent from the deviation of the sum of the relative quantum yields from one. The plots of the neutral in the D_2O solution shows an increased, less quenched, response at higher acid strengths than in H_2O, while the anion yields are essentially the same. Quantitative evaluations from fluorescence titration curves are not directly possible. At first glance it might appear that, as with normal, ground state titration curves, the pK_a^* might be read from the inflection point of the plots. Interestingly, such an inspection would give a pK_a value of ~2.6 when determined from the anion (for either solution), which is a value not far from what would be calculated by the Forster cycle[16]. However, the position of the inflection point is a function of the kinetics, specifically the relative excited state lifetimes and the quenching rates[31]. Without a knowledge of these rates, the inflection points only give a crude estimate of pK_a^*.

Quantitative results require a plot of the ratio of the neutral to the anion relative quantum yields (Table V and VI for H_2O and D_2O, respectively, and Eq. (A71)) versus corrected proton activities. Equation (A71) shows that both the ratio k/k_1, and the sum, $k_2 + k_q'$ can be obtained from such a plot. Plots of Eq. (A71) for H_2O and D_2O are given in Figs. 31 and 32, respectively. They yield: k/k_1 = 0.27 (H_2O) and 0.27 (D_2O); $(k_2 + k_q') = 0.104\ ps^{-1}$ (H_2O, at pH 5.3, $G_2 = k' = 1.32 \times 10^{-4}\ ps^{-1}$,) and $(k_2 + k_q') = 0.077\ ps^{-1}$ (D_2O, at pD = 4.6, $k' = 5.8 \times 10^{-5}\ ps^{-1}$). Again, the ratio k/k_1 is found to be independent of the isotope. These plots are useful only for moderate acid strengths where ϕ_A/ϕ_A' may be accurately determined. Non-linear quenching effects not accounted for by the model are thought to become

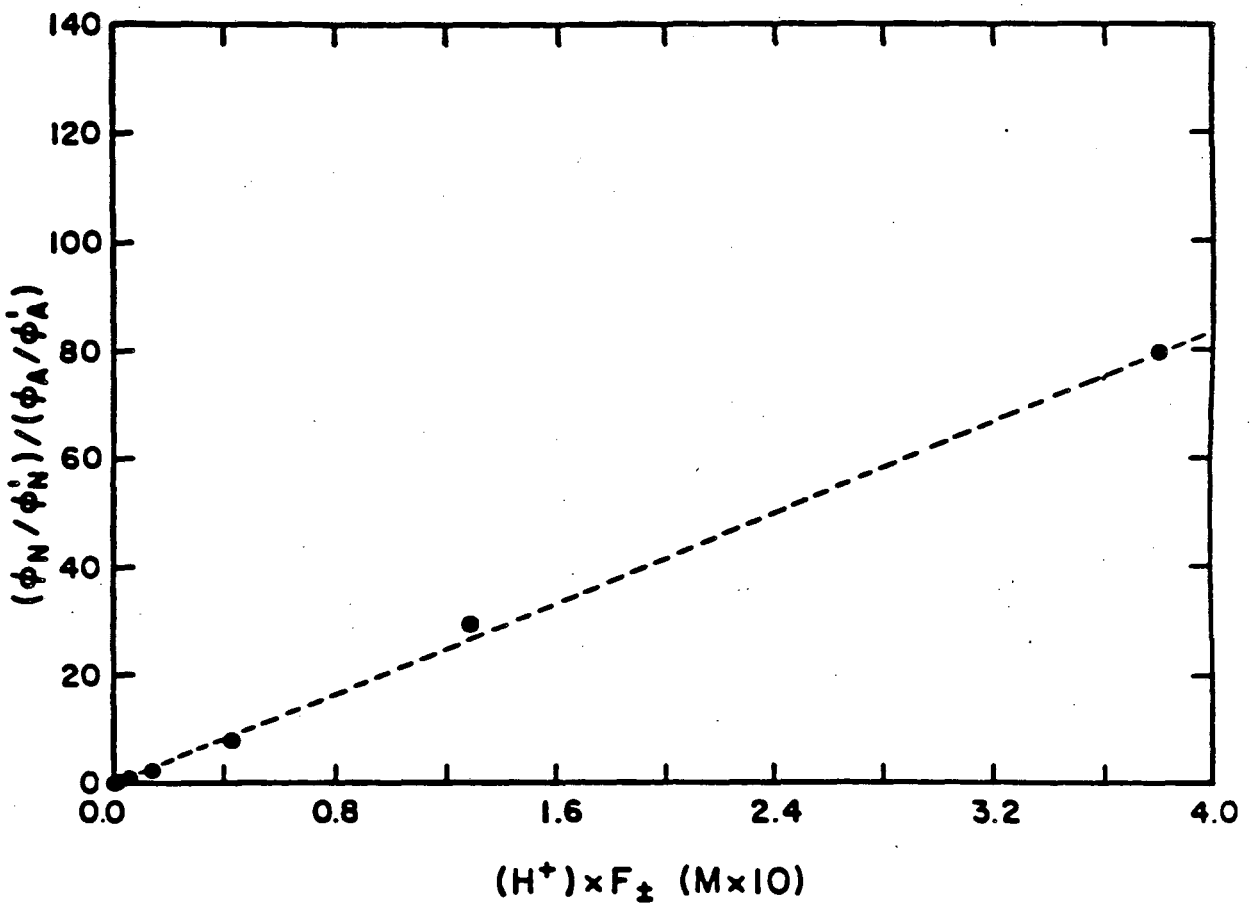

Fig. 31: Plot of Eq. (A71) from the values given in Table V for 1-naphthol in H_2O, see text for the meaning of these plots. In this case, the dashed line is both a least square's fit to the data and the plot from the computer simulation.

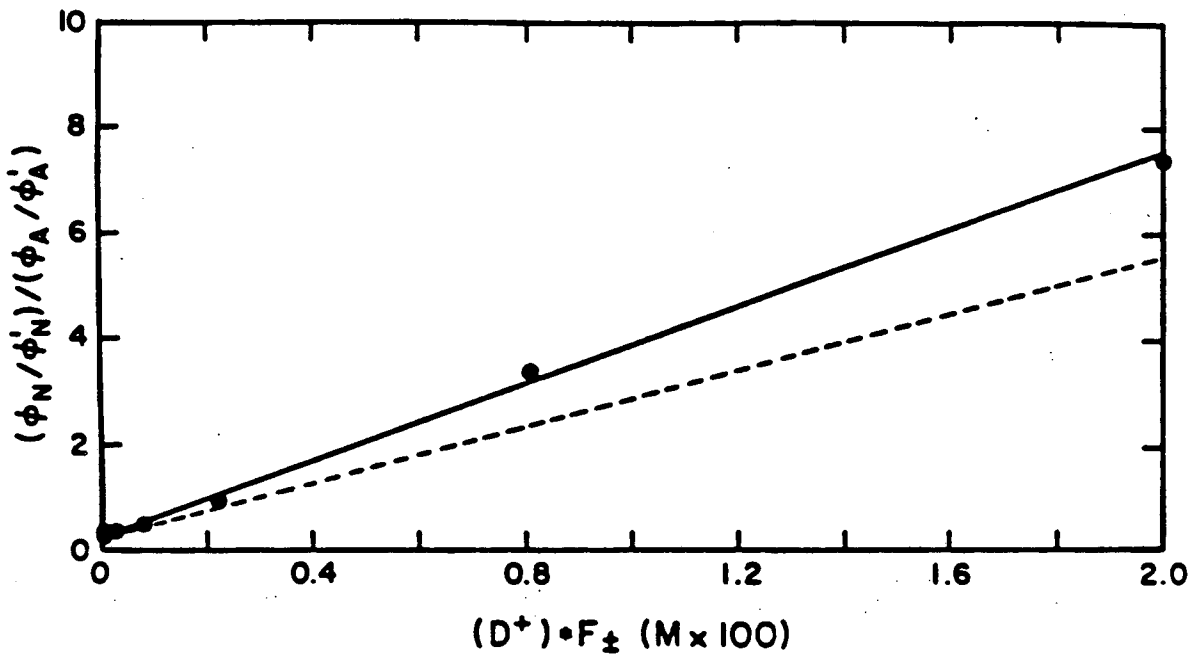

Fig. 32: Plot of Eq. (A71) from the values given in Table VI for 1-naphthol in D_2O, see text for the meaning of these plots. The solid line is a least square's fit to the data. The dashed line is the plot to the computer simulated data.

important at higher acid concentrations. The dashed line in these and future plots of the data show the computer-generated line using the final values listed in Table XI. The solid lines are the best-fit lines to the data.

The time resolved technique of plotting $G_1 + G_2$ versus corrected hydrogen ion activity (Eq. (A72), Tables VII and VIII) gives the necessary additional information to solve for k_1 and k when used in conjunction with Eq. (A71). The intercept, which is very reliable, establishes the sum, $k_1 + k + k'$, as 0.032 ps^{-1} (H_2O, Fig. 33) and 0.010 ps^{-1} (D_2O, Fig. 34). These results give a value for k_1 of 0.025 ps^{-1} (H_2O) and 0.0079 ps^{-1} (D_2O), and a value for k of 0.0068 ps^{-1} (H_2O) and 0.0021 ps^{-1} (D_2O). These values validate the estimates made earlier using the proton transfer quantum yield and the value of G_1 at pH 7. The slope of these plots are sensitive to quenching and the corrections. Over the range used, however, the data compares reasonably well to the computer-derived line. The linearity of the computer-derived line justifies the estimation that these data will be linear versus corrected hydrogen ion activity. As discussed Chapter three, the equation is not a linear function of the hydrogen ion activity with the corrections involved. The slope from these plots gives the sum of the proton dependent terms, $k_2 + k_q + k_q'$, (where the correction on k_q is ignored) as: 0.097 ps^{-1} (H_2O) and 0.048 ps^{-1}(D_2O). Compared to the results of Eq. (A71), the discrepancies are apparent. The slope of Eq. (A71) is steeper (larger value) than Eq. (A72), yet the former slope represents a smaller quantity, $k_2 + k_q'$, than the latter, $k_2 + k_q + k_q'$. For both solvents this difference is of the same magnitude and direction. The only recourse is to average the two methods, since both techniques

Table VII

(H^+)	$(H^+)*F_\pm$	$G_1+G_2(1/ps)$	$G_1*G_2-k_3*k_4(1/ps^2)^\dagger$
7.9×10^{-8}	7.9×10^{-8}	0.0301	-2.0×10^{-7}
1.0×10^{-5}	9.9×10^{-6}	0.0341	2.4×10^{-7}
1.3×10^{-3}	1.2×10^{-3}	0.0402	-1.6×10^{-6}
7.9×10^{-3}	6.6×10^{-3}	0.0293	-1.8×10^{-5}
2.7×10^{-2}	2.0×10^{-2}	0.0297	-4.9×10^{-5}
5.2×10^{-2}	3.6×10^{-2}	0.0383	-7.5×10^{-5}
8.0×10^{-2}	5.2×10^{-2}	0.0350	-1.1×10^{-4}
1.2×10^{-1}	7.4×10^{-2}	0.0432	-1.2×10^{-4}
2.4×10^{-1}	1.3×10^{-1}	0.0461	-2.3×10^{-4}
5.1×10^{-1}	2.3×10^{-1}	0.055	-3.7×10^{-4}
1.2	5.4×10^{-1}	0.069	-1.2×10^{-3}

Table VII presents the calculated, time resolved, kinetic parameters used in Eqs. (A72) and (A73) for graphing vs. $(H^+)*F_\pm$ to yield linear plots.

† k_3 is the term $[(k_1 + k) + k_q(H^+)]$ with $(k_1 + k) = 0.032\ ps^{-1}$, $k_q = 0.006\ ps^{-1}$, and k_4 is the term $[k' + (k_2 + k_q')(H^+)*F_\pm]$ with $k' = 1.32 \times 10^{-4}\ ps^{-1}$ and $(k_2 + k_q') = 0.1\ ps^{-1}$.

Table VIII

(D^+)	$(D^+)*F_\pm$	$G_1+G_2(1/ps)$	$G_1*G_2-k_3*k_4(1/ps^2)^\dagger$
7.9×10^{-8}	7.9×10^{-8}	9.51×10^{-3}	-3.0×10^{-8}
3.2×10^{-6}	3.2×10^{-6}	9.61×10^{-3}	-1.9×10^{-9}
7.9×10^{-4}	7.4×10^{-4}	9.81×10^{-3}	-3.7×10^{-7}
2.0×10^{-3}	1.8×10^{-3}	1.01×10^{-2}	-8.3×10^{-7}
5.0×10^{-3}	4.3×10^{-3}	9.92×10^{-3}	-2.0×10^{-6}
1.4×10^{-2}	1.1×10^{-2}	1.05×10^{-2}	-4.7×10^{-6}
2.2×10^{-2}	1.7×10^{-2}	9.92×10^{-3}	-6.9×10^{-6}
4.2×10^{-2}	3.0×10^{-2}	1.02×10^{-2}	-1.2×10^{-5}
8.0×10^{-2}	5.2×10^{-2}	1.73×10^{-2}	-1.5×10^{-5}
1.2×10^{-1}	7.4×10^{-2}	1.38×10^{-2}	-2.3×10^{-5}
9.7×10^{-1}	4.5×10^{-1}	3.14×10^{-2}	$-1.7\ 10^{-4}$

Table VIII presents the calculated, time resolved, kinetic parameters used in Eqs. (A72) and (A73) for graphing vs. $(D^+)*F_\pm$ to yield linear plots.

† k_3 is the term $[(k_1 + k) + k_q(D^+)]$ with $(k_1 + k) = 0.010\ ps^{-1}$, $k_q = 0.004\ ps^{-1}$, and k_4 is the term $[k' + (k_2 + k_q')(D^+)*F_\pm]$ with $k' = 5.8 \times 10^{-5}\ ps^{-1}$ and $(k_2 + k_q') = 0.060\ ps^{-1}$ (ave. of (A71) and (A72)).

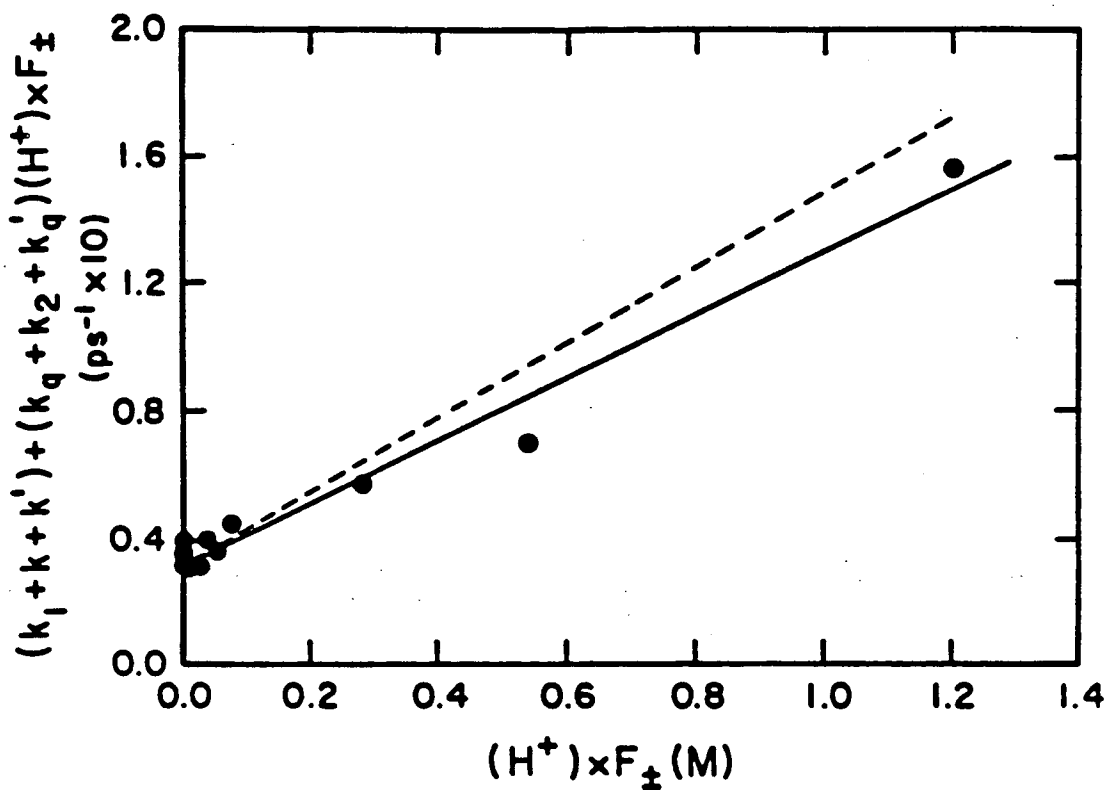

Fig. 33: Plot of Eq. (A72) from the values given in Table VII for 1-naphthol in H_2O, see text for the meaning of these plots. The solid line is a least square's fit to the data. The dashed line is the plot to the computer simulated data.

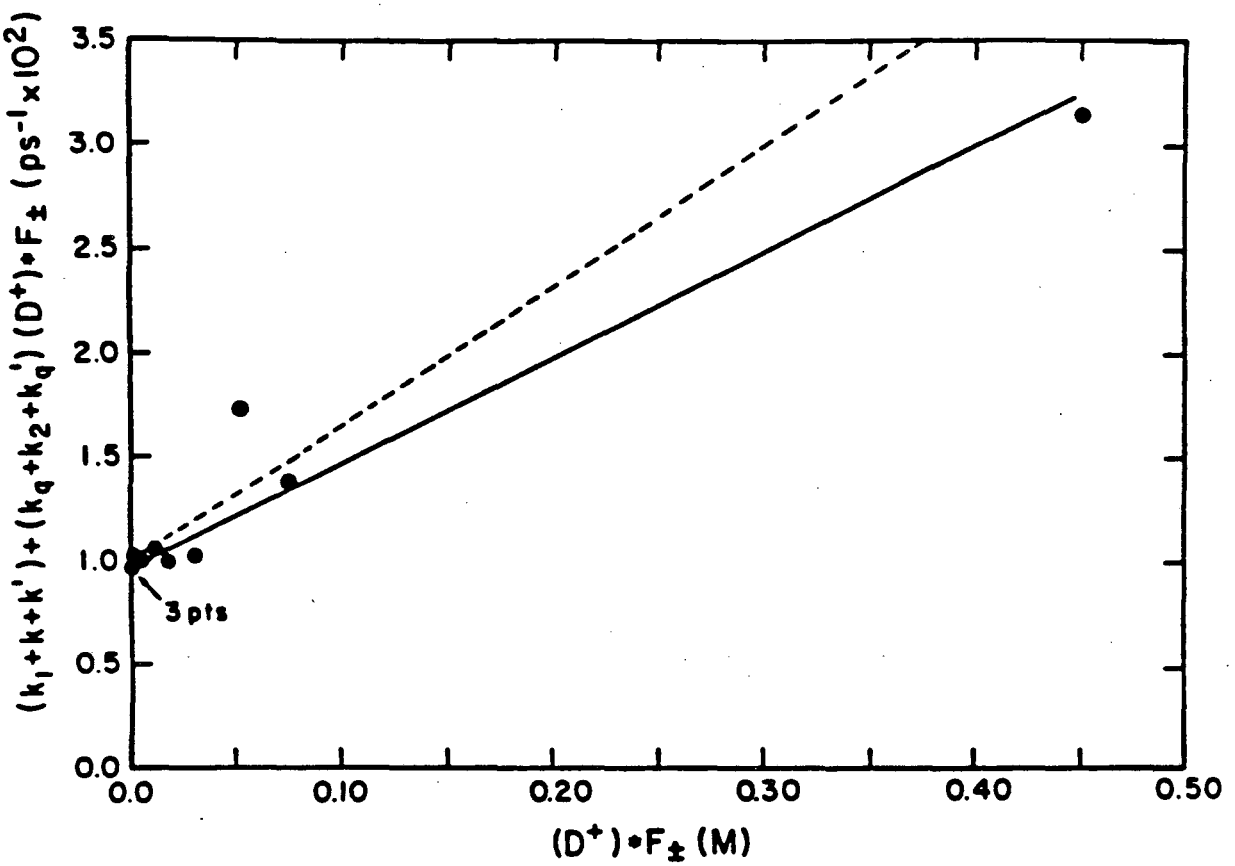

Fig. 34: Plot of Eq. (A72) from the values given in Table VIII for 1-naphthol in D_2O, see text for the meaning of these plots. The solid line is a least square's fit to the data. The dashed line is the plot to the computer simulated data.

are equally valid. The final check on this averaging scheme is evaluated later by a comparison of the real data to the computer-calculated "data".

A unique equation is given by Eq. (A66b). The plot of this complex function, Tables IX and X and Figs. 35 and 36, provides a way to determine the two proton dependent quenching rate constants. Due to the complexity of the function, an evaluation of the appropriate plotting region and an estimate of the accuracy of the resulting values is difficult. Since quenching terms are prominent in both the slope and intercept of this equation, a reasonable assumption would be to use the full range of values, including high acid data where quenching is more dominant. Actually, the plot illustrates that it is the low acid strength data which show the most scatter. The results from these graphs are (using the previously established rates and with $k_2 + k_q'$ from Eq. (A71)): $k_q' = 0.048$ (0.0091 in D_2O) ps^{-1} and $k_q = 0.006$ (0.004 in D_2O) ps^{-1}. The plots from the computer model for these two solvents show that the accuracy of this equation is only qualitative and should only be used as a check on the results from other equations. The estimate for k_q obtained from this equation is needed in the next analysis, the calculation of Eq. (A73). Since the contribution of k_q in that calculation is relatively small, the estimate found here is probably sufficient.

The last plot (Eq. (A73)) links together all the results found previously. The product, $G_1 * G_2$, is determined from the data, Tables VI and VII. The values of k_3 and k_4 may be taken directly from any previous result, average of results, or an iteration of results and plots. For the H_2O case a single evaluation from this

Table IX

(H^+)	$(H^+)*F_\pm$	$F_\pm$	$[(H^+)*F_\pm]^{-1}*[(\phi_A/\phi_A'+\phi_N/\phi_N')^{-1}-1]*[1+k_1/k+(k_2+k_q')(H^+)*F_\pm/k']^\dagger$	$[1/F_\pm+(k_2+k_q')(H^+)/k']$
4.0×10^{-4}	3.8×10^{-4}	0.96	1145.	1.36
2.5×10^{-3}	2.2×10^{-3}	0.90	1195.	3.08
7.9×10^{-3}	6.6×10^{-3}	0.84	1189.	7.4
1.8×10^{-2}	1.4×10^{-2}	0.78	1407.	15.1
6.4×10^{-2}	4.3×10^{-2}	0.67	1561.	52.
2.4×10^{-1}	1.3×10^{-1}	0.56	1593.	190.
8.2×10^{-1}	3.8×10^{-1}	0.47	1800.	647.
4.7	1.8	0.39	3032.	3700.

Table IX shows the steady state parameters (with kinetic rates from Eq. (A71)) which yield a yield a linear plot as described by Eq. (A66b).

† $k_1/k = 1/(0.27)$ and $(k_2 + k_q') = 0.104\ ps^{-1}$ from the plot of Eq. (A71).

Table X

(D^+)	$(D^+)*F_\pm$	$F_\pm$	$[(D^+)*F_\pm]^{-1}*[(\phi_A/\phi_A'+\phi_N/\phi_N')^{-1}-1]*[1+k_1/k+(k_2+k_q')(D^+)*F_\pm/k']^\dagger$	$[1/F_\pm+(k_2+k_q')(D^+)/k']$
2.5×10^{-5}	2.5×10^{-5}	.99	0	1.04
2.0×10^{-4}	1.9×10^{-4}	.97	- 770	1.2
7.9×10^{-4}	7.4×10^{-4}	.94	890	1.9
2.5×10^{-3}	2.2×10^{-3}	.90	320	3.7
1.0×10^{-2}	8.2×10^{-3}	.82	530	11.6
2.7×10^{-2}	2.0×10^{-2}	.75	600	29.
6.4×10^{-2}	4.3×10^{-2}	.67	1000	68.
2.0×10^{-1}	1.2×10^{-1}	.57	1170	210
8.2×10^{-1}	3.8×10^{-1}	.47	2100	850

Table X shows the steady state parameters (with kinetic rates from Eq. (A71)) which yield a yield a linear plot as described by Eq. (A66b).

† $k_1/k = 1/(0.27)$ and $(k_2 + k_q') = 0.060\ ps^{-1}$ from the average of the plots of Eqs. (A71) and (A72).

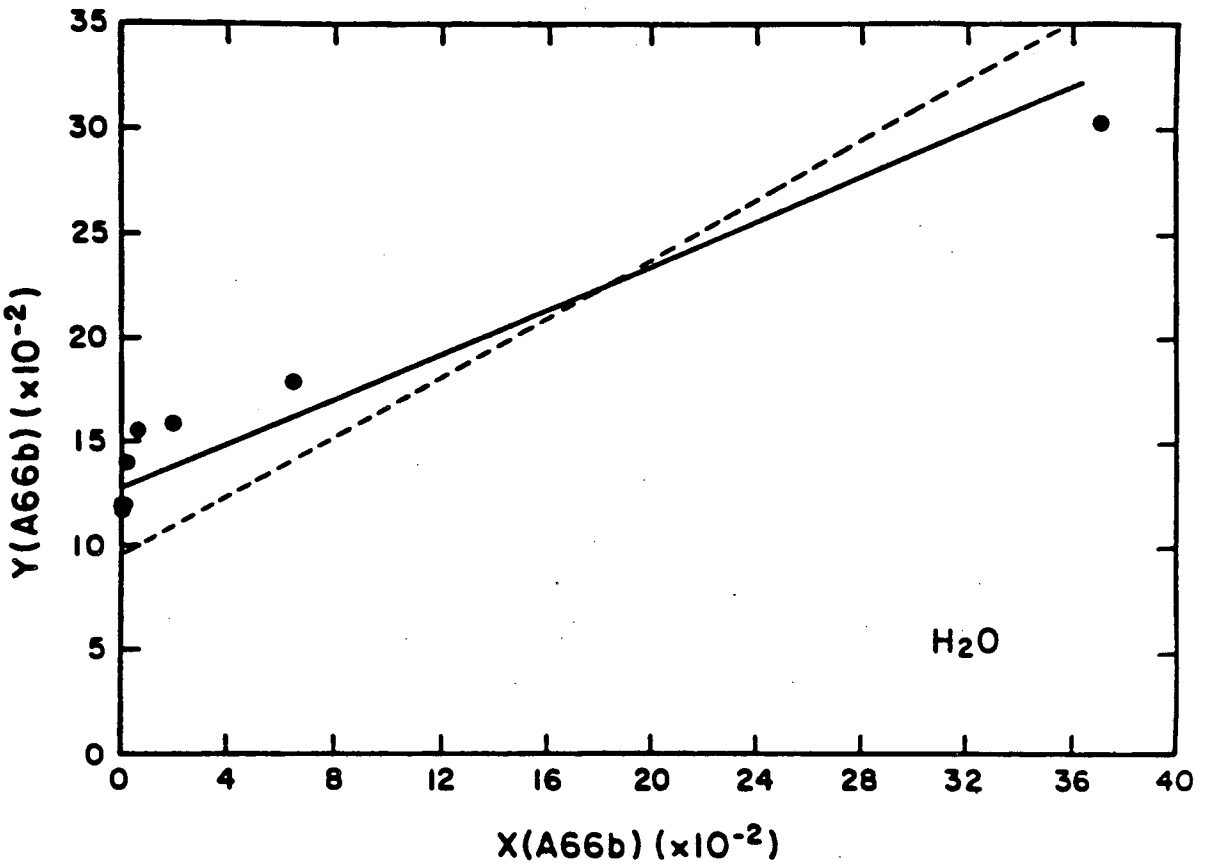

Fig. 35: Plot of Eq. (A66b) from the values given in Table IX for 1-naphthol in H_2O, see text for the meaning of these plots. The solid line is a least square's fit to the data. The dashed line is the plot to the computer simulated data.

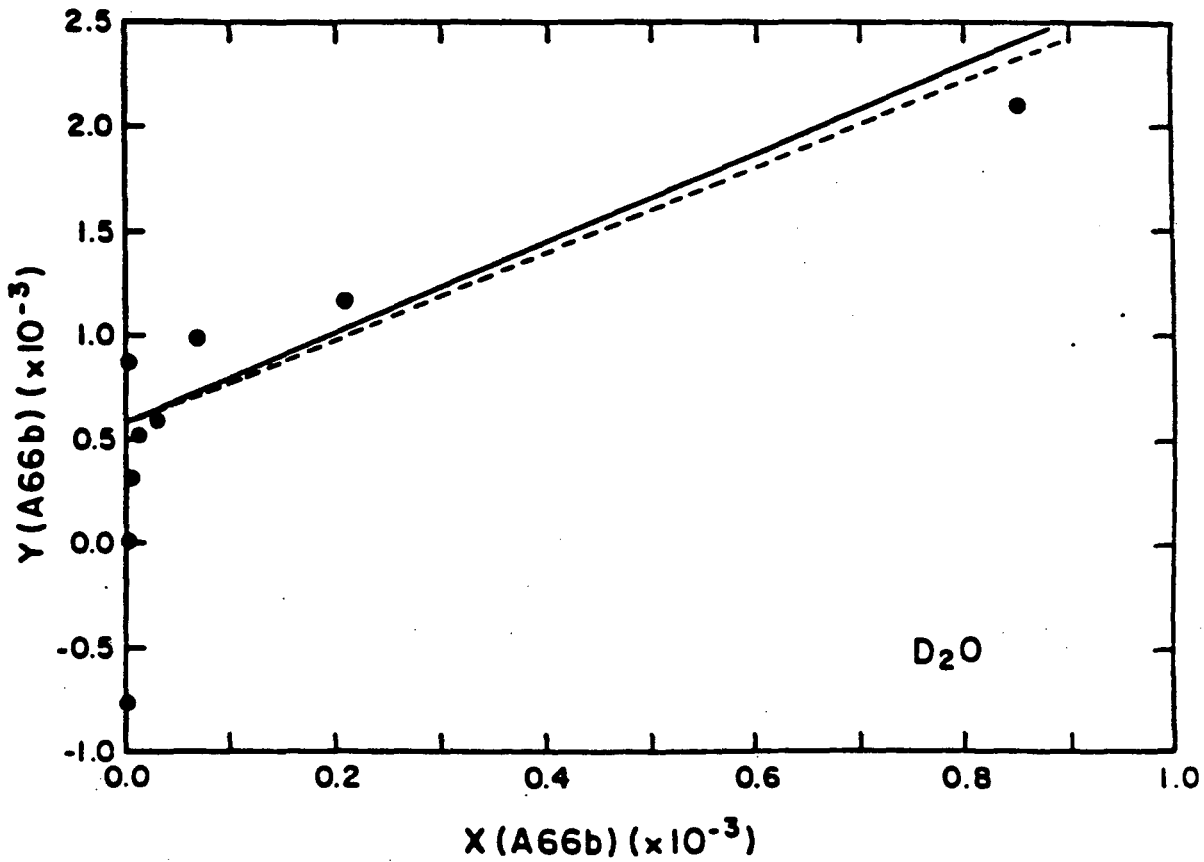

Fig. 36: Plot of Eq. (A66b) from the values given in Table X for 1-naphthol in D_2O, see text for the meaning of these plots. The solid line is a least square's fit to the data. The dashed line is the plot to the computer simulated data.

equation was performed, which produced results which correlated well with the previously determined numbers. The value for $k_2 + k_q'$ of 0.10 ps^{-1} came from Eq. (A71). The slope of the line gave (Fig. 37) a value for k_2 of 0.08 ps^{-1} and therefore a k_q' of 0.02 ps^{-1}. These values were then averaged with the results of Eq. (A72) (where $k_2 + k_q' = 0.097 - k_q \cong 0.091$) and Eq. (A66b) to yield the final values of $k_2 = 0.068$ ps^{-1} and $k_q' = 0.033$ ps^{-1}. For the D_2O case, the iterative method was found to work with equal accuracy. The iterative procedure was started using an initial $k_2 + k_q'$ value (from (A72)) of 0.044 ps^{-1}. These conditions returned a value for k_2 of 0.049 ps^{-1}, demonstrating that an averaged value from Eq. (A71) and Eq. (A72) would be appropriate. A second step through Eqs. (A66b) and (A73) (Figs. 36 and 38, respectively), using an average value for ($k_2 + k_q'$) of 0.060 ps^{-1}, gave the results reported above for Eq. (A66b) and a value of 0.048 ps^{-1} for k_2. This value for k_2 was reasonably close to the number obtained in the first iteration by Eq. (A73). This determination of k_2 can serve as a second check on the value of k_q' found from Eq. (A66b) of 0.0091 ps^{-1}. By calculating k_q' from the previous results ($k_q' = 0.060 - 0.048 = 0.012$ ps^{-1}) the internal consistency of these results is demonstrated. The computer plots of Eq. (A73) show very good agreement for both solvents.

The method of analysis described above demonstrates the utility of using "overlapping" techniques that depend on both time dependent and steady state results. No single equation nor set of equations for either of these methods can give the most accurate results. The averaging of values is only possible with both time dependent and steady state data. The final results from this complete analysis are given

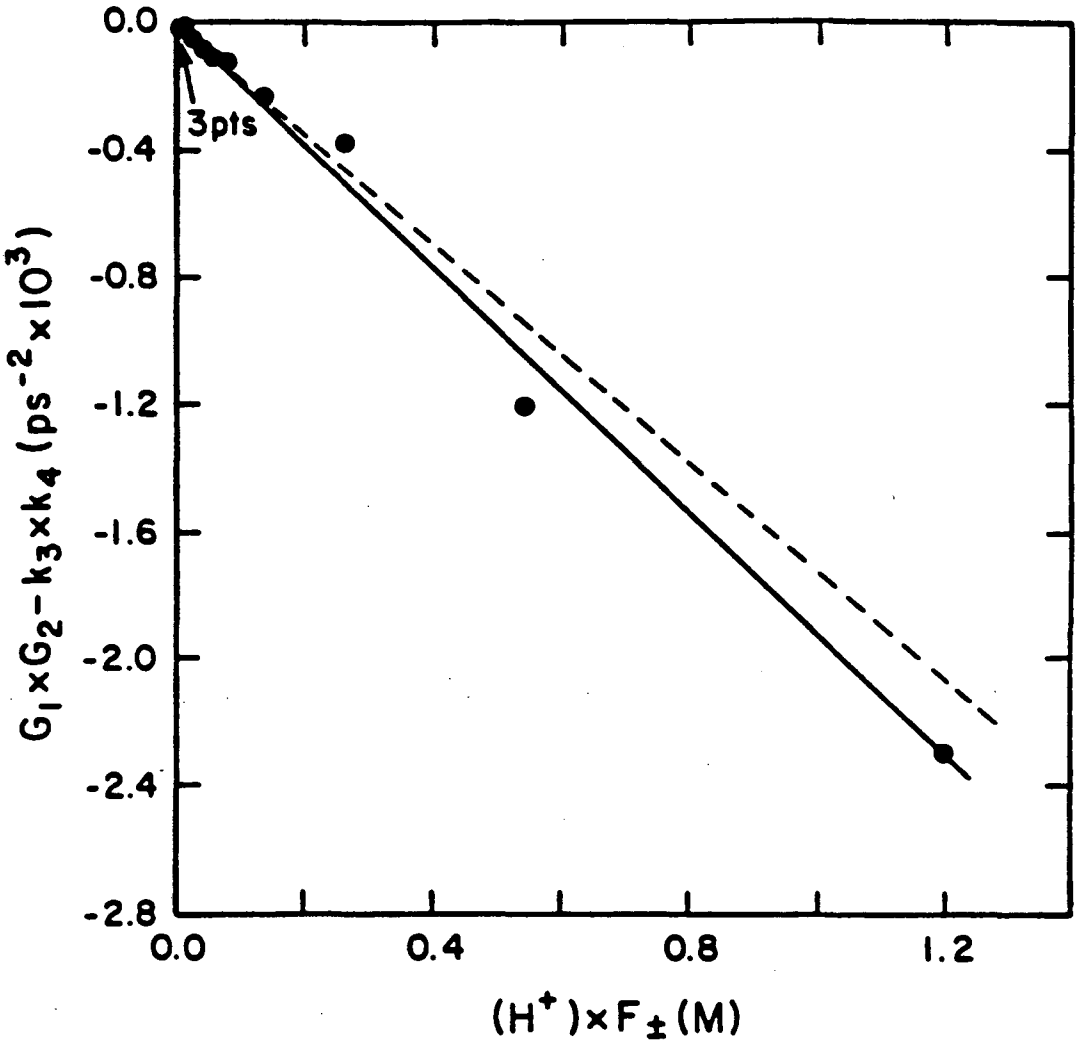

Fig. 37: Plot of Eq. (A73) from the values given in Table VII for 1-naphthol in H_2O, see text for the meaning of these plots. The solid line is a least square's fit to the data. The dashed line is the plot to the computer simulated data.

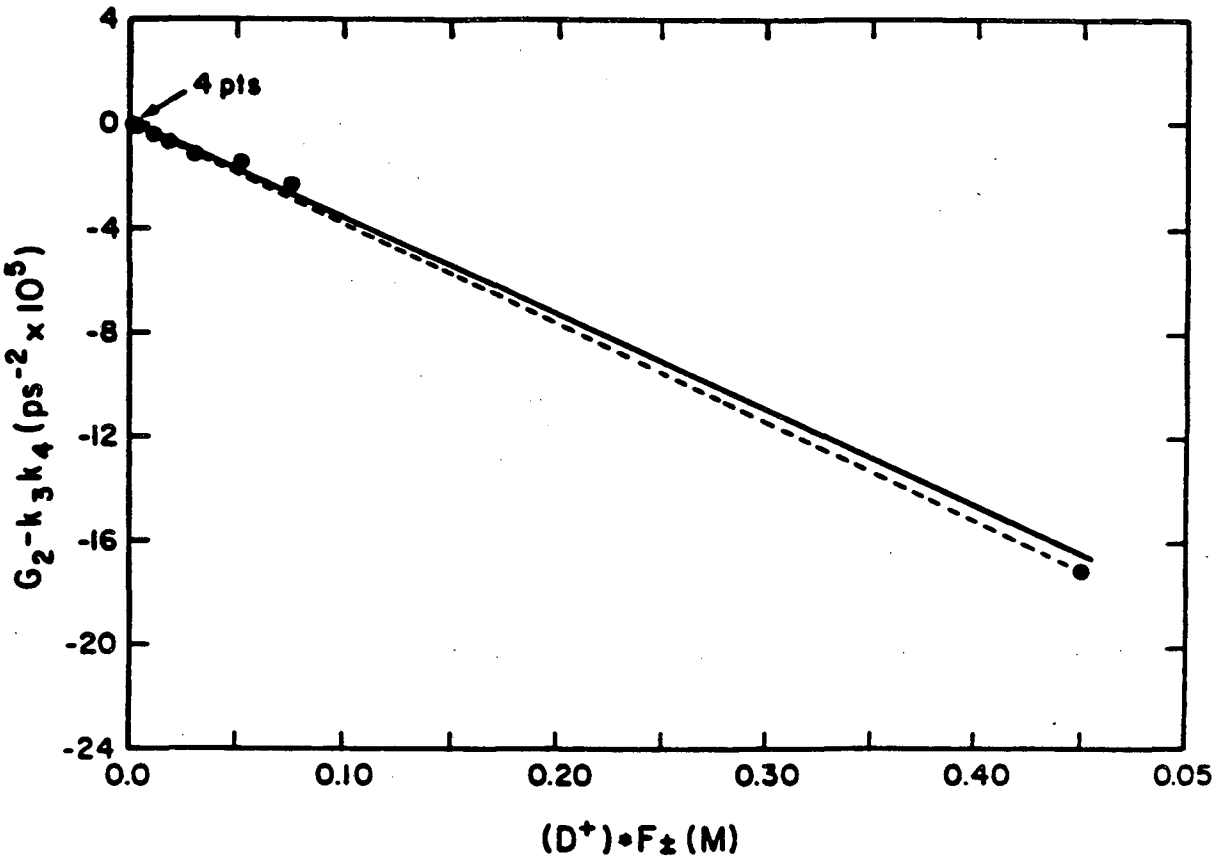

Fig. 38: Plot of Eq. (A73) from the values given in Table VIII for 1-naphthol in D_2O, see text for the meaning of these plots. The solid line is a least square's fit to the data. The dashed line is the plot to the computer simulated data.

in Table XI.

The final values were inserted into the computer program for the generation of simulated data. The computer-derived titration curves, plotted from Eqs. (A65a and A65b), are shown in Figs. 39 (H_2O) and 40 (D_2O).

The marked points are the actual data taken from Figs. 29 and 30. The match is qualitatively good. For the H_2O solution, the anion curve is nearly exact. However, the neutral appears insufficiently quenched in the simulation around pH 1, but does demonstrate similar curvature, compared to the raw data at very low pHs. The exact determination of how the various rates control these features is as yet unclear. More extensive modelling and/or sensitivity analyses would be required to see how each parameter changes the magnitude and shape of the simulations. For the D_2O titration curves the observations are reversed. The computer-plotted titration curve for the neutral matches reasonably well with the data throughout the entire pH range. However, the anion which has the same overall slope misses at the inflection point.

The time resolved data also shows good agreement with the computer curves. Figure 41 (H_2O solution) exhibits remarkably good, essentially quantitative agreement for the three, randomly chosen pHs. Both the neutral and anion kinetics are well matched. As previously mentioned, the computer-modelled data was simply scaled and shifted to best coincide with the real data, but the shapes of the curves are solely dependent on the kinetic parameters. The D_2O case, Fig. 42, is not as well matched, especially at high acid concentrations. The anion "fits" at the higher two pHs are very good, while the neutral

Table XI

Values ‡	H_2O/HCl	D_2O/DCl	H_2O/HCl †	2-Napthol §
τ_o''(pH 12)	8000 ± 400	20000 ± 1000	8000	9000
τ_o'(pH 7)	7550 ± 400	17200 ± 1000	---	---
τ_o(pH 7)	150 ± 30	480 ± 90	440	7900
Φ_A/Φ_A''	0.71 ± 0.05	0.66 ± 0.05	0.68	0.62
Φ_A/Φ_A'	0.76 ± 0.05	0.77 ± 0.05	---	---
k_1	2.5 ± 0.5	0.79 ± 0.16	0.47	0.0075
k	0.68 ± 0.14	0.21 ± 0.04	0.23	0.0125
k'	0.0132 ± 0.0007	0.0058 ± 0.0003	0.0125	0.011
k_2	6.8 ± 1.4	4.8 ± 1.8	1.4	4.6
k_q	0.6 ± 0.2	0.4 ± 0.2	0.17	0.0024
k_q'	3.3 ± 1.4	0.91 ± 0.3	2.8	0.6
pK*	0.4 ± 0.2	0.8 ± 0.3	0.5	2.78

Table XI lists the best fit and averaged kinetic values for the ESPT processes for 1-naphthol in H_2O and D_2O solutions along with previous 1-naphthol/H_2O and 2-naphthol results.

‡ All the rate constants are reported in ps^{-1} (x100) and $M^{-1}ps^{-1}$ x100) for unimolecular and bimolecular processes, respectively. All times, τ, are in picoseconds. Errors in temporal measurements are based on the maximum deviations observed, errors in rate constants are based on an estimate from the fits and averaging.

† See ref. 16

§ See ref. 15

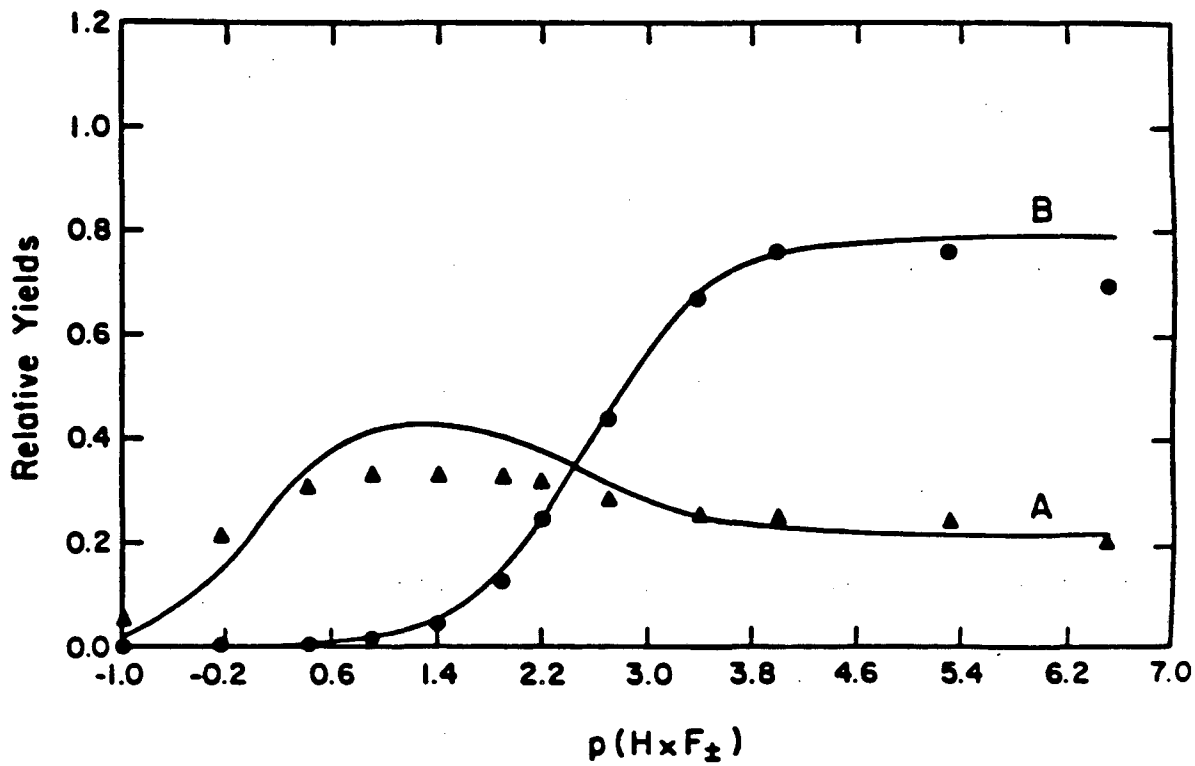

Fig. 39: Computer simulated fluorescence titration curves (solid lines) for the neutral and the anion (A and B, respectively) in H_2O, using the final results from the data as given in Table XI. The plotted points are the actual data as given in Fig. 29.

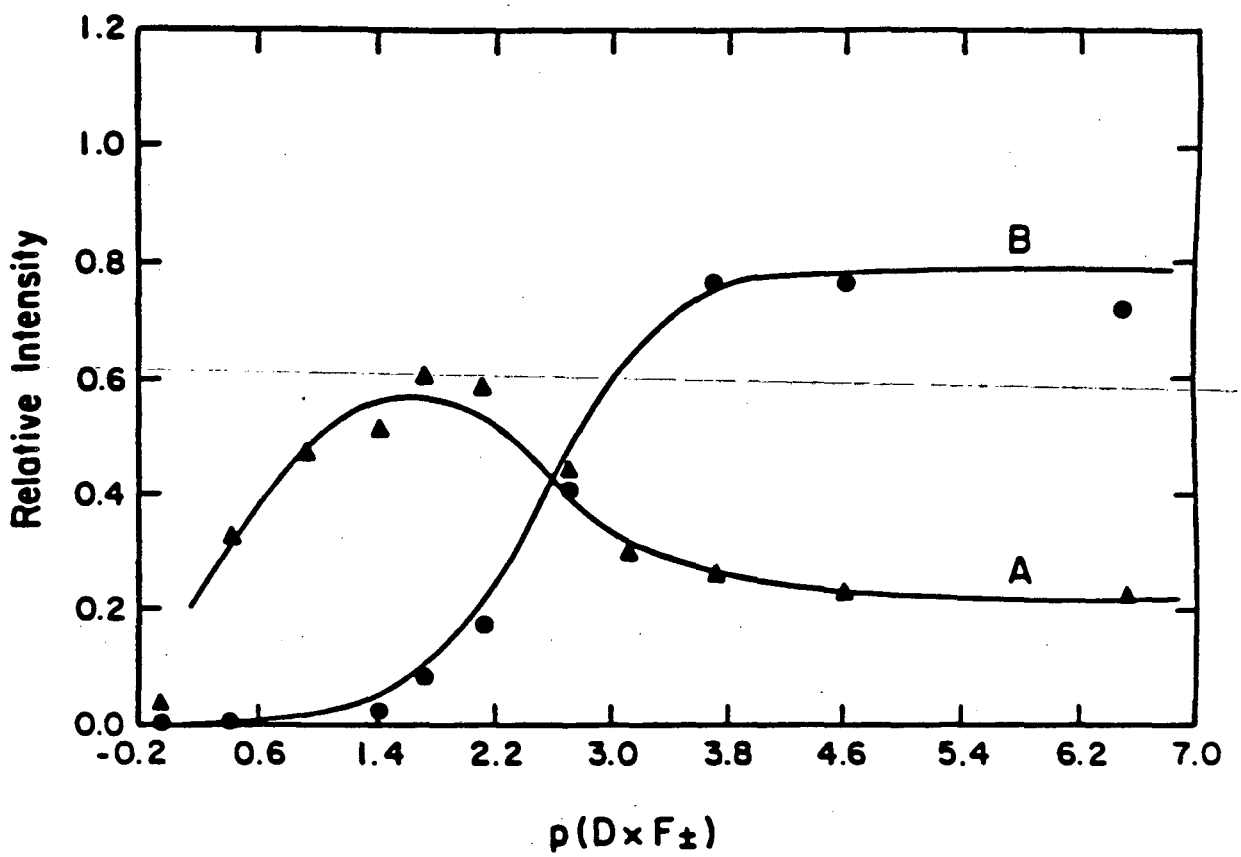

Fig. 40: Computer simulated fluorescence titration curves (solid lines) for the neutral and the anion (A and B, respectively) in D_2O, using the final results from the data as given in Table XI. The plotted points are the actual data as given in Fig. 30.

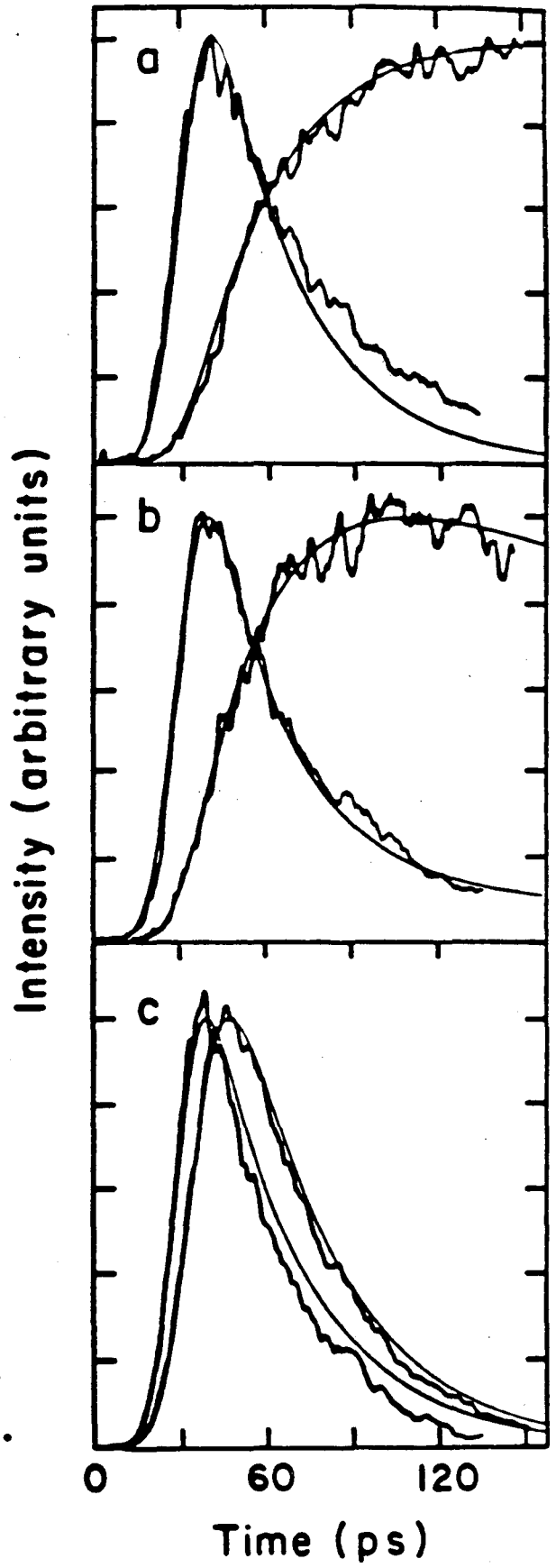

Fig. 41:
Computer simulated fluorescence decay curves (smooth lines) for the neutral (falling curve) and the anion (rising curve) at 3 pHs: 7.1 (a), 1.3 (b), and -0.08 (c). The data have only been scaled and shifted to best match the generated curves (arbitrary intensity and time "zero" point).

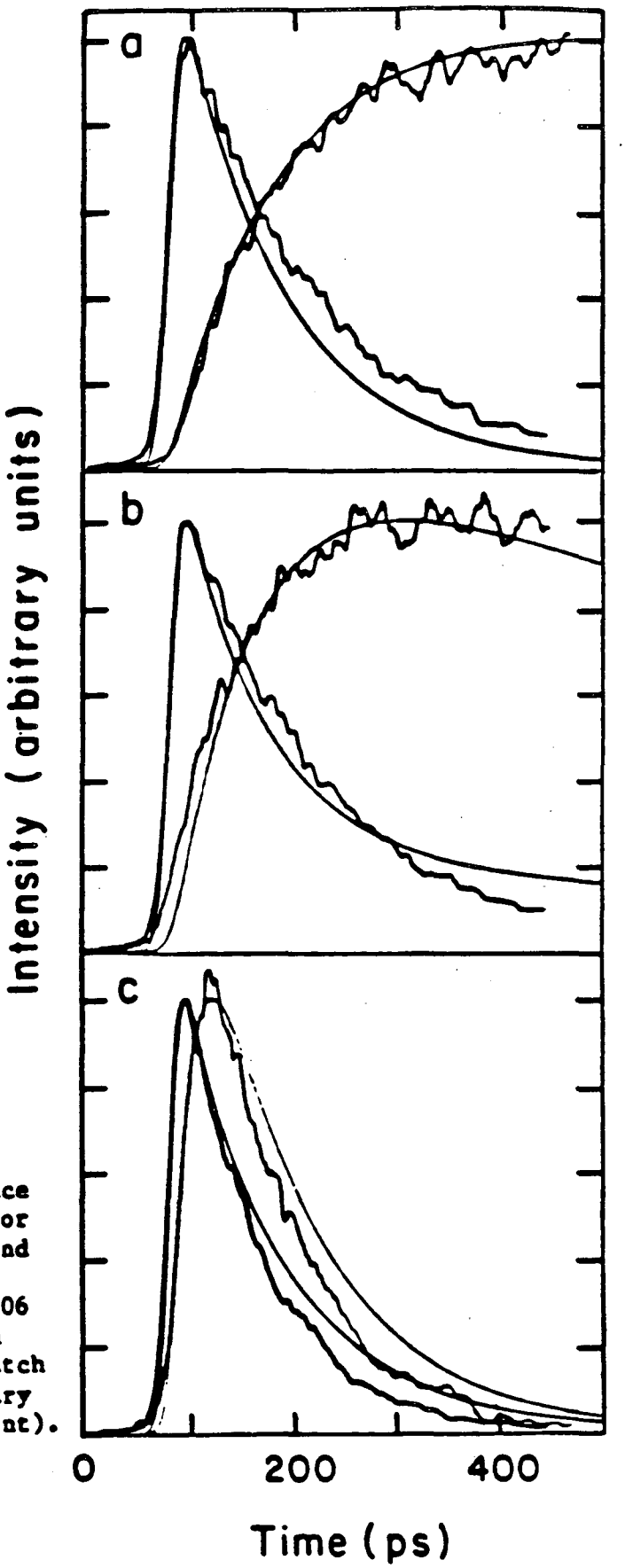

Fig. 42:
Computer simulated fluorescence decay curves (smooth lines) for the neutral (falling curve) and the anion (rising curve) at 3 pDs: 5.5 (a), 1.3 (b), and 0.06 (c). The data have only been scaled and shifted to best match the generated curves (arbitrary intensity and time "zero" point).

misses slightly at each pH, being over-compensated at one extreme and under-compensated at the other. Since the fluorescence titration data for the neutral matched well with the model using these same parameters, this result is surprising. Also, an interesting result is that the anion matches at the two higher pHs yet the accuracy of the fit for the neutral, with the same kinetic parameters, seems poor. Nonetheless, it is concluded that the resulting kinetic scheme and values are correct within the error of the analysis.

The model can be evaluated in terms of the final "fits" to the steady state and time dependent data. Qualitatively and within the error of the measurements, the kinetic scheme presented does account for the observed data. This favorable comparison does not, of course, guarantee that the proposed scheme presents the only possible mechanism, nor that it is complete. Only the major processes have been considered. Further, while the final values may be internally consistent with the model, it is important to remember that they are dependent on the form of the applied corrections, especially the factor, $F_{\pm}$, that is used to correct for ionic screening. The model also simplifies the real conditions at high acidities (low pH). The known[16] quenching effect of the counter ion, Cl^-, is included in the proton quenching rates. The (H^+) and (Cl^-) dependent quenching rates may may not be linearly additive at each pH. Also, the disruption of the solvent shell by these ions is not completely accounted for, regarding its affects on the non-radiative components of the rate constants, k and k'. In non-aqueous solutions, the radiative lifetime of the 1-naphthol neutral (τ_o) is considerably longer than in aqueous solution (see the following section). Such a disruption of the solvent occurs in

concentrated sulfuric acid as well. One group, Tsutsumi and Shizuka[13], reported a value for τ_o of 7800 ps, measured in concentrated sulfuric acid. This value does not fit the model nor their data for the other pH solutions. Also, it does not agree with the data presented here. The use of extreme conditions of pH to determine k is analogous to comparing gas phase to solution phase acidities. The correlation is inaccurate, since the surroundings are so very different.

The final values found in this study can be compared to those found by Harris and Selinger for 1-naphthol[16] and 2-naphthol[15] in H_2O, Table XI. Their analysis for 1-naphthol represents the best previous work. They relied on the steady state approach, coupled with a temporal measurement of τ_o' and a guess for τ_o. The analysis for 2-naphthol is acceptable, since the ESPT reaction in this molecule is more easily determined than in 1-naphthol. Interesting comparisons can be drawn between 1-naphthol in the two solvents, H_2O and D_2O, and between 1- and 2-naphthol.

As mentioned above, the deuterium isotope effect seems to have a similar influence on the two unimolecular rates for the neutral, k_1 and k. Both of these rates must therefore be similarly dependent on the solvent.

The greatest difference in the rates for the two solvents occurs in the forward and reverse proton transfer rates. In the former a large isotope effect (factor of 3.1) is found while in the latter a much smaller change (1.4 times) is measured. The slowed deprotonation rate upon isotopic exchange is reasonable if breaking the O-D bond is the rate-determining step. The reprotonation does not deviate much from the diffusion controlled rate (0.045 ps^{-1}, calculated by Weller[67])

for either solvent. All the rates varied either by this ratio of three (k_1,k,k',k_q') or by approximately one and a half (k_2,k_q). Thus by comparison, the proton (deuteron) is significant in the former rate processes and is of a secondary nature in the latter.

Stryer[44] noticed similar factors in the isotope effect for the forward and reverse rates in 2-naphthol. He saw generally that the absolute quantum yields, which are reflective of the processes given by k and k', all show isotope effects of between 3 and 4 when ESPT processes were involved. Even when proton transfer was slow (relative to the excited state lifetime), molecules with a labile proton displayed an isotope effect in the quantum yields. In cases without a labile proton, no isotope effect was seen. These observations, in accord with the complete kinetics presented here, suggest that hydrogen-bonding in these systems with labile protons is an important feature in the solvent quenching of the excited state.

A pronounced isotope effect is not seen for the proton dependent quenching of the neutral, given by k_q. This observation may be an indication that the counter ion, Cl^-, dominates the quenching of the neutral. Another possible explanation for this small difference is that the quenching occurs at the naphthalene ring. Such a process would reflect the activation barrier of the protonation (deuteration) step and not the effect of the electrophile (H^+ or D^+). In either case, this quenching does not appear to be influenced by either the solvent hydrogen-bonding nor the interaction of the solvent with labile protons.

The comparison of the reaction rates for 1- and 2-naphthol reveal important differences between these two molecules. Additionally, although it is not shown in Table XI, the neutral lifetime in non-aqueous

solvents in not much different for 1- and 2-naphthol. In water, the similarities between the lifetimes of the neutral species vanish. This large difference between the lifetimes of the neutrals emphasizes the curious similarity between the lifetimes of the anions. These lifetimes suggest that the anomalous effects in 1-naphthol are mostly due to features in the neutral rather than the anionic species.

The most significant difference between these two molecules in water is the deprotonation rate, k_1. Since a similar diffusion controlled reprotonation, k_2, exists for both systems, this factor of 300 in the increased rate of k_1 means that 1-naphthol is a much stronger acid in the excited state. This factor of 300 for k_1 also partly explains why so little fluorescence from the protonated species is seen in neutral pH solutions. However, the proton transfer quantum yield for 1-naphthol is only twice that of 2-naphthol, despite the much larger k_1 for 1-naphthol. The reason for this relatively small increase in the quantum yield in 1-naphthol is the equally large increase which occurs for the non-radiative rate, k. Since both of these rates are equally influenced by the solvent in contrast to the rates in 2-naphthol, different solute/solvent interactions between the two systems is suggested.

Both neutral (protonated) species have comparable quenching constants, k_q, relative to their proton transfer rates. The corresponding anion quenching rate, k_q', is proportionately much larger for 1-naphthol. Since this quench is solvent dependent (D_2O study), 2-naphthol must be much less influenced by solute/solvent interactions. This large quenching rate constant further explains why so little emission is seen for this system even as the pH approaches the pK_a^*.

The exact cause for these large differences is not clear and is beyond the scope of the experiments described here. The D_2O study, however, indicates that the solvent definitely plays a role. Also, the electronic structure of the solute greatly affects the ESPT rates, as demonstrated by the comparison of the 1- and 2-naphthol isomers. The survey work presented in the next section will begin to elucidate some of the details of what is occurring in the ESPT reaction of 1-naphthol.

D. Investigations of the Effects of Solvent Structure on ESPT in 1-Naphthol

The observations presented below describe some initial investigations into the solute/solvent interactions which make 1-naphthol/H_2O such a unique system. The study of the ESPT reaction in these altered, aqueous systems will help deduce these interactions[32]. The experiments presented here are solvent effects brought about by: added salts, mixed organic solvents (with water), and increased pressure. Again, both time resolved and steady state measurements were performed. All the studies reported here involve measurements at either neutral or very high pH. The observations were made on the effect of various perturbations on the rapid kinetics described by G_1, i.e., the rate processes reflected in k_1 and k. In the past, investigations of the neutral fall (or the anion rise) times have been linked solely to changes in the proton transfer rate constant, k_1, without regard for the potential changes which may be occurring in k[23-26]. The optimum analysis would measure both the relative quantum yield, ϕ_A/ϕ_A', and G_1 to obtain directly both k_1 and k (see Eq. (9)). Proton transfer quantum yields in many of these experiments are difficult to relate accurately since numerous solvent parameters change upon going from

pH 7 to pH 12 solutions, especially for the mixed solvents. A further complication is the determination of the absorption isosbestic point, which must be carried out for for each solution, prior to measuring the relative quantum yields. The measurements made in this survey were done using 266 nm excitation, thus being directly comparable to the laser excitation wavelength used for the time resolved studies. Reported below are the general observations of the fast kinetics and, when applicable, the features apparent in the steady state spectra. These qualitative findings are informative.

In addition to the solution studies, the 1-naphthol isomer, 5,8-dideutero-1-naphthol, was also investigated. Only time resolved processes were analyzed in this system. A pH 7 solution was investigated to determine if the isotopic substitution had any pronounced affect on the proton transfer kinetics. As expected, the analysis of the neutral and anion kinetics duplicated those of normal 1-naphthol at this one pH. The study of the full pH range, in both H_2O and D_2O, is warranted. The anticipated result is a change in the quenching constant, k_q, and possibly in k_q'. These proton dependent constants are expected and are observed to be unaltered at pH 7.

Analyses involving the modification of the solvent by various external means seem to be a fruitful venture, not only for understanding more about ESPT processes, but also for learning about the solvent "structure" itself[27,47]. Huppert[26] investigated the kinetics of some hydroxyaromatic compounds in various salt solutions. These solutions are expected to have an effect on the solvent organization. He found a linear relationship between the deprotonation rate (measuring G_1 and claiming that $k_1 \gg k$) and the activity of the water determined

from vapor pressure measurements. An attempt was made to rationalize the solute/solvent processes of ion pair formation, recombination, and diffusion with respect to the ionic screening and the restructuring of the water cage. He concluded that the dominant effect of the added ions was the hindering of the ion pair formation process. These investigations were performed on molecules with ESPT rates of, at least, a factor of 3 slower than 1-naphthol.

The preliminary results presented in Table XII agree with the above study, except for Na_2SO_4, which shows no effect even at 1 M. In summary, no deviation is demonstrated up to ionic strengths of one, whereupon the neutral lifetime shows an increase, Fig. 43. The effect of these salts on the other rate processes may be expected to be equally important. The disruption of the rapid, proton transfer is further revealed in the steady state spectra, since emission from the neutral is directly apparent in the higher concentrations of salts. However, without accurate quantum yield measurements, the possibility remains that these observations are due solely to changes in k rather than k_1, or most likely, to changes in both rate constants. The quantum yield of the anion is apparently diminished at increased salt concentration, for example by about 80% on going from, 0.1 to 1. M CsCl. The ratio of the quantum yields, pH 6.5 to pH 12, is unchanged for these salt solutions. This crude result, with the time resolved measurements, suggests that k_1 is most strongly affected by the added salt.

Experiments which alter the solvent provide information about the role of solute/solvent interactions in ESPT. Similar to the D_2O solvent comparison, mixed solvent studies can give insight into the influence of solvent on the processes given by k_1 and k[28,35]. Water

Table XII

Salt	[Conc.] M	[Anion Conc.] M	μ (uncorr.)† M	ΔTime‡
NaCl	0.1	0.1	0.1	0
	1.0	1.0	1.0	6
	5.0	5.0	5.0	58
CsCl	0.1	0.1	0.1	0
	1.0	1.0	1.0	5
$MgCl_2$	0.04	0.08	0.1	0
	0.33	0.6	1.0	3
	1.0	2.0	3.0	28
KSCN	0.1	0.1	0.1	0
	1.0	1.0	1.0	3
Na_2SO_4	0.04	0.04	0.1	0
	0.33	0.33	1.0	0
	1.0	1.0	3.0	0

Table XII shows the difference in lifetime ($1/G_1$) for 1-naphthol in various salts and concentrations at pH 6.5.

† Simple ionic strength: $\mu = 1/2\ \Sigma\ C_n Z_i^2$

‡ ΔTime is the increase in the lifetime (in ps) of 1-naphthol in the salt solution relative to pure water (32±5 ps).

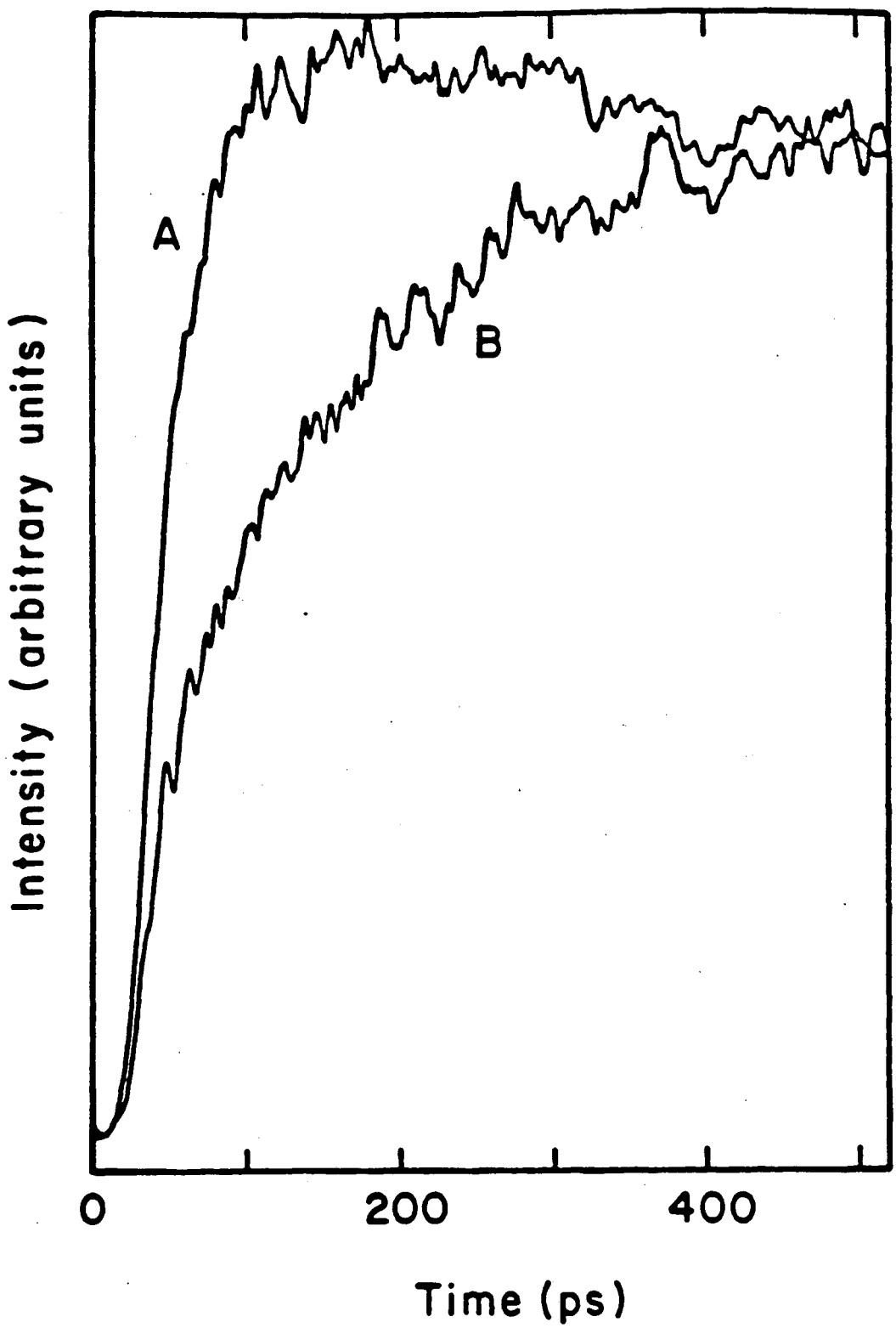

Fig. 43: Temporal response of the anion rise time (550 nm detection) as a function of the concentration of added NaCl at pH 6.5. Curve B shows the dramatic lengthening of the anion rise (90 ps) at 5 M NaCl as compared to pure H_2O (curve A, 32 ps).

clustering around the solute is also observable[25]. However, these studies involve complex analyses. Comparisons between systems with changing solvents are not unambiguous[45]. Martynov, et al.[24], investigated the change of (k_1 + k) in polar and non-polar solvents as a function of added water for 1-naphthol. They used mainly steady state techniques on the anion since they lacked the time resolution and sensitivity to investigate both species. They noticed a basic difference between strong hydrogen bonding and low hydrogen bonding solvents (ethanol and DMF versus heptane and acetonitrile). In the pure solvents they found a pronounced difference in the anion lifetime (shorter for ethanol and DMF) and fluorescence spectra (more diffuse for the hydrogen bonding solvents). They concluded that partial removal of the labile proton in the excited state by these hydrogen bonding solvents assisted in the deactivation. They further hypothesized that the ability to hydrogen bond created an inversion in the excited state manifold (from ^1L_b to ^1L_a)[13,40,41]. Further, this inversion of states distinguishes 1-naphthol from 2-naphthol where the ^1L_b is the emitting state[17].

Robinson, et al.[25], studied the clustering of water as determined by the kinetics of the ESPT reaction of 2-naphthol in methanol/water mixtures. They noticed a disappearance of the anion emission in solutions greater than 50% methanol. They modelled the proton transfer rate as being a function of water cluster size, which is modulated by the amount of methanol. By comparing their data to this scheme, they predicted that the optimal cluster size of water, suitable for accepting a proton, is four. They concluded that the proton transfer process is activated by the appropriate water structure. This conclusion

is similar to that reached by Huppert[23], where salts were found to modify the water activity with regard to the ion-formation (proton transfer) step.

Time resolved and steady state measurements of ESPT with regard to solvation processes were obtained for 1-naphthol in the mixed solvents ethanol/water and acetonitrile/water. For a given concentration of 1-naphthol, the absorption intensity for the neutral shows a gradual decrease with increasing water concentration for both solvent mixes. This change signals a probable difference in the radiative lifetime of the neutral as a function of the mixture. At high pH, the anion absorption displays no such trend with the solvent. In the emission spectra the intensities of the anion greatly increase at the expense of the neutral, as the concentration of water is increased, as expected for the increased ESPT. The emission from the neutral is structured in the mixed solvents compared to the diffuse structure in pure water[24]. Throughout the ethanol mixtures some structure remains while for acetonitrile the structure disappears as soon as water is added. These observations suggest that broadening occurs as a result of interactions of 1-naphthol and water. The quenching by water, observed by reduced neutral emission, is more severe in the acetonitrile/water mix than in the ethanol/water case. Together these observation show that 1-naphthol/H_2O interactions are more hindered in the ethanol solutions compared to the acetonitrile solutions.

The time resolved data are extremely complex and difficult to model even at pH 7. The data would involve multiple kinetic components if inhomogeneous micro-environments are possible. Thus, the decay rates would be dependent on the particular orientation or

type of solvent nearby[45]. Since the proton transfer process to water is so fast for 1-naphthol, such non-statistical behavior might be seen on these very fast timescales. Another concern is that emission from the neutral might be appearing at the detection wavelength of the anion. This effect will increase the observed rise time. The traces in Fig. 44 display the trend in the data. As the water concentration is reduced, the decay processes for the neutral, k_1 and k, are similarly reduced. The data listed in Tales XIII and XIV present some further trends. A disconcerting feature is the apparent mismatch between the neutral, 1-naphthol, fall time and the anion, 1-naphtholate, rise time. According to the model ascribed for pure water, these two times, measured at the same pH, should represent the same kinetic properties (given by G_1). The discrepancy shown here is a factor of two. Additionally, it is the rise time (formation rate of the indirectly produced species) which shows the shorter time. Other explanations exist, in addition to the two mentioned above. One explanation considers a local, ground state micro-environment which promotes direct excitation of the anion. The absorption spectrum gives no hint of ground state anion at neutral pH, nor is it reasonable to expect ionization to be favored by the addition of these organic solvents. The possibility of a non-vertical transition, where excitation of the neutral species directly produces the excited anion, is not a new concept. It is simply a rephrasing of the excited state micro-environment argument. In this case, deprotonation takes place "instantaneously" relative to <u>any</u> emission from the neutral. If this were not the case, the neutral lifetime would also display this initial rapid loss. Such kinetics require sub-picosecond reaction times even

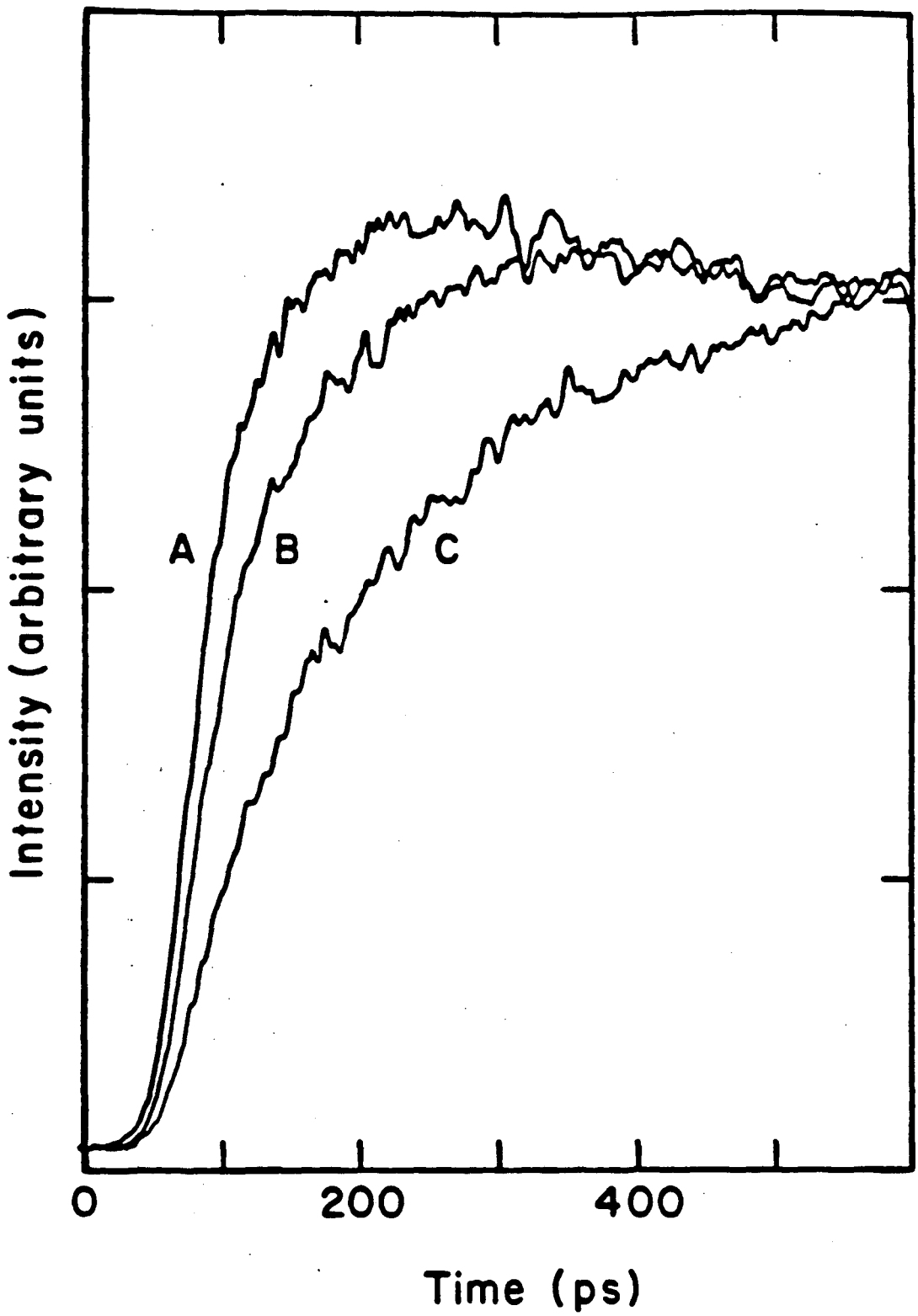

Fig. 44: Temporal response of the anion rise time (550 nm detection) as a function of the concentration of mixed solvent (ethanol in water) at pH 6.5. Curves A to C shows the response of pure H_2O (32 ps), 20 % ethanol (94 ps), and 40 % ethanol (306 ps), respectively.

Table XIII

CH_3CN/H_2O			$EtOH/H_2O$		
v/v %	Neutral Fall time	Anion Rise time	v/v %	Neutral Fall time	Anion Rise time
0	32	30	0	32	30
20	105	54	20	94	50
40	310	160	40	306	135
60	650	250	60	570	280
80	1200	300	80	1300	360
100	6600	—	100	5700	—

Table XIII lists the apparent lifetimes of 1-naphthol in various volume/volume mixes of acetonitrile/water and ethanol/water, assuming single exponential kinetics. All solutions are at approximately pH 6.5. Both fall and rise measurements should reflect the same process, namely $1/G_1$ (see text). All reported times are in picoseconds and are accurate to no better than 10%.

Table XIV

Anion lifetimes CH_3CN/H_2O			Anion lifetimes $EtOH/H_2O$		
v/v %	pH 6.5	pH 12	v/v %	pH 6.5	pH 12
0	7.5	8.0	0	7.5	8.0
20	10.7	11.2	20	8.8	9.2
40	12.6	14.0	40	9.9	10.3
60	12.5	13.8	60	10.0	11.0
80	11.5	11.7	80	9.5	10.7
100	6.1	—	100	7.5	—

Table XIV presents the 1-naphtholate emission lifetime (λ(detect) > 550 nm) at pH 6.5 and 12 as a function of solvent mixtures. All time are in nanoseconds ± 10 %.

for a nanosecond, natural lifetime[53]. Continued investigations into these processes are warranted.

An important feature of the mixed solvents data is that both polar solvents, one a hydrogen bond donnor and acceptor (ethanol) and the other only a hydrogen bond acceptor (acetonitrile), act in an identical, albeit unusual, manner as reflected in their various emission times. Also, both solvent mixes display an increasing anion lifetime with the addition of solvent at both pH 6.5 and 12 until maximizing at approximately a 50/50 mix. Although these lifetimes are is not directly connected to the ESPT process, the long lifetime of the 50% mixture suggest that this solvent structure is somehow unique. In part of his study, Robinson[25] found a minimum in the sum of k_1 and k at 50% methanol/water for 2-naphthol. He attributed this minimum to a competition between the two rates. The proton transfer process, k_1, being large and dominant in pure water and the intra-molecular deactivation, k, being large and dominant in pure methanol. For unexplained reasons he claimed that the sum of these processes reaches a minimum at the 50% point. The observations here show qualitatively that the proton transfer rate does rapidly decrease (increasing neutral lifetime, Table XIII) with increasing organic solvent, while the intramolecular rate processes (as a function of solvent, Table XIV) reach a slight minimum (maximum in lifetime) at the 50% mix. These results agree very well with the shape of the plot of $k + k_1$ versus solvent mixture given by Robinson.

The study of ESPT processes and water structure as a function of pressure is a relatively new topic. Recently, Huppert and Rentzepis[26] presented results showing the effect of pressure on the proton transfer

of a trisulfonated pyrenol in water and D_2O. They measured the lifetime of the protonated species in neutral water versus pressure to investigate the effect of the activation volume and water structure on k_1. They found a linear increase in the rate by a factor of three over the pressure range of 0-8 kbar (about 1 to 8000 atm). This rate increase was attributed to either the increased freedom of motion afforded to the water, because of the weakening internal hydrogen-bonding, or the closer arrangement of solute to solvent due to increased pressure. They assumed that under the pressures studied that no intrinsic change occurred in the solute. Again, it appears that it is the short range interaction, the orientation of the adjacent water molecules, that fascilitates the proton transfer.

The results presented in Table XV and shown in Fig. 45 follow the same trend as those given by Huppert[26]. In fact, the ratio of the fall (or rise) time at room pressure versus that at 3 kbar falls within the error of his data. The ratio of the anion rise time from atmospheric pressure to 5 kbar also falls on this line. This observation implies that the pressure effect on the proton transfer rate is independent of the solute. Further, G_1 rates of up to 7×10^{10} sec^{-1} (the reciprocal rise time of the anion at 5 kbar) demonstrate that rapid interactions occur at high pressure. Additionally, it was found that the anion lifetime at neutral pH ($G_2 \approx k'$) was independent of pressure up to 5 kbar. This fact indirectly supports Huppert's claim that the pressure has little affect on the intra-molecular processes for the neutral, k, since both k' and k might be similarly affected by pressure. The simple proof of this conclusion would come from relative quantum yield measurements of the anion (resulting in the proton transfer quantum yield) as

Table XV

Pressure (kbar)	Fall time	Rise time
0.001	38 ± 5	30 ± 4
1.5	30 ± 4	20 ± 3
2.0	27 ± 4	19 ± 3
3.0	21 ± 3	17 ± 3
4.0	†	17 ± 3
5.0	†	14 ± 4

Table XV gives the neutral fall time and anion rise time, $1/G_1$, for 1-naphthol at pH 6.2 as a function of pressure. All times are in picoseconds.

† Signal too weak to determine accurately.

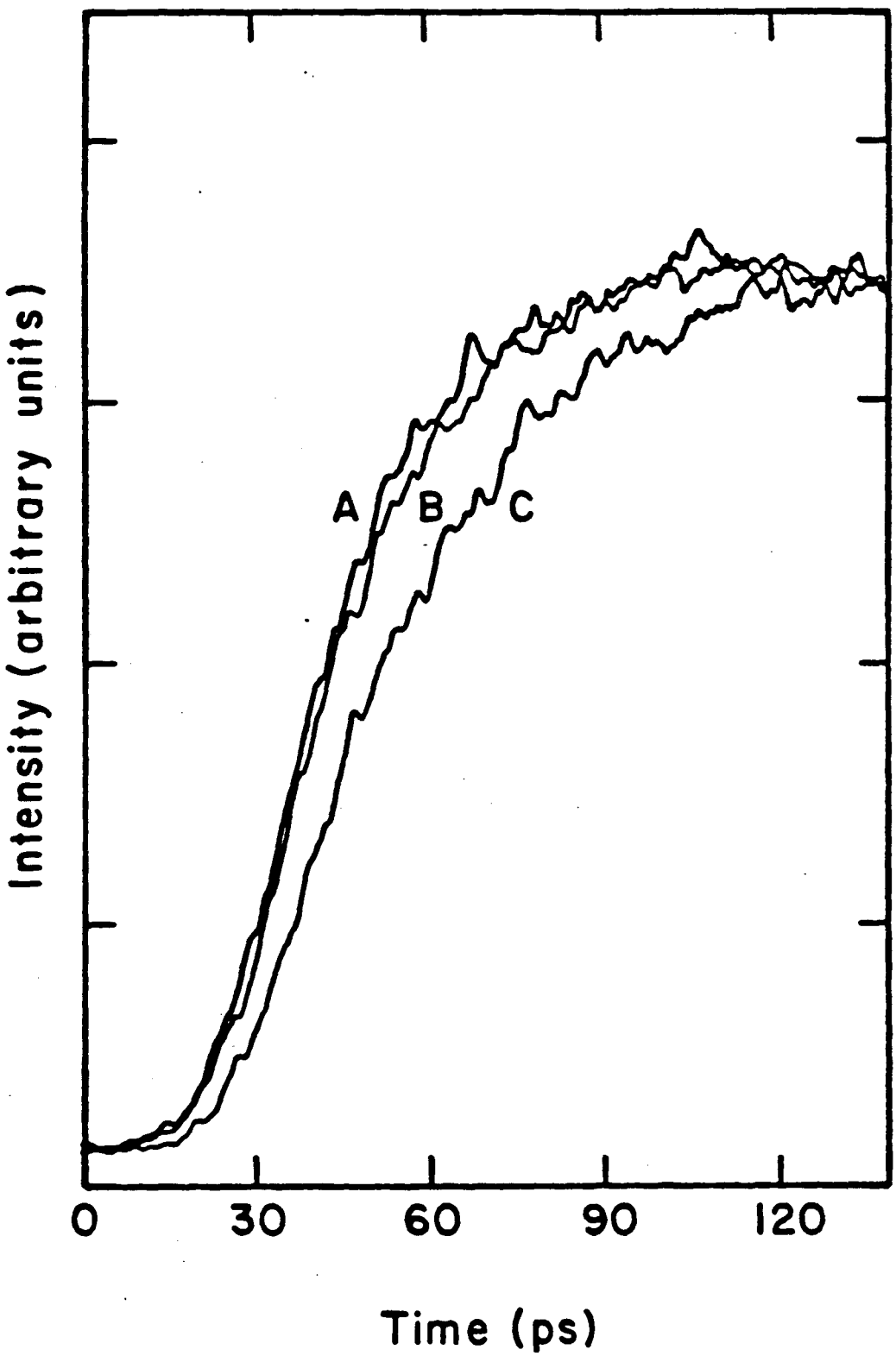

Fig. 45: Temporal response of the anion rise time (550 nm detection) as a function of applied pressure for 1-naphthol in water at pH 6.2. Curves C to A shows the response of pure H_2O at 1 bar (32 ps), 1500 bar (20 ps), and 3000 bar (17 ps), respectively.

a function of pressure. The expected outcome would be an increase in the proton transfer quantum yield with increasing pressure. Such experiments await the coupling of the pressure cell to the fluorimeter.

Chapter Five

Conclusion

The work presented here represents the first direct, real time measurements of the fluorescence decay of the neutral 1-naphthol molecule. Such determinations, when compared with the rise time of the fluorescence signal of the anion, show the 1:1 coupling of the two species on the excited potential surface. An adiabatic, excited state proton transfer is indicated. The combination of steady state techniques with fast, time resolved methods produces the most accurate, composite picture for the processes of an ESPT reaction, especially when diabatic, proton dependent quenching is included. Previous studies of ESPT reactions have rarely coupled these two techniques. Failure to include all the temporal and quantum yield measurements results in inaccurate representations of the processes given by the ESPT model[13,15]. Isolation of the proton transfer rate process (given by k_1) fron the nonradiative paths (given by k), requires either an *a priori* knowledge of the magnitude of these rate constants or an investigation of both time resolved and steady state measurements, for example as given in Eq. (9).

Since a model was selected for the proposed reactions of excited 1-naphthol, direct comparisons can be made between the theoretical responses of the system and the actual data. Such comparisons have been made for both pulsed laser (time resolved) experiments and for continuous wave spectrofluorimeter (steady state) experiments. The results validated the proposed mechanisms within the framework and limitations of the model. Using the final, derived rate constants,

the model was demonstrated to simulate accurately many of the features of the data as determined by either time resolved or steady state means. Deviations of the simulated "data" from the actual data help to elucidate the more subtle aspects of the problem. When used in conjunction with improved experimental data, further computer modelling will aid in the understanding of how the system reacts to its changing environment.

Full kinetic analyses of 1-naphthol in H_2O and D_2O point out the importance of the solvent on the various rate processes. Comparisons of 1- and 2-naphthol present further implications regarding the effect of solute structure on the ESPT processes. The exact mechanisms for these solute/solvent interactions are not yet fully understood. The important aspects to be considered in future work are: 1) the nature of the excited state, i.e., how the charge transfer characteristics activate a group with a labile proton by removal of charge density from the heteroatom; 2) the structure of the solute; i.e., the ability to hydrogen-bond to the solvent and thereby diabatically relax to the ground state; 3) the intrinsic structure of the solvent, i.e., the long and short range interactions and aggregations; and 4) the solvent orientation, i.e., whether the proton transfer is directly possible or if solvent re-positioning is necessary. Preliminary tests by solute and solvent schemes have been tried and can be compared to the conditions in "pure" water, but additional work is needed. Further, in depth studies and new experiments are necessary to explore areas such as the dependence on excitation wavelength and the effect of temperature. The results presented here demonstrate the power of the combination of time resolved and steady state analyses for the study of these complex systems.

References

1. T.H. Lowry and K.S. Richardson, Mechanism and Theory in Organic Chemistry, Harper and Row, N.Y., 1976.

2. a) Th. Förster, Naturwissenschaften, 1949, 36, 186; b) Th. Förster, Z. Electrochem., 1950, 54, 531.

3. A. Weller, Z. Electrochem., 1952, 56, 662.

4. A. Weller, Prog. React. Kinet., 1961, 1, 187.

5. A. Weller, Z. Phys. Chem. (Wiesbaden), 1958, 17, 224.

6. L.D. Derkacheva, Opt. Spectrosc. (Engl. Trans.), 1960, 9, 110.

7. J.L Rosenberg and I. Brinn, J. Phys. Chem., 1972, 24, 3558.

8. J.H. Clark, S.L. Shapiro, A.J. Campillo, and K.R. Winn, J. Am. Chem. Soc., 1979, 101, 746.

9. S. Hou, W.M. Hetherington, G.M. Korenowski, and K.B. Eisenthal, Chem. Phys. Lett., 1979, 68, 282.

10. K.K. Smith, K.U. Kaufmann, D. Huppert, and M. Gutman, Chem. Phys. Lett., 1979, 65, 164.

11. H. Shizuka, K. Tsutsumi, H. Takeuchi, and T. Tanaka, Chem. Phys. Lett., 1979, 62, 408.

12. H. Shizuka, K. Tsutsumi, H. Takeuchi, and T. Tanaka, Chem. Phys., 1981, 59, 183.

13. K. Tsutsumi an H. Shizuka, Z. Phys. Chem. (Wiesbaden), 1980, 122, 129.

14. W.R. Laws and L. Brand, J. Phys. Chem., 1979, 83, 795.

15. C.M. Harris, and B.K. Selinger, J. Phys. Chem., 1980, 84, 891.

16. C.M. Harris, and B.K. Selinger, J. Phys. Chem., 1980, 84, 1366.

17. S.P. Webb, S.W. Yeh, L.A. Philips, M.A. Tolbert, and J.H. Clark, J. Am. Chem. Soc., 1984, 106, 7286.

18. G.W. Robinson, J.M. Morris, R.J. Robbins, and G.R. Fleming, J. Mol. Struct., 1978, 47, 221.

19. G.A. Kenney-Wallace, Phil. Trans. R. Soc. Lond. A, 1980, 298, 309.

20. K.B. Eisenthal, Accts. Chem Res., 1975, 8, 118.

21. G.R. Fleming, G. Porter, R.J. Robbins, and J.A. Synowiec, Chem. Phys. Lett., 1977, 52, 228.

22. F. Franks, Water A Comprehensive Treatise, V. II, F. Franks (ed.), Plenum Press, N.Y., 1972, 323.

23. D. Huppert, E. Kolodney, M. Gutman, and E. Nachliel, J. Am. Chem. Soc., 1982, 104, 6949.

24. I.Yu. Martynov, N.K. Zaitsev, I.V. Soboleva, B.M. Uzhinov, and M.G. Kuz'min, Zh. Prikl. Spektrosk. (Engl. Trans.), 1978, 28, 1075.

25. J. Lee, R.D. Griffin, and G.W. Robinson, to be submitted.

26. D.H. Huppert, A. Jayaraman, R.G. Mains, Sr., D.W. Steyert, and P.M. Rentzepis, J. Chem. Phys., 1984, 81, 5596.

27. D.H. Huppert, E. Kolodney, and M. Gutman, Picosecond II, Springer Ser. Chem. Phys., 1980, 242.

28. M. Swaminathan and S.K. Dogra, J. Chem., Soc., Perkin Trans. 2, 1984, 947.

29. K.Z. Weber, Phys. Chem. B, 1931, 15, 18.

30. N.J. Turro, Modern Molecular Photochemistry, Benjamin/Cummings, Menlo Park, 1978.

31. J.F Ireland and P.A.H. Wyatt, Adv. Phys. Org. Chem., 1976, 12, 131.

32. a) E. Vander Donckt, Prog. React. Kinet., 1966, 5, 273; b) I.Yu. Martynov, A.B. Demyashkevich, B.M. Uzhinov, and M.G. Kuz'min, Usp. Khim. (Engl. Trans.), 1977, 46, 3.

33. S.G. Schulman, Spectrosc. Lett., 1973, 6, 197.

34. N.M. Trieff and B.R. Sundheim, J. Phys, Chem., 1965, 69, 2044.

35. N.K. Zaitzev, A.B. Demyashkevich, and M.G. Kuz'min, Khim. Vys. Energ. (Engl. Trans.), 1978, 12, 430.

36. Th. Förster, Chem. Phys. Lett., 1972, 17, 309.

37. a) The sample of 5,8-Dideutero-1-naphthol was prepared by photochemical substitution of 1-naphthol in D_2O. The sample was gratiously donated by Prof. Laren Tolbert of the University of Kentucky. b) S. Tobita and H. Shizuka, Chem. Phys. Lett., 1980, 75, 140.

38. S.I. Druzhinin and B.M. Uzhinov, Chem. Phys., 1983, 78, 29.

39. H. Shizuka and S. Tobita, J. Am. Chem. Soc., 1982, 104, 6919.

40. A. Matsuyama and H. Baba, Bull. Chem. Soc. Jpn., 1971, 44, 1162.

41. S. Suzuki and T. Fujii, J. Mol. Spetrosc., 1976, 61, 350.

42. S. Suzuki, T. Fujii, and K. Sato, Bull. Chem. Soc. Jpn, 1972, 45, 1937.

43. H. Baba and S. Suzuki, J. Chem. Phys., 1961, 35, 1118.

44. L. Stryer, J. Am. Chem. Soc., 1966, 88, 5708.

45. E.L. Simmons, Progr. React. Kinet., 1977, 8, 161.

46. S. Scheiner, P. Redfern, and M.M. Szczesniak, J. Phys. Chem., 1985, 89, 262.

47. L.A. Philips, S.P. Webb, S.W. Yeh, and J.H. Clark, J. Phys. Chem., 1985, 89, 17.

48. K.P. Ghiggino, A.J. Roberts, and D. Phillips, J. Phys. E: Sci. Instrum., 1980, 13, 446.

49. E.L. Quitevis and G.A. Kenney-Wallace, Rev. Sci. Instrum., 1984, 55, 1265.

50. S. Kinoshita, H. Ohta, and T. Kushida, Rev. Sci. Instrum., 1981, 52,572.

51. D.B. McDonald, J.L. Rossel, and G.R. Fleming, IEEE J. Quantum Electron., 1981, QE-17, 1134.

52. S.P. Webb, S.W. Yeh, L.P. Philips, M.A. Tolbert, and J.H. Clark, Rev. Sci. Instrum., to be submitted.

53. L.A. Philips, W.T. Brwn, S.P. Webb, S.W. Yeh, and J.H. Clark, to be submitted.

54. D. Waldeck, A.J. Cross, Jr., D.B. McDonald, and G.R. Fleming, J. Chem. Phys., 1981, 74, 3381.

55. D.W. Phillion, D.J. Kuizenga, and A.E. Siegman, Appl. Phys. Lett., 1975, 27, 85.

56. D.R. Lutz, K.A. Nelson, C.R. Gochanour, and M.D. Fayer, Chem. Phys., 1981, 58, 325.

57. D.M. Guthals, C.C. Hayden, H. Nathel, D.W. Anthon, and J.H. Clark,

58. G.W. Scott, J.H. Clark, M.A. Tolbert, S.P. Webb, A.J. Cox, and G. Renz, IEEE J. Quantum Electron., 1983, QE-19, 544.

59. H.P. Kortz, A.J. Cox, G.W. Scott, D.M. Guthals, H. Nathel, S.W. Yeh, S.P. Webb, and J.H. Clark, J. Phys. Chem., to be submitted.

60. H. Nathel, D.M. Guthals, and J.H. Clark, to be submitted. to be submitted.

61. L.A. Philips, S.P. Webb, H. Nathel, S.W. Yeh, and J.H. Clark, Chem. Phys.Lett., to be submitted.

62. G.R. Fleming, J.M. Morris, and G.W. Robinson, Chem. Phys., 1976, 17, 91.

63. S.W. Yeh, L.A. Philips, L.F. Buhse, S.P. Webb, and J.H. Clark, Ultrafast Phenomena IV, D.H. Austin and K.B. Eisenthal (eds.), 1984, 359.

64. a) A.N. Glazer, S.W. Yeh, S.P. Webb, and J.H. Clark, Science, 1985, 227, 419; b) The experiments were conceived and the phycobilisomes were isolated by Professor Alex Glazer of the Microbiology Department, University of California, Berkeley. Without his input these experiments would be impossible.

65. L.A. Philips and J.H. Clark, Rev. Sci. Instrum., to be submitted.

66. L.A. Philips, S.P. Webb, and J.H. Clark, J. Chem Phys., to be submitted.

67. A. Weller, Z. Phys. Chem. (Frankfurt am Main), 1958, 17, 224.

68. H.S. Harned and B.B. Owens, The Physical Chemistry of Electrolytic Solutions, Reinhold Co., N.Y., 1950, 343.

69. C.C. Wescott, pH Measurements, Academic Press, N.Y., 1978, 154.

70. N.J. Turro, V. Ramamurthy, W. Cherry, and W. Farneth, Chem. Rev., 1978, 78, 125.

Appendix

A. The ESPT Rate Equations

The kinetic schemes pictured in Figs. 17 and 18 are typical for the study of ESPT in 1- and 2-napthol, respectively. In general we could write for a equilibrating excited state pair, N and A (signifying an excited neutral and anion, respectively):

$$\xleftarrow{\Sigma k_i} \quad N \underset{k_2'}{\overset{k_1}{\rightleftharpoons}} A \quad \xrightarrow{\Sigma k_i'} \tag{A1}$$

where $k_2' = k_2(H+)$ and is therefore a constant at any given pH; (H+) is to denote hydrogen ion activity as opposed to [H+] which will be used to describe the concentration as determined by titration or dilution; and Σk_i (or k_i') refers to all the non-ESPT (other than k_1 and k_2') processes which occur from the excited neutral or anion, respectively, and further specified below. For the case of 1-napththol, we define Σk_i as:

$$\Sigma k_i = k_f + k_r + k_q(H+) = k + k_q(H+) \tag{A2}$$

The analogous rate constants for the anion are denoted with primed superscripts. Some further definitions to simplify the form of the rate equations are:

$$a_1 \equiv \text{processes which deplete the neutral}$$
$$= \Sigma k_i + k_1 \quad \text{and} \tag{A3}$$

$$a_2 \equiv \text{processes which deplete the anion}$$
$$= \Sigma k_i' + k_2' \tag{A4}$$

We can then write the differential rate expressions as follows:

$$\dot{N} = -a_1 N + k_2' A \tag{A5}$$

which can be rearranged and the derivative taken with respect to time to yield,

$$A = (\dot{N} + a_1 N)/k_2' \tag{A5a}$$

$$\dot{A} = (\ddot{N} + a_1 \dot{N})/k_2' \tag{A5b}$$

and the expression for the anion concentration,

$$\dot{A} = -a_2 A + k_1 N \tag{A6}$$

where $\dot{N}$ and $\dot{A}$ mean the usual time derivatives of the concentrations, and $\ddot{N}$ is the second derivative with respect to time. Equations (A5a and b) can be inserted into (A6) to yield:

$$\ddot{N} + (a_1 + a_2)\dot{N} + (a_1 a_2 - k_1 k_2')N = 0. \tag{A7}$$

We then define the following substitutions:

$$G_1 + G_2 = a_1 + a_2 \quad \text{and} \tag{A8}$$

$$G_1 * G_2 = a_1 a_2 - k_1 k_2', \tag{A9}$$

which gives for G_1 and G_2:

$$G_1 = .5[(a_1+a_2) + \sqrt{(a_1-a_2)^2 + 4k_1 k_2'}\,] \tag{A10}$$

$$G_2 = .5[(a_1+a_2) - \sqrt{(a_1-a_2)^2 + 4k_1 k_2'}\,] \tag{A11}$$

The general solution of the coupled differential equations is

$$N = c_1 e^{-G_1 t} + c_2 e^{-G_2 t} \tag{A12}$$

for which the initial conditions are such that at t=0 only the neutral species is formed at a concentration equal to N_o. This condition is true in these experiments since the neutral is the only ground state species present to absorb the incident light. Equation (A12) becomes:

$$N_o = c_1 + c_2 \tag{A13}$$

$$\dot{N} = -G_1 c_1 e^{-G_1 t} - G_2 c_2 e^{-G_2 t}$$

and (A5a) is

$$k_2'A = (a_1c_1-G_1c_1)e^{-G_1t} + (a_1c_2-G_2c_2)e^{-G_2t} \tag{A14}$$

At the initial conditions:

$$k_2'A(0) = 0. = a_1c_1 - G_1c_1 + a_1c_2 - G_2c_2 \tag{A15}$$

which allows for the solution of c_1 and c_2 as:

$$c_1 = (a_1-G_1)N_o/(G_1-G_2) \tag{A16}$$

$$c_2 = (G_1-a_1)N_o/(G_1-G_2) \tag{A17}$$

The final, complete form for the integrated rate equations which give the time dependent concentrations relative to the initial concentration, N_o, is:

$$N/N_o = \frac{1}{(G_1-G_2)}\left[(a_1-G_2)e^{-G_1t} + (G_1-a_1)e^{-G_2t}\right] \tag{A18}$$

$$A/N_o = \frac{k_1}{(G_1-G_2)}\left[e^{-G_2t} - e^{-G_1t}\right] \tag{A19}$$

B. Equilibrium Conditions:

For any pulsed experiment, where the species are initially formed and then decay to zero concentration, thermodynamic equilibrium, K, is established only for an instant in time as given by the following considerations:

$$K = A'/N \tag{A20}$$

or the kinetic definition

$$K = k_1/k_2 \tag{A21}$$

where A' equals A * (H^+). We have at some time, t', an equivalence between the thermodynamic and kinetic equilibrium:

$$k_1N = k_2'A \tag{A22}$$

$$\frac{k_1}{(G_1-G_2)}\left[(a_1-G_2)e^{-G_1t'} + (G_1-a_1)e^{-G_2t'}\right] =$$

$$\frac{k_1k_2'}{(G_1-G_2)}\left[e^{-G_2t'} - e^{-G_1t'}\right] \qquad \text{(A23)}$$

which, solving for t', yields

$$t' = \frac{1}{(G_1-G_2)}\ln[(a_1+k_2'-G_2)/(a_1+k_2'-G_1)] \qquad \text{(A24)}$$

An approximate, stationary state condition can be set up for an appreciable time when the equilibrium rates, k_1 and k_2', are large compared to the rates which depopulate the excited states. The following conditions then hold:

$$k_1,\ k_2' >> k,\ k',\ k_q, k_q', \ldots \qquad \text{(A25)}$$

$$a_1 \cong k_1 \qquad \text{and} \qquad a_2 \cong k_2' \qquad \text{(A26)}$$

$$G_1 \cong a_1 + a_2 \qquad \text{and} \qquad G_2 \cong 0 \qquad \text{(A27)}$$

For $k_1 \cong k_2'$ the equilibrium concentrations, which will be reached within a few (~5) lifetimes of $k_1 + k_2'$, can be expressed as:

$$A_{eq}/N_o = \frac{k_1}{G_1}\left(1-e^{-G_1t}\right) = \frac{k_1}{k_1+k_2'}\left(1-e^{-(k_1+k_2')t}\right) \qquad \text{(A28)}$$

$$N_{eq}/N_o = \frac{1}{G_1}\left[a_1e^{-G_1t} + (G_1-a_1)\right]$$

$$= \frac{1}{k_1+k_2'}\left(k_1e^{-(k_1+k_2')t} + k_2'\right) \qquad \text{(A29)}$$

which, as $t \to \infty$, gives the correct equilibrium condition:

$$\frac{A_{eq}}{N_{eq}} = \frac{k_1}{k_2'} \qquad \text{(A22)}$$

Therefore, there exist conditions for which thermodynamic equilibrium can be directly determined from the excited state populations.

Similarly, when $k_2' >> k_1$, equations (A28) and (A29) reduce to give

$$A/N = k_1\left(1-e^{-k_2't}\right)\Big/\left(k_1e^{-k_2't} + k_2'\right) \quad , \tag{A30}$$

which will reduce to equation (A22) when $t \gtrsim 5/k_2'$. The case where $k_1 >> k_2'$ is somewhat more complex since the equilibrium constant evolves in time as:

$$A/N = k_1\left(1-e^{-k_1t}\right)\Big/\left(k_1e^{-k_1t} + k_2'\right) \quad , \tag{A31}$$

which reduces to (A22) when both:

$$\text{i.} \qquad 1 - e^{-k_1t} \longrightarrow 1 \qquad \text{and} \tag{A32}$$

$$\text{ii.} \qquad k_1e^{-k_1t} + k_2' \longrightarrow k_2' \tag{A33}$$

Condition (i) is met when n (the number of forward proton transfer lifetimes: $t = n/k_1$) is greater than or equal to 5. Condition (ii) is met as a function of the ratio of k_1/k_2' as:

$$k_1/k_2'\ e^{-n} \leq .01 \tag{A34}$$

for which, using a typical k_2' of 10^{10}, we can see for two examples

$$\text{if} \quad k_1/k_2' = 100, \text{ then } n \geq 9,\ t = 9.2 \text{ ps} \tag{A35}$$

or

$$\text{if} \quad k_1/k_2' = 10^5, \text{ then } n \geq 16,\ t = 1.6 \times 10^{-2} \text{ps} \tag{A36}$$

Thus, the number of lifetimes for equilibration becomes greater, but the overall time for equilibrium to be established is less. We have, therefore, a simple means to evaluate the equilibrium conditions, but

only in the regime where equilibrium can be well established relative to the decay of the two excited states. This condition is seldom realized in practice. However, there is a second technique which relies on steady state concentrations of the excited states, yet does not require that equilibrium ever be established between them. This technique is derived in the next section.

C. Steady State Method and Quantum Yields:

The steady-state method differs little from a single pulse analysis with regards to the kinetic expressions already derived. A prerequisite is that the conditions of the analysis must be such that there is no time-dependent absorption or emission over the time of the measurement. These conditions mean that sufficiently small absorption occurs so as to not "bleach" the sample and to not deplete significantly the excitation source. Under these conditions each photon which is absorbed acts as a "single pulse" and so the whole system responds as the sum of many single pulse experiments. Therefore, as long as the integration time is constant (or normalized) from experiment to experiment, the relative intensities of the system under different conditions (i.e., pH) can be compared.

Let us consider a simple case for the coupled, two state scheme outlined for the ESPT reaction, but assume that the only deactivating process is the fluorescence of the two excited species. We will continue to use the normalizing value, No, as in the initial conditions but having the slightly new meaning as being the sum total of the absorption directly into the neutral (no directly produced anion as

before). Obviously, we expect to find the total emission quantum yield, ϕ, to equal one. We have

$$\phi \equiv \phi_N + \phi_A \tag{A37}$$

$$= \frac{1}{N_o} \; k_f \int_o^\infty N \, dt + k_f' \int_o^\infty A \, dt) \tag{A38}$$

$$a_1 = k_f + k_1 \quad \text{and} \quad a_2 = k_f' + k_2' \tag{A39}$$

where k_f and k_f' are the fluorescence rates for the neutral and anion, respectively. The time integrated yields can be considered as originating from all emission wavelengths or any particular wavelength, assuming that the kinetics are wavelength independent. From equations (A18) and (A19) we can write

$$\int_o^\infty N \, dt = \frac{N_o}{G_1 - G_2} \int_o^\infty \left[(a_1 - G_2) e^{-G_1 t} + (G_1 - a_1) e^{-G_2 t} \right] dt \tag{A40}$$

$$\int_o^\infty A \, dt = \frac{N_o k_1}{G_1 - G_2} \int_o^\infty \left(e^{-G_2 t} - e^{-G_1 t} \right) dt \tag{A41}$$

which solve to give:

$$\int_o^\infty N \, dt = N_o a_2 / (a_1 a_2 - k_1 k_2') \tag{A42}$$

$$\int_o^\infty A \, dt = N_o k_1 / (a_1 a_2 - k_1 k_2') \tag{A43}$$

and

$$\phi = \frac{k_f (k_f + k_2') + k_f' k_1}{(k_f + k_1)(k_f' + k_2') - k_1 k_2'} = 1 \tag{A44}$$

which is the desired result. We can easily expand this solution, (A44), to include any and all deactivating rates, including the proton quenching rates, k_q and k_q', to yield:

$$\phi = (k_f a_2 + k_f' k_1)/(a_1 a_2 - k_1 k_2')$$

$$= (k_f a_2 + k_f' k_1)/D \qquad \text{(A45)}$$

$$\phi_N = k_f a_2/D \qquad \text{(A46)}$$

$$\phi_A = k_f' k_1/D \qquad \text{(A47)}$$

$$\phi_{pt} = k_1 a_2/D \qquad \text{(A48)}$$

where ϕ_{pt} is the proton transfer quantum yield.

The absolute quantum yields are simplified by relating them to quantum yields in pH regions where the kinetic expressions simplify. What is tried is to measure the quantum yields in regions where there is no proton transfer, that is measure the anion at a pH much greater than the ground state pK and the neutral at a pH much less than the excited state pK*. Under these conditions the kinetics reflect two, separate, uncoupled states. This seemingly straightforward analysis, assuming one can guess the pK*, would yield the following simple rate equations:

$$dA'/dt = -(k_f' + k_r')A' \qquad \text{(A49)}$$

$$dN'/dt = -(k_f + k_r)N' \qquad \text{(A50)}$$

and the following quantum yields (normalized as above, $N_o = 1$)

$$\phi_A' = k_f'/(k_f' + k_r') \qquad \text{(A51)}$$

$$\phi_N' = k_f/(k_f + k_r) \qquad \text{(A52)}$$

where the primes denote the special condition of no proton transfer.

Two difficulties must be considered before accepting these data. Since these normalizing values are generally measured at extremes of pH one must consider: 1) are the states (solute + solvent) in the ground and excited states the same at all pH's or, in other words, are these extreme pH's reflective of the same rate processes at mild pH's; and 2) are there additional processes which may be important and occurring at these pH's? Since this work has been concerned with the 1-naphthol case, the consideration of the above points will be addressed relative to 1-naphthol.

First, with regard to the anion, it should be noticed, and will be shown below, that the fluorescence lifetime of the anion at a neutral pH (between 6 and 7) should be the same as at high pH (for example, 12, noting that the ground state pK = 9.2). This equivalence is due to the fact that at pH 7 the dominant processes for the anion are: k_1, k_f', k_r' since the other rate constants, k_2 and k_q', are bimolecular with proton concentration and are thus negligible. Since these two lifetimes are different and if we assume that k_f' is intrinsic to the molecule itself, then the rate constant k_r'(pH 7) is not equal to k_r''(pH 12). A simple correction can be made for this difference which will allow us to find an effective quantum yield of the anion relative to the yield in the absence of proton transfer under conditions at pH 7. The following definitions and calculations apply:

$$\phi_A''(\text{pH } 12) = k_f'/(k_f' + k_r'') = k_f' \tau_o'' \tag{A53}$$

$$\phi_A'(\text{pH } 7) = k_f'/(k_f' + k_r') = k_f' \tau_o' = k_f'/k' \tag{A54}$$

So

$$\phi_A'(\text{pH } 7) = \phi_A''(\text{pH } 12)\ \tau_o'/\tau_o'' \tag{A55}$$

where the τ's are the measured lifetimes.

Similarly, for the neutral species, the conditions actually determined in high acid solution (pH<<pK*) must be expressed as:

$$\phi_N^* = k_f \tau_o^* \tag{A56}$$

$$\tau_o^* = (k_f + k_r + k_q(H_o^+))^{-1} \tag{A57}$$

where τ_o^* is the measured lifetime at known hydrogen ion activity, (H_o^+). This expression is a constant only at a given acidity and is further valid only if k_1 is negligible as outlined below. What is often done, and is true under the kinetics of the assumed model scheme, is to note that at pH 7 (far from both the pK and pK*) all quenching terms dependent on the proton concentration vanish. This means that:

$$\phi_N/\phi_N' + \phi_A/\phi_A' = 1 \tag{A58}$$

$$\phi_N' \equiv k_f/(k_f + k_r) \quad . \tag{A59}$$

Since ϕ_N, ϕ_A, ϕ_A' are all measurable, ϕ_N' can be determined.

For the above statements to hold three points need to be shown: 1) the fluorescence lifetime of the anion, unperturbed by the presence of the neutral, must be measurable at pH 7; 2) τ_o^* must be unaffected by k_1; and 3) equation (A58) should be verified.

Point (1) can be rephrased to state: is the kinetically measurable quantity, G_2, equal to $(\tau_o')^{-1}(= k_f' + k_r' \equiv k')$ at pH 7? The kinetics simplify in this region to the following: 1) $k_1 >> k_2'$ and 2) k_2', k_q, k_q' are all small since they are proton dependent, bimolecular rate constants and limited to effective maximum size of 10^4 $M^{-1}sec^{-1}$ (since the diffusion controlled rate is ~10^{11} $M^{-1}sec^{-1}$) which is much less than normal radiative rates. We have, then:

$$a_1 = k_1 + k \tag{A60}$$

$$a_2 = k' = 1/\tau_o' \tag{A61}$$

which means that G_2 must equal a_2 and therefore G_1 must equal a_1 (from (A8)). From (A9) we know that

$$a_1a_2 = G_1{*}G_2 = a_1a_2 - k_1k_2' \tag{A62}$$

which can be true only if $k_1k_2' << a_1a_2$, but since part of the product, a_1a_2, is k_1k', then (A62) holds since we know, at least, that $k' >> k_2'$.

The proof of eq. (A58) involves the same approximations as above, which are proper at this pH. From equations (A46) and (A47) and noting that D is equal to $G_1{*}G_2(=a_1a_2)$ we have:

$$\phi_N = k_f a_2/a_1a_2 = k_f/a_1 \tag{A63}$$

$$\phi_A = k_f' k_1/a_1a_2 \tag{A64}$$

Combining (A63) with (A59), (A64) with (A54), and using (A60) and (A61) we get the desired result:

$$\phi_N/\phi_N' + \phi_A/\phi_A' = \frac{ka_2}{a_1a_2} + \frac{k_1k'}{a_1a_2}$$

$$= \frac{k\ k' + k_1k'}{(k_1+k)\ k'} = 1 \tag{A64}$$

Lastly, we must consider the applicability of (A56) and (A57) to see when τ_o^* is independent of k_1. Two cases can be considered which will effectively decouple the k_1 process. First, $k_q(H_o^+) >> k_1$: this condition simply means that the neutral will decay via this proton quenching and very little neutral will deprotonate to form the anion. The measured decay will then reflect soley this quench, though these

conditions also imply very little fluorescence intensity whenever $k_q(H_o^+) >> k_f$. A further consideration is that k will likely be equivalent to k_1 (same order of magnitude) or smaller. Thus, this term will also be lost in this lifetime measurement. The second case is when $k_2' >> k_1$ <u>and</u> $k_2' >> k_q'(H_o^+)$, where k_2' is equal to $k_2(H_o^+)$. The rationale here is that, at the low pH necessary to be below the pK*, k_2' will dominate, forcing the equilibrium (if ever established) to the neutral (Le Chatlier's principle). That k_2' must be larger than $k_q'(H_o^+)$ is necessary so that a "sink hole" does not exist for the anion which can effectively siphon out the neutral via the anion even though k_2' may be much larger than k_1. We make the assumption in the above argument that $k_q'(H_o^+)$ is the dominant deactivating path, as seems likely considering the low pH. All these points must be known <u>a priori</u> if analyses containing τ_o^* or ϕ_N^* are used.

D. Analytic Expression Employing Steady State and Kinetic Measurements vs. pH:

There are many possible ways to combine and analyze the data to extract the desired rate expressions. This analysis will follow a route applicable to the 1-naphthol experiments. The general scheme is to apply a formalism which uses the most reliable data. Assessment of reliability will depend on the particular experiment. We will assume in these analyses that G_1, G_2, ϕ_N, ϕ_A, ϕ_N', ϕ_A', τ_o^*, τ_o'', and τ_o' are all experimentally obtainable. The first four terms are the primary measurables; the first two being from kinetic determinations and the latter two from steady state analyses. All four are pH dependent. The other terms come from similar experiments but at particular pH's

and serve as normalizing functions which allow for the calculation of these rate constants which are not directly measured.

We have the following relative quantum yield expressions:

$$\phi_A/\phi_A' = k_1k'/(G_1{*}G_2) = k_1k'/D \qquad \text{(A47)/(A54) = (A65a)}$$

$$\phi_N/\phi_N' = ka_2/D \qquad \text{(A46)/(A59) = (A65b)}$$

$$\left(\frac{\phi_A}{\phi_A'} + \frac{\phi_N}{\phi_N'}\right)^{-1} =$$

$$\frac{[k_1/k+1+k_q(H^+)/k][1+(k_2+k_q')(H^+)/k'] - k_1k_2(H^+)/(k\ k')}{k_1/k + 1 + (k_2+k_q')(H^+)/k'} \qquad \text{(A66a)}$$

which can be rearranged to:

$$(\phi_A/\phi_A' + \phi_N/\phi_N')^{-1} -1 \quad 1+k_1/k + (k_q'+k_2)(H^+)/k' \ /(H^+) =$$

$$k_1k_q'/(kk') + k_q[1 + (k_2+k_q')(H^+)/k']/k \qquad \text{(A66b)}$$

a formidable but useful equation. For completeness we can also write:

$$\phi_A/\phi_A^7 = D_7/D = (k_1+k)(k')/D\ , \qquad \text{(A67)}$$

where $$\phi_A^7 = k_f' \int_0^\infty A(\text{pH } 7)\ dt = k_f'k_1/D_7 \qquad \text{(A68)}$$

with $$D_7 = (G_1{*}G_2)_{\text{pH } 7} = (k_1+k)k' \quad \text{and} \qquad \text{(A69)}$$

$$\phi_N/\phi_N^* = a_2(k+kq(H_o^+))/D \quad . \qquad \text{(A46)/(A56) = (A70)}$$

We will concern ourselves with equations (A65a), (A65b), and (A66b). A further, useful combination comes from dividing (A66) by (A65) to obtain:

$$\frac{\phi_N/\phi_N'}{\phi_A/\phi_A'} = k_2a_2/(k_1k') = \frac{k}{k_1} + \frac{k}{k_1}\left[\frac{(k_2 + k_q')}{k'}\right](H^+) \qquad (A71)$$

From the kinetic analysis we already have:

$$G_1 + G_2 = a_1 + a_2 = (k_1+k+k') + (k_2+k_q+k_q')(H^+) \qquad (A72)$$

$$G_1{*}G_2 = a_1a_2 - k_1k_2'$$

$$= [k_1+k+k_q(H^+)][k'+(k_2+k_q')(H^+)] - k_1k_2(H^+) \quad . \qquad (A73)$$

One final consideration is the simplifications which can be made at pH 7. Equation (A65a) can be used to describe the relative emission of the anion under conditions where the proton dependent rates can be considered negligible. This phenomenon occurs at all pHs where the hydrogen ion concentration is small and the solution pH is well above the excited state pK*. Over this region the relative quantum yield of the anion is given approximately as:

$$\phi_A/\phi_A' = k_1k'/(k_1+k)(k') = k_1/(k_1+k), \qquad (A74)$$

where (k_1+k) is simply G_1.

For 2-naphthol or similar systems where quenching is negligible, much of the analysis can be simplified. In actuality quenching effects have been determined in 2-naphthol, but the corrections do not change the relative ESPT rates (that is, the pK* does not change significantly). A determination solely from kinetic measurements is capable of determining the desired rate constants. Equations (A72) and (A73) become:

$$G_1 + G_2 = (k_1+k+k') + k_2(H^+) \qquad (A75)$$

$$G_1 * G_2 = (k_1k'+kk') + kk_2(H^+)$$

$$= (k_1+k)\ k' + kk_2(H^+) \qquad (A76)$$

from which plots versus (H^+) will give k_2 and k. Since k' is the lifetime of the anion and is found from either a separate experiment at pH 12 or from G_2 at pH 7, k_1 is obtainable from the intercepts. A solution also exists for the kinetics of a system which includes proton quenching of the anion by a completely time dependent method. The new equations for G_1+G_2 and G_1*G_2 are now:

$$G_1 + G_2 = (k_1+k+k') + (k_2+k_q')(H^+) \qquad (A77)$$

$$G_1 * G_2 = (k_1+k)[k' + (k_q'+k_2)(H^+)] - k_1k_2(H^+) \qquad (A78)$$

which may be combined with equation (A77) to give the final equation:

$$G_1 * G_2 = (k_1+k)k' + k[(G_1+G_2)-(k_1+k+k')] + (k_1k_q')(H^+) \qquad (A79)$$

Therefore a plot of (A77) versus (H^+) will give (k_1+k+k') as the intercept and (k_2+k_q') as the slope, which can both be used in (A79). Since the determination of k' (= $1/\tau_o'$, the reciprocal lifetime of the anion) is possible, the unique evaluation of k (and therefore k_1) is possible from the intercept, which then allows for the calculation of k_q' from the slope and, further, yields k_2.

This report was done with support from the Department of Energy. Any conclusions or opinions expressed in this report represent solely those of the author(s) and not necessarily those of The Regents of the University of California, the Lawrence Berkeley Laboratory or the Department of Energy.

Reference to a company or product name does not imply approval or recommendation of the product by the University of California or the U.S. Department of Energy to the exclusion of others that may be suitable.

TECHNICAL INFORMATION DEPARTMENT
LAWRENCE BERKELEY LABORATORY
UNIVERSITY OF CALIFORNIA
BERKELEY, CALIFORNIA 94720